Politecnico di Milano

FACOLTÀ DI INGEGNERIA DEI SISTEMI
Corso di Laurea in Ingegneria Fisica

TESI DI LAUREA

OPTIMIZATION OF HOT ELECTRON EMITTERS

Candidato:
Paolo Malacrida
Matricola 720224

Relatore:
Prof. Ib Chorkendorff

Relatore interno:
Prof. Riccardo Bertacco

Anno Accademico 2009–2010

Contents

Acknowledgements **V**

Abstract **VII**

Sommario **IX**

Introduction **1**

1 The hot electron emitters **5**
1.1 Theory of MIS structures . . . 5
1.1.1 MIS structure at equilibrium . . . 6
1.1.2 Tunneling regimes . . . 8
1.1.3 Tunneling current . . . 10
1.1.4 Transmission probability . . . 13
1.1.5 Emission current . . . 16
1.2 Design of hot electron emitters . . . 18
1.2.1 Substrate . . . 19
1.2.2 Thin oxide . . . 19
1.2.3 Metal gate . . . 20
1.2.4 Thick oxide . . . 21
1.2.5 Backside metal . . . 22
1.3 Fabrication sequence . . . 22

2 Electrical characterization **27**
2.1 Introduction to the measurement techniques . . . 27
2.2 Experimental setup . . . 28
2.3 Current-voltage characteristics . . . 30
2.3.1 Reproducibility of IV curves . . . 30
2.3.2 Effects of the work function . . . 32
2.3.3 Fowler plot . . . 34
2.4 Emission curves . . . 36
2.4.1 Reproducibility of emission curves . . . 37

3 Emission under gas pressure 39
3.1 Comparison of the results in UHV and in air 40
3.2 Pressures of Argon 44

4 Model for transport of electrons under air pressure 47
4.1 Idea of the model 48
4.2 Theory of slow electron motion in gases 49
4.2.1 Electron energies and Townsend factor 50
4.2.2 Drift velocity in steady state 50
4.2.3 Energy loss per collision 53
4.2.4 Assumptions and modifications 54
4.3 Model for the electron transmission probability in gases 58
4.3.1 Idea of the model 58
4.3.2 Classical electron motion between collisions 59
4.3.3 Probability distribution functions 62
4.3.4 Initial conditions 65
4.3.5 Iterations and transmission probability 65
4.4 Comparison with the experimental results 67
4.4.1 Emission as a function of the electric field 68
4.4.2 Emission as a function of pressure 71
4.4.3 Conclusions about the model 72

5 Optimization of hot electron emitters 75
5.1 Thickness of titanium wetting layers 75
5.2 Different materials 78
5.3 Work function lowering 80

6 Time dependence of emission and durability 83
6.1 Time evolution of the IV curves 84
6.2 The repairing role of oxygen 85
6.3 Durability 86

7 Hot electron emitters for mass spectrometry 91
7.1 Preparation of the mass spectrometer 92
7.2 Experimental results 93

Conclusion 97

A List of symbols 101

B Hot electron surface chemistry 105

C Measurement setup and holders 109

Bibliography a

Optimization of Hot Electron Emitters

Acknowledgements

This work was accomplished at the Center for Individual Nanoparticle Functionality (CINF) as a master thesis under the Department of Physics of the Technical University of Denmark (DTU). The experimental activities were carried out in the period of time between November 2008 and June 2009. A period of time which I will always remember for the satisfactions and everyday intensity. I thank DTU for the provided resources and facilities but also for the courses of these last two years. At the same time I thank my Italian university, the Politecnico di Milano, where fundamental studies in the three previous years constituted the basis of my technical knowledge and allowed me to be prepared for this project. A project I hope to have enriched with the qualities of both these worlds and cultures. I am particularly grateful to Professor Ib Chorkendorff, my supervisor during these months; I offer him my sincere thanks for his help while choosing the subject of this thesis and later during all its development, for the suggested ideas and the always inspiring discussions. I thank my Italian supervisor at Politecnico di Milano, Professor Riccardo Bertacco, for his interest in accepting to follow my project despite the long distance and for correcting my thesis in perspective of my Italian graduation. Thanks are directed to Professor Martin Johansson and Professor Ole Hansen who never hesitated to share their deep knowledge about semiconductor technologies and vacuum technologies, guiding and assisting me in the laboratories of CINF. I thank all of them for their patience when answering my sometimes ingenuous questions. Special acknowledgments are dedicated to PhD student Lasse Thomsen with whom I performed several experiments. His ideas and enthusiasm aroused my interest and curiosity about a subject he deeply studied for more than three years. I offer the same thanks to PhD students Gunver Nielsen and Robert Jensen for assisting me everyday, for the efficient team work and for the pleasant conversations. I express my appreciation for the opportunity to work and to exchange arguments, intentions and thoughts with all the members of the hot electron group and more in general with all the staff of CINF and of the Center of Atomic-scale Material Design (CAMD). Special thanks go to my friends Elisa Fiordaliso and Marco Vanin. Their agreeable company, the pleasant conversations and our afternoon teas contributed to the creation of an enjoyable environment. Finally I thank all my friends who supported me during these months and to my parents who even being far away in Italy have constantly represented a point of reference.

Abstract

A Metal-Insulator-Semiconductor (MIS) structure may constitute the foundation for the realization of hot electron emitters. A theoretical description of the heterostructure is presented with a particular reference to emission. The derived parameters are the basis for the design of real devices; these are fabricated through cleanroom technologies. The fabrication sequence is illustrated. The experimental results from standard IV measurements and emission measurements taken in UHV environment are compared with the theoretical predictions and show good agreement. The possibility of emitting electrons under gas pressures up to 1 bar was observed and exploited for a qualitative characterization of the devices. A model for the transport of electrons through a gas, originally due to Townsend (1928), is modified in order to estimate the transmission probability of electrons from the device to the collector where emission is measured. Measurements of emission as a function of the accelerating electric field and of the pressure are taken and compared to the model. Various combinations of metals are tested in order to maximize the emission and the efficiency of the devices. The deposition of 2 Å of titanium (Ti) as wetting layer and of 100 Å of gold (Au) produced the best results: an emission of 5µA/cm^2 and an efficiency of 3.4×10^{-4} is reached at 6V. The possibility of enhancing the emission current by lowering the work function of the metal is demonstrated: the dramatic effects of the covering metals on the electrical properties of the devices due to the deterioration of the oxide, however, does not allow to produce real improvements. The durability of the devices is investigated. The results support the project of substituting the traditional electron sources of a mass spectrometer with hot electron emitters. These have the advantage not to generate heat and outgassing in a UHV chamber. The spectra measured with these devices and with thermionic filaments are compared: the good agreement between the two measurements confirms the possibility of employing hot electron emitters in mass spectrometry.

Sommario

Il principale scopo di questa tesi è stato lo studio e l'ottimizzazione di emettitori di elettroni caldi. Da alcuni anni, questi dispositivi vengono realizzati nei laboratori del dipartimento di fisica del DTU, Technical University of Denmark, ed in particolare presso il centro Danchip, specializzato nella fabbricazione di microchip basati su tecnologia dei semiconduttori. Esistono due principali ragioni di interesse per questi dispositivi: da una parte sono stati studiati in relazione alla possibilità di aumentare la reattività chimica delle superifici, con l'obiettivo di creare nuovi e più efficienti catalizzatori [1, 2, 3]. Dall'altra, sono considerati un'innovativa e promettente sorgente elettronica, in grado di aggirare alcune delle problematiche legate ai tradizionali filamenti a effetto termoionico [10] o agli emettitori basati su effetto di campo [11, 12, 13]. Questa tesi si è concentrata sulla seconda di queste possibili applicazioni, valutando la possibilità di superare quelli che sono fino ad ora i due principali limiti dei nuovi emettitori, la bassa densità di corrente e la scarsa durevolezza [14]: requisiti necessari per entrambe le applicazioni ma certamente fondamentali per una sorgente elettronica. I vantaggi consistono invece nella possibilità di avere emissione con trascurabile produzione di calore e in presenza di gas, applicando piccole tensioni; le ridotte dimensioni dei dispositivi e le basse temperature, in particolare, rendono interessante l'implementazione in ultra alto vuoto, per esempio, come mostrato in questa tesi, in uno spettrometro di massa.

La presentazione dei dispositivi parte necessariamente dalla definizione di *elettroni caldi*: con questo termine si intendono quegli elettroni che, tramite meccanismi di eccitazione diversi, assumono un'energia superiore a quella del livello di Fermi di un materiale. Nonostante in letteratura siano stati proposti vari metodi per la produzione di elettroni caldi [4, 5, 6, 7, 8], tra cui ad esempio eterostrutture a film sottile metallo-isolante-metallo (MIM), questo progetto di ricerca si è focalizzato su eterostrutture di tipo metallo-isolante-semiconduttore (MIS).

Il primo capitolo di questa tesi contiene una descrizione degli emettitori, prima da un punto di vista strettamente teorico, procedendo poi, sulla base di tale modello, al progressivo dimensionamento della struttura, fino alla sequenza di fabbricazione vera e propria dei dispositivi. Normali conoscenze di fisica dello stato solido permettono di delineare la struttura a bande dei dispositivi e di identificare i diversi regimi di funzionamento quando una tensione è applicata ai capi della struttura MIS. In regime di Fowler-Nordheim tunneling [19], in particolare, una tensione positiva applicata al metallo è in grado di generare una cospicua corrente di tunneling

che immette elettroni caldi nel metallo stesso. Questi elettroni possono propagarsi senza subire collisioni fino alla superficie del metallo dove, se la loro energia supera quella della funzione lavoro, possono essere emessi. Una formula, originariamente derivata da Tsu e Esaki [22],

$$J = \frac{4\pi m^{\star} q}{h^3} \int_{E_{min}}^{E_{max}} T(E)\, N(E)\, dE$$

viene impiegata al fine di predire la corrente di tunneling una volta che la probabilità di tunneling T(E) e la funzione di alimentazione N(E) sono state modellizzate e inserite. La dipendenza esponenziale della probabilità di tunneling rispetto allo spessore dell'isolante, nonché della probabilità di attraversare il metallo in modo balistico rispetto allo spessore del metallo, impongono strette condizioni di dimensionamento. Su un substrato di silicio (Si) altamente drogato, tipici spessori di 5 nm di ossido di silicio (SiO_2) e di 10 nm di un metallo di transizione, in genere oro (Au) o platino (Pt), costituiscono la struttura MIS. L'ampia superficie dei dispositivi, unita a questi spessori nanometrici, rende particolarmente impegnativa e critica la fase di fabbricazione: la regione attiva ha infatti un'area di $1cm^2$.

Il secondo capitolo fornisce una prima caratterizzazione elettrica dei dispositivi; a tal fine, viene illustrato lo schema circuitale impiegato per la misura delle correnti di tunneling attraverso la struttura MIS e delle correnti di emissione. A prova della riuscita fabbricazione degli emettitori, entrambe tali correnti sono misurate su un notevole numero di dispositivi mostrando una buona riproducibilità. Inoltre, alcune caratteristiche IV dei dispositivi sono analizzate in relazione al modello teorico: la dipendenza della corrente dalla funzione lavoro del metallo e dalla tensione applicata sono evidenti prove del fatto che il trasporto elettronico avvenga mediante un meccanismo di tunneling ed in particolare nel regime di Fowler-Nordheim tunneling, nell'intervallo di tensioni utile al fine di avere emissione.

Nel terzo e quarto capitolo viene affrontato il vasto tema dell'emissione elettronica in una pressione di gas o in aria. Sebbene misure di emissione che abbiano valenza quantitativa debbano essere realizzate in ultra alto vuoto, dove gli elettroni possono essere raccolti da un anodo posto a distanza dalla superficie del metallo, senza che essi subiscano collisioni, è possibile effettuare questo genere di misure anche in aria. Se l'anodo è posto a breve distanza dalla superficie e il campo applicato fra di essi sufficientemente intenso, la diminuzione della probabilità di trasferimento non è drammatica. Queste evidenze sperimentali hanno consentito di effettuare in aria una caratterizzazione rapida, seppur qualitativa, dei dispositivi. Il terzo capitolo evidenzia invece alcune delle differenze che è possibile osservare effettuando questo genere di misure: la diminuzione della corrente di emissione misurata in corrispondenza di un aumento di pressione di argon oppure, in opportune condizioni, l'aumento di tale corrente dovuto alla ionizzazione del gas.

Il desiderio di comprendere meglio i diversi fenomeni che determinano la funzione di trasferimento dalla superficie dell'emettitore all'anodo, ovvero la probabilità che un elettrone emesso venga rivelato, è alla base del quarto capitolo. Le misure effettuate sotto pressione di un gas saranno infatti tanto più significative

quanto minore è l'incertezza su tale funzione di trasferimento: un modello in grado di descrivere il moto degli elettroni in un gas è stato dunque introdotto per stimare questa funzione. Tre principali cause sono ritenute responsabili delle variazioni della probabilità di trasmissione: ionizzazione delle molecole di gas, perdite geometriche, dovute al posizionamento e al dimensionamento imperfetto dell'anodo e perdite di retro-diffusione, dovute agli elettroni che a seguito di un certo numero di collisioni vengono riassorbiti dall'emettitore. Poiché le prime due possono essere ridotte drasticamente rispettivamente limitando i campi elettrici applicati e progettando un anodo opportuno, il capitolo si concentra sul fenomeno della retro-diffusione.

Un modello teorico ideato da Townsend [40] e in seguito modificato da Huxley e Zaazou [41], è stato adottato per descrivere il moto di elettroni soggetti a campo elettrico in un gas e per ricavare alcune grandezze tipiche del moto: il tempo medio fra due urti, la perdita di energia media dovuta a un urto, e il fattore di Townsend che descrive quanto il sistema è lontano dall'equilibrio termodinamico. Queste grandezze vengono poi impiegate per simulare il trasporto di elettroni tra la superficie dell'emettitore e quella dell'anodo. La simulazione sfrutta un metodo iterativo che assume la propagazione degli elettroni come completamente libera tra un urto e quello successivo: permette perciò di far evolvere iterativamente la densità elettronica tra le due superfici metalliche e di ricavare la probabilità di trasmissione. Nella fine del capitolo, la funzione di trasferimento così stimata è confrontata con i risultati sperimentali. Nonostante le correnti predette dal modello siano sensibilmente inferiori a quelle reali e non abbiano di conseguenza alcun valore quantitativo, la dipendenza da tutte le grandezze di interesse corrisponde. Oltre a spiegare la prevedibile diminuzione di corrente per alte pressioni o bassi campi elettrici, in particolare, il modello consente di spiegare la diminuzione di corrente per gli elettroni emessi con maggiore energia cinetica. Un'alta energia cinetica infatti agisce rendendo più casuale il moto degli elettroni che quindi saranno meno sensibili all'azione deterministica del campo elettrico che li accelera, subendo più facilmente retro-diffusione.

Il capitolo quinto e sesto rappresentano il presupposto essenziale per una possibile applicazione degli emettitori di elettroni caldi: quelle che sono le principali problematiche relative a questi dispositivi, la bassa densità di corrente e la limitata durevolezza, vengono affrontate al fine dell'ottimizzazione. Nel capitolo quinto, in particolare, diverse strategie vengono impiegate al fine di massimizzare la corrente di emissione ed in particolare l'efficienza degli emettitori, definita come il rapporto fra corrente emessa e la corrente totale che attraversa l'eterostruttura MIS. Questa efficienza è in genere molto bassa e raramente supera il valore di $\eta = 10^{-5}$; la principale motivazione va ricercata nell'attenuazione della corrente di tunneling dovuta agli urti inelastici degli elettroni che si propagano attraverso il metallo fino a raggiungerne la superficie. In un modello continuo tale attenuazione è esponenziale:

$$\eta \propto \exp\left(-\frac{L}{\lambda}\right)$$

Essendo necessario avere un minimo spessore L del film metallico al fine di assicurare un buon contatto elettrico, è necessario scegliere materiali in cui il libero cammino medio degli elettroni λ sia elevato. Inoltre è preferibile scegliere un metallo con bassa funzione lavoro per poter osservare uguali correnti di emissione applicando tensioni minori. Questi requisiti hanno motivato un'intensa ricerca del miglior materiale; molti dei metalli impiegati, tuttavia, compromettono irrimediabilmente le proprietà isolanti dell'ossido di silicio, comportando il breakdown della struttura. Il miglior compromesso è stato trovato depositando un film sottile di Ti, seguito da un film di Au: lo strato di titanio, necessario per assicurare buona adesione tra SiO_2 e Au, tuttavia, incide fortemente sull'efficienza e il suo spessore deve essere minimizzato; pochi angstrom di spessore si sono rivelati sufficienti. Una tecnica promettente per innalzare l'efficienza di emissione consiste nella riduzione della funzione lavoro superficiale del metallo [51, 52, 53]; nonostante i tentativi effettuati, depositando piccoli spessori di cesio (Cs) su oro (Au) o di argento (Ag) su platino (Pt), abbiano innalzato le correnti di emissione e l'efficienza, la funzionalità dei dispositivi è velocemente crollata a causa della probabile migrazione di atomi superficiali fino all'ossido [54] con il conseguente breakdown.

Il capitolo sesto valuta la possibilità di mantenere in funzionamento gli emettitori per lunghi periodi di tempo, concentrandosi su campioni realizzati con due film sottili di Ti/Au. Nonostante questo genere di dispositivi abbia esibito la maggiore durevolezza, resistendo alle tensioni applicate per molte ore e provando la buona qualità dell'ossido, uno studio dell'evoluzione temporale delle caratteristiche IV mostra il progressivo deterioramento dello strato isolante e il graduale aumento della corrente attraverso la struttura. Si ritiene che tale aumento sia dovuto alla formazione di difetti e di micro-canali conduttivi nello strato di ossido [55, 56]. Evidenze sperimentali suggeriscono inoltre che la resistenza degli emettitori alle tensioni applicate sia inferiore quando impiegati in ultra alto vuoto: l'ossigeno dell'aria potrebbe avere un'azione riparatrice sulla superificie dei dispositivi. Nel complesso tuttavia, la capacità di mantenere una discreta corrente di emissione per diverse ore, senza variazioni eccessive ma subendo una lenta flessione, con buona approssimazione lineare, ha motivato l'idea di impiegare gli emettitori in uno spettrometro di massa.

Il settimo e ultimo capitolo di questa tesi descrive la preparazione di uno spettrometro di massa per ospitare un emettitore di elettroni caldi come sorgente elettronica, sostituendo il tradizionale filamento ad effetto termoionico. A tale scopo è stato scelto uno dei migliori dispositivi realizzati in Ti/Au, la cui massima corrente di emissione misurata è stata $5\mu A/cm^2$, con una efficienza $\eta = 3.4 \times 10^{-4}$ per una tensione applicata di 6V. Alcuni accorgimenti sono stati adottati per poter acquisire misure impiegando alternativamente l'emettitore di elettroni caldi o il filamento, così da rendere più significativo possibile il confronto tra gli spettri; per la stessa ragione è stata immessa una pressione parziale di argon (Ar) nella camera a ultra alto vuoto come valore di riferimento rispetto al quale normalizzare le misure.

Le due misure sono decisamente confrontabili e provano l'applicabilità degli emettitori; poiché tuttavia la corrente generata dal filamento è all'incirca uno o due

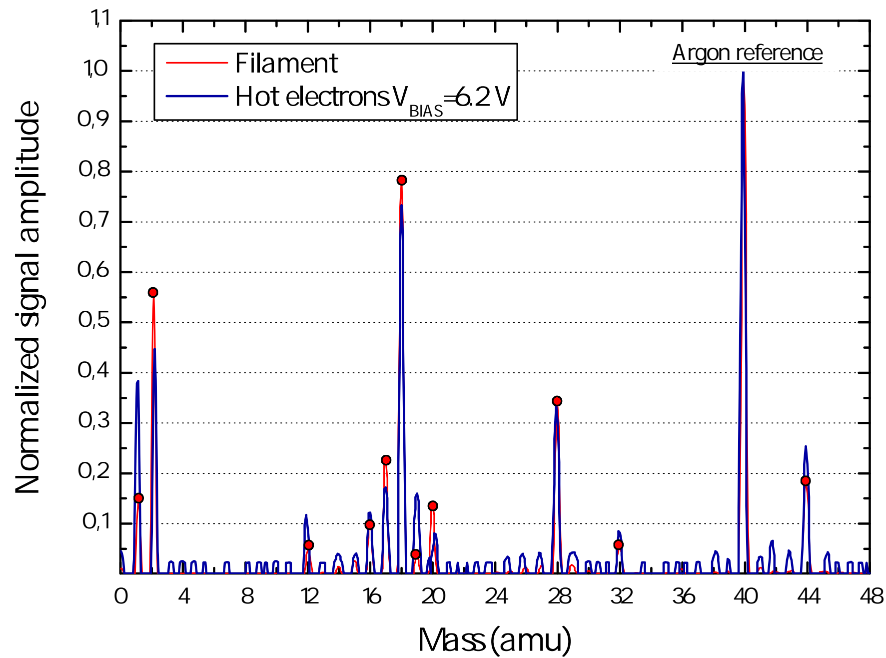

Figura 1: *Confronto tra gli spettri con le due sorgenti elettroniche. H_2O (17,18amu), H_2 (2amu), CO (28amu), CO_2 (16,44amu)*

ordini di grandezza superiore, la sensibilità garantita da questa sorgente è maggiore e il rumore di fondo osservato minore. La superiorità degli emettitori basati struttura MIS dovrebbe invece riguardare i segnali provenienti da molecole quali: H_2O, H_2, CO, CO_2 che facilmente possono evaporare dalle superfici della camera ad ultra alto vuoto per effetto delle alte temperature prodotte dal filamento, falsando la misura. Mentre le pressioni parziali di H_2O e H_2 sembrano effettivamente sostenere questa tesi, il segnale di CO_2 è inferiore per la misura con il tradizionale filamento, ed è difficile trarre una conclusione definitiva sulla natura di queste differenze.

Introduction

The main drive for this thesis has been the characterization of hot electron devices and their optimization as electron emitters. There are two main reasons why the investigation of the properties of such devices arouses much interest: first it fits into the broad challenge to enhance the chemical reactivity of surfaces, in order to realize new or better catalysts. Secondly, it opens the doors to the fabrication of innovative electron emitters with all the associated implications and applications. This thesis mostly focuses on the latter motivation of this research, thereby providing an analysis of hot electron emitters and some suggestions about their applications, in particular the possibility of employing them as an electron source in mass spectrometry.

The basic idea, the theoretical principles and the fabrication sequence of these hot electron devices were studied in the last few years at the Department of Physics of the Technical University of Denmark: the actual design is the result of the collaboration of the Center for Individual Nanoparticle Functionality (CINF) and the Center of Atomic-scale Material Design (CAMD). The central notion of this project concerns hot electrons themselves; these are electrons which have been excited above the Fermi Energy of the considered material. Their energy is typically a fraction, up to some electron volts higher than the energy of ordinary thermally excited electrons. Because of this high energy, when reaching the interface between a metal and a gas phase, these electrons may be able to interact with an adsorbate on the surface and induce a chemical reaction. This possibility leaded to the first hypotheses of employing hot electrons for enhancing the reactivity of surfaces [1, 2, 3], a technique known as hot electron femtochemistry at surfaces (HEFatS). On the other hand, if this energy, above the Fermi level, exceeds the work function of the metal, electrons can also be ejected into the gas phase producing emission. Although HEFatS is not directly considered in this thesis, a brief description of the previous studies at CINF is presented in appendix B.

There have been various attempts to produce hot electrons: Metal-Insulator-

Metal (MIM) and Metal-Insulator-Semiconductor (MIS) heterostructures were suggested and found to be promising [4, 5, 6, 7, 8]. Both these systems rely on the opportunity for the electrons to elastically tunnel through the junction. In this project the focus was directed toward the realization of MIS devices: as a matter of fact the technologies required are compatible with the semiconductor technologies available at Danchip in the Technical University of Denmark. Furthermore semiconductor technologies, especially silicon-based ones, are well known and standardized allowing a high reproducibility of the devices for reasonable costs.

Hot electron emitters differ from the previous electron sources for several reasons. The traditional hot filaments which still represent the majority of electron emitters have a series of drawbacks. They are based on the thermionic effect: a current is supplied to a filament, typically a thoriated tungsten one [9], which consequently heats up. When a sufficient amount of thermal energy is provided, the necessary energy to overcome the work function of the metal, electrons can be emitted. Such devices obligatorily involve high temperatures and intense light emission with the consequent heating of the surroundings and outgassing [10]. They need vacuum conditions to operate and because of these reasons a fairly big amount of space.

More recently, cold cathode electron emitters relying on the field effect were fabricated on chip. In these devices high electric fields are build up nearby a sharp tip of the cathode, accelerating electrons from this extremity into vacuum. As a consequence of the high fields and the production of electric discharges at high pressure, also these emitters can only operate in vacuum [11, 12, 13].

The MIS devices proposed here have the advantage not to produce significant amount of heat. This peculiarity ensures a negligible outgassing and depicts hot electron emitters as promising electron sources in a mass spectrometer, where the minimum level of noise is often limited by the presence of traditional filaments. The possibility of producing devices of any shape and dimension, even extremely small, makes them flexible and adaptable to different conditions. Furthermore they have been demonstrated to operate successfully under a wide range of pressures: from vacuum up to atmospheric pressure at least [14]. The energy of the emitted electrons can be tuned and their energy spectrum is rather narrow. These properties introduce the prospect of other application; the capability of emitting electrons from a particular very well defined pattern on a wafer is exploited in Hot Electron Emission Lithography [15]. The possibility of producing spin-selective emitters, thanks to the different mean free path of electrons of different spin in

transition metals could be a further application [16, 17].

The main drawbacks of hot electron emitters are the low emission current density and their durability. Due to the high probability of breakdown during operation the electrical properties of the device are easily compromised. Such deterioration easily affects the stability of the device and its emission efficiency. Purpose of this project was to enhance the emission current, possibly maintaining it constant in time and stable, as any kind of application requires.

The first chapter of this thesis introduces the concept of hot electron emitters, first describing them from a theoretical point of view, later proceeding with the actual design of a device towards the practical fabrication procedure. The second chapter presents the first experimental results providing a general electrical characterization of the devices. Chapter three and four approach the complicated topic of electron emission under gas pressure; a model for the electron transport in a gas phase is derived and compared with the performed measurements. Chapter five and six represent the prerequisite for a real application of hot electron emitters: the problems of the low current density and of the limited durability are assessed in order to optimize the devices. Finally in chapter seven the hot electron emitters are employed as an electron source for mass spectrometry, the results are compared with the spectra achieved using a traditional filament.

Chapter 1

The hot electron emitters

This first chapter is aimed at providing a general description of the hot electron emitters, starting from a theoretical treatment and proceeding toward real devices. First it considers the theory of MIS structures: the tunneling of the electrons through the oxide barrier and how they can be emitted in vacuum. Secondly it focuses on the geometry of a device showing the role and the peculiarities of each of its parts. Finally the practical processes involved in the fabrication of hot electron emitters are reported.

1.1 Theory of MIS structures

This section analyzes the physical fundamentals of MIS devices, the basic principles from whence the idea of hot electron devices was originated. More in detail the objective is to understand how electrons propagate across the devices, to predict the expression of the IV characteristics and the origin of the emission current. In order to approach the matter the complete description of a real device is deferred to the next section while here the interest is focused on its essential part: the MIS heterostructure itself.

This is a sequence of three solid layers: a highly n-doped semiconductor, an insulator and a metal. Unless specified otherwise a silicon layer (Si) doped with antimony (Sb) will represent the semiconductor, silicon dioxide (SiO_2) will be the insulator and platinum (Pt) will be chosen as a typical metal. The following considerations also apply to other materials but the characterizing constants and parameters in the band diagrams will refer to these illustrative choice. A list of the symbols and the numerical parameters used can be found in appendix A. The three layers are separated by two heterojuctions whose physical description is particularly in-

teresting as a consequence of their completely different properties in solid-state physics.

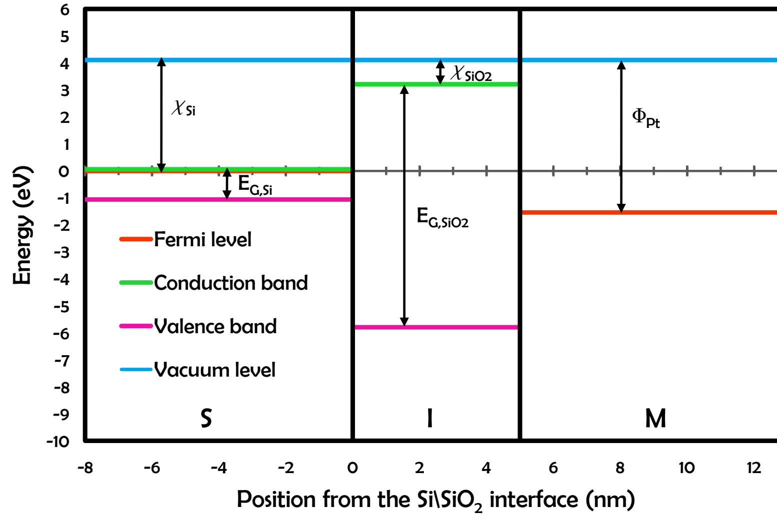

Figure 1.1: *The band structure of the MIS device is illustrated with numerical values from layers of silicon, silicon dioxide and platinum. When disconnected these materials are represented with a common vacuum level. The energy gaps* E_G*, the electron affinities* χ *and the work function in the metal* Φ *are shown.*

1.1.1 MIS structure at equilibrium

In order to define the band diagram of the MIS structure the characteristic parameters of each of the three layers must be considered. The electrical properties of the semiconductor are described by the distance between the valence and conduction band: for silicon this energy bandgap is $E_{G,Si} = 1.12eV$ at room temperature. Furthermore the electron affinity defines the distance between the bottom of the conduction band and the vacuum level which represents the energy the electrons need to gain in order to depart from the solid: for silicon $\chi_{Si} = 4.05eV$. The position of the Fermi level in the semiconductor strongly depends on the doping; for a highly n-doped silicon layer and a concentration of antimony donors of $N_D = 3 \times 10^{18} cm^{-3}$ the position of the Fermi level is very close to the conduction band. A simple approximated calculation assuming the concentration of electrons

in conductive band to be equal to the concentration of ionized donors is given by:

$$E_F - E_{V,Si} = \frac{E_{G,Si}}{2} + K_B T \ln \frac{N_D}{n_i} = 1.057eV \tag{1.1}$$

Where the position of the Fermi level E_F is referred to the top of the valence band $E_{V,Si}$ of the semiconductor: K_B is the Boltzmann constant, T the temperature in Kelvin and n_i the concentration of carriers of the intrinsic semiconductor. The

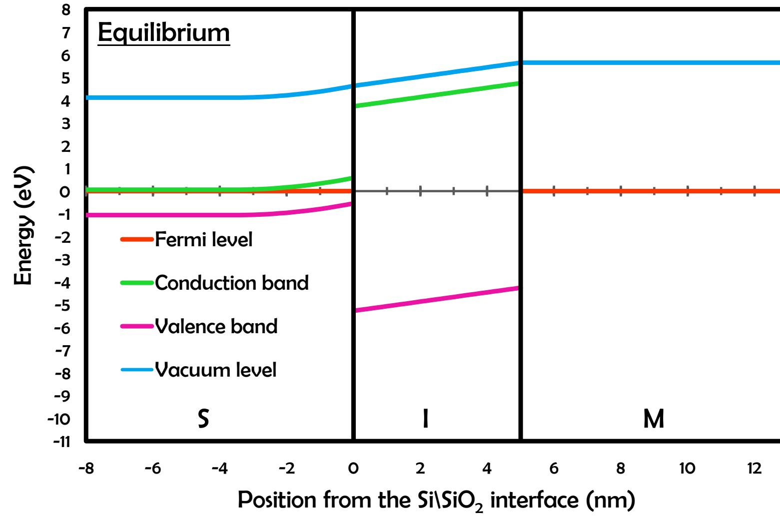

Figure 1.2: *At the equilibrium the Fermi energies of the semiconductor and of the metal are equal. This causes the bands of the insulator to be tilted in order to avoid discontinuities in the vacuum level. The band bending at the interface between the semiconductor and the insulator causes the* depletion *of a part of the semiconductor. At this interface the surface potential is negative.*

distance of the Fermi energy from the conduction band $E_{C,Si} - E_F = 0.063eV$ is low enough for being comparable with a thermal energy $K_B T = 0.026eV$ at $T = 300K$: the Fermi distribution ensures a good occupation probability of the conductive band and the low resistance of the semiconductor itself. The insulator is characterized by a higher energy bandgap: $E_{G,SiO_2} = 9eV$ and an electron affinity $\chi_{SiO_2} = 0.9eV$. The metal layer is represented by the position of the Fermi level with respect to the vacuum level: such distance, by definition, is the work function of the metal. In the case of platinum : $\phi_{Pt} = 5.65eV$ [18].

When the materials are considered separately, without being connected, their band energies are referred to the common vacuum level: the resulting band diagram is plotted in figure 1.1. Nonetheless if the three layers are connected and the MIS structure is formed these energy bands rearrange in order to establish the equilibrium. By definition at the equilibrium there is no net current and the Fermi level is the same in the whole heterostructure. Consequently the bands of the oxide exhibit a slope, which is admissible because of the absence of free carriers in the oxide. Figure 1.2 shows the band structure at the equilibrium.

1.1.2 Tunneling regimes

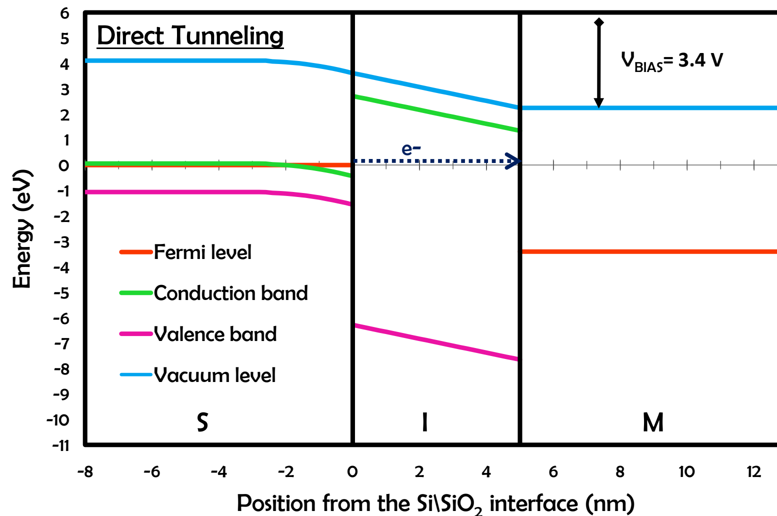

Figure 1.3: *In the direct tunneling regime a positive bias voltage is applied at the metal. The resulting potential barrier across the insulator is trapezoidal and the electrons tunnel from the semiconductor directly into the metal. Because of the negative slope of the insulator bands the surface potential is positive; the band bending is also shown in the resulting* accumulation *regime.*

When a gate bias voltage is applied across the MIS structure, the equilibrium is broken and currents may be originated as a consequence of the different Fermi levels in the semiconductor and in the metal. Despite the presence of the insulator and of the potential barrier it originates, quantum physics predicts a non-zero probability for the electrons to cross the oxide and generate a tunneling current.

Particularly interesting for the purposes of this project is the case of a positive voltage applied to the gate metal since it enhances the probability of an electron to tunnel from the semiconductor to the metal: if not differently specified the MIS structure will always be considered in this condition. Since the electrons do not lose energy while tunneling, they enter the metal with an energy which can be significantly higher than the local quasi-Fermi energy. For this reason they are defined as hot electrons. Depending on the intensity of the applied bias voltage different regimes can be found as the shape of the tunnel barrier changes. The shape of the barrier also depends on the energy of the tunneling electrons in the semiconductor, nevertheless the narrow distribution of their energies above the Fermi level at room temperature allows to establish a correlation between these regimes and the bias voltage. For low positive voltages the potential barrier extends over the full

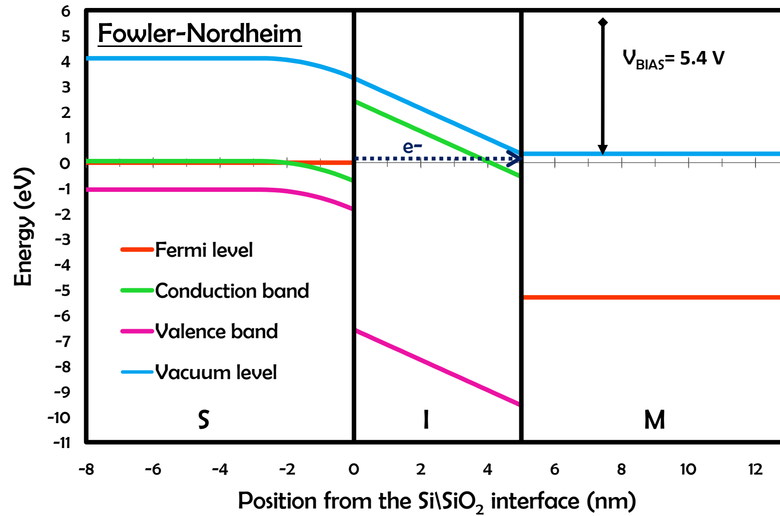

Figure 1.4: *When the positive applied bias voltage is even higher and it exceeds* $V_{FN} = \Phi_{Pt} - \chi_{SiO_2}$*, the shape of the potential barrier in the insulator is triangular and the electrons tunnel from the semiconductor into the conduction band of the oxide. This is referred to as Fowler-Nordheim tunneling. The surface potential is still positive but bigger in modulus and the* accumulation *is more evident.*

thickness of the oxide, the tunneling electrons are directly injected from the semiconductor into the metal and the transport is labeled as *direct tunneling*. When the applied voltage is higher and it exceeds a threshold voltage $V_{FN} = \Phi_{Pt} - \chi_{SiO_2}$ the en-

ergy bands are so tilted that the electrons tunnel into the conduction band of the insulator and no direct tunnel is possible anymore. In this case the electrons need to travel a certain distance in the oxide before reaching the metal and the effective tunneling distance is reduced. This regime is referred to as *Fowler-Nordheim tunneling* from the names of the first researchers who observed the phenomenon [19]. After the tunneling of the electrons in the Fowler-Nordheim regime the electrons may be scattered in the conduction band of the insulator losing a part of their energy: for the estimation of the current passing through the heterojunction these scattered electrons will be assumed to all reach the metal. If the bias voltage is even bigger the energy of the tunneling electrons will be higher than the vacuum level of the metal; this approximately happens when the bias voltage is bigger than the work function of the metal. If these electrons are not scattered they will propagate ballistically through the insulator and the metal for being emitted into vacuum. A plot of the energy bands in the two regimes is shown in figures 1.3 and 1.4.

1.1.3 Tunneling current

In order to estimate the current of electrons through the defined structure some assumptions need to be made. The disperison relation for the electrons in the semiconductor under the parabolic approximation is:

$$\mathrm{E} = \frac{\hbar^2 k^2}{2m_\mathrm{S}^\star} = \frac{\hbar^2 \left(k_x^2 + k_y^2 + k_z^2\right)}{2m_\mathrm{S}^\star} \tag{1.2}$$

where $m_\mathrm{S}^\star$ is the effective mass of the electron in the semiconductor and k the wavevector. If the x direction is chosen to be perpendicular to the junctions, the particular geometry of the system suggests to assume the wavevector k to be conserved along the y,z directions during the tunneling process; this parallel component of the wavevector is defined as $k_p = k_y\vec{e_y} + k_z\vec{e_z}$. The energy itself can be written as the sum of a parallel component and a perpendicular one: $\mathrm{E} = \mathrm{E}_x + \mathrm{E}_p$.

$$\mathrm{E}_x = \frac{\hbar^2 k_x^2}{2m_\mathrm{S}^\star}, \qquad \mathrm{E}_p = \frac{\hbar^2 k_p^2}{2m_\mathrm{S}^\star} \tag{1.3}$$

Under these assumptions the net current through the device is achieved as the difference of the current intensity in the two opposite directions [20].

$$\mathrm{J} = \mathrm{J}^+ - \mathrm{J}^- \tag{1.4}$$

where J is the total current density and J^+,J^- the components in the positive and negative direction of the x axis respectively: J^+ is taken to represent the current from the semiconductor to the metal in agreement with the previous figures. These currents will be calculated as an integral over the full range of values for the perpendicular wavevector k_x.

$$
\begin{aligned}
dJ^+ &= qT(k_x)\, v_x(k_x)\, g_S(k_x)\, f_S(E)\left(1 - f_M(E)\right) dk_x \\
dJ^- &= qT(k_x)\, v_x(k_x)\, g_M(k_x)\, f_M(E)\left(1 - f_S(E)\right) dk_x
\end{aligned} \tag{1.5}
$$

here q is the electron charge, T is the transmission coefficient which is assumed to be only a function of the perpendicular component k_x, v_x the perpendicular component of the velocity. g_S and g_M are the densities of k_x states in the semiconductor and in the metal respectively, while f_S,f_M are the correspondent Fermi distributions representing the occupancy of the two states. The density of states is calculated as:

$$
g(k_x) = \int_0^\infty \int_0^\infty g\left(k_x, k_y, k_z\right) dk_y dk_z \tag{1.6}
$$

and for simplicity $g\left(k_x, k_y, k_z\right)$ is considered to be the same for the conduction band of the semiconductor and for the metal, g_S=g_M=g, equal to the three-dimensional density of states in the momentum space for a cube of side length L. Periodic boundary conditions impose the quantization of k along its three components:

$$
k_i L = 2n\pi \quad \Rightarrow \quad k_i = \frac{2n\pi}{L} \quad \Rightarrow \quad \Delta k_i = \frac{2\pi}{L} \tag{1.7}
$$

where $i = x, y, z$ refers to the generic direction. The density of states becomes:

$$
g\left(k_x, k_y, k_z\right) = \frac{2}{\Delta k_x \Delta k_y \Delta k_z} \frac{1}{L^3} = \frac{1}{4\pi^3} \tag{1.8}
$$

The factor 2 includes the spin degeneracy. With this expression of the density of states and remembering that under the parabolic approximation $v_x = \frac{1}{\hbar}\frac{dE_x}{dk_x}$,equation 1.5 can be written as:

$$
\begin{aligned}
dJ^+ &= \frac{q}{4\pi^3\hbar} T(E_x)\, dE_x \int_0^\infty \int_0^\infty f_S(E)\left(1 - f_M(E)\right) dk_y dk_z \\
dJ^- &= \frac{q}{4\pi^3\hbar} T(E_x)\, dE_x \int_0^\infty \int_0^\infty f_M(E)\left(1 - f_S(E)\right) dk_y dk_z
\end{aligned} \tag{1.9}
$$

Integrating these expressions over the full range of energies E_x:

$$J^+ = \frac{4\pi m_S^\star q}{h^3}\int_{E_{min}}^{E_{max}} T(E_x)\,dE_x \int_0^\infty f_S(E)\left(1 - f_M(E)\right) dE_p$$
$$J^- = \frac{4\pi m_S^\star q}{h^3}\int_{E_{min}}^{E_{max}} T(E_x)\,dE_x \int_0^\infty f_M(E)\left(1 - f_S(E)\right) dE_p \tag{1.10}$$

which has been expressed as a function of the energy components. The integration along E_x is performed between two values E_{min} and E_{max}, which take into account the presence of forbidden bands: for instance within the energy gap of the semiconductor. According to equation 1.4 the net current is:

$$J = \frac{4\pi m_S^\star q}{h^3}\int_{E_{min}}^{E_{max}} T(E_x)\,dE_x \int_0^\infty \left(f_S(E) - f_M(E)\right) dE_p \tag{1.11}$$

This expression, known as the Tsu-Esaki formula, was originally proposed by Duke [21] and later employed by Tsu and Esaki [22] for modeling the tunneling current of similar devices; more often it may be found in the form:

$$J = \frac{4\pi m_S^\star q}{h^3}\int_{E_{min}}^{E_{max}} T(E_x)\,N(E_x)\,dE_x \tag{1.12}$$

where N is referred to as the supply function. In order to estimate the current density the transmission probability and the supply function can be modeled in different ways depending on the system or the chosen approximation [23]. With the previous choice, the supply function is:

$$N(E_x) = \int_0^\infty \left(f_S(E) - f_M(E)\right) dE_p \approx \int_0^\infty f_S(E)\,dE_p \tag{1.13}$$

The last approximation is understood when the range of integration energies is considered, the minimum energy is represented by the bottom of the conduction band in the insulator. If the bias voltage is considerably higher than the thermal energy $V_{BIAS} > K_b T$, which is always true in the cases of interest, the conduction band is much higher than the Fermi level of the metal, therefore the occupancy in the metal is negligible. Being $E_{F,S}$ the Fermi energy in the semiconductor the integral becomes:

$$N(E_x) = \int_0^\infty \frac{1}{1 + exp\left(\frac{E - E_{F,S}}{K_b T}\right)}\,dE_p = K_b T\, ln\left(1 + exp\left(-\frac{E_x - E_{F,S}}{K_b T}\right)\right) \tag{1.14}$$

1.1.4 Transmission probability

The probability for the electrons to tunnel across the potential barrier of the MIS structure can be derived from the time-independent Schröedinger equation [24]:

$$-\frac{\hbar^2}{2m_I^\star}\frac{d^2\Psi(x)}{dx^2} + q\mathrm{V}(x)\Psi(x) = \mathrm{E}\Psi(x) \tag{1.15}$$

where $\hbar$ is the reduced Planck's constant, $m_I^\star$ is the electron effective mass in the insulator, $\Psi(x)$ is the mono-dimensional wavefunction, $\mathrm{V}(x)$ is the potential and E is the total energy of the electron. Equation 1.15 is easily rewritten as:

$$\frac{d^2\Psi(x)}{dx^2} = \frac{2m_I^\star\left(q\mathrm{V}(x) - \mathrm{E}\right)}{\hbar^2}\Psi(x) \tag{1.16}$$

Nonetheless an approximation needs to be considered in order to find an analytic solution: a slow varying potential along the insulator is assumed. This means that the wavefunction at a certain position $x + dx$ can always be related to the wavefunction at the position x; this assumption is the so called Wentzel-Kramers-Brillouin (WKB) approximation [25]. More precisely the kinetic energy of the electron $\mathrm{E} - q\mathrm{V}(x)$ is considered constant in an interval dx: in this way the arbitrary shape of the potential barrier is approximated by subsequent rectangular barriers each of width dx. From the quantum theory of tunneling for a simple rectangular barrier:

$$\Psi(x + dx) = \Psi(x)\exp\left(-\int_x^{x+dx} k\,dx\right) \tag{1.17}$$

where k is the wave vector defined as $k = \frac{\sqrt{2m_I^\star(q\mathrm{V}(x)-\mathrm{E})}}{\hbar}$. The probability of tunneling from a position x to a position $x + dx$ is defined as:

$$\mathrm{T}_{x\to x+dx} = \frac{\Psi(x+dx)\Psi^*(x+dx)}{\Psi(x)\Psi^*(x)} = \exp\left(-2\int_x^{x+dx} k\,dx\right) \tag{1.18}$$

In order to calculate the total transmission probability the shape of the barrier needs to be evaluated; this depends both on the energy of the approaching electrons and on the applied bias voltage which tilts the barrier itself. Furthermore the band bending effect, not explicitly considered in this thesis, increases the effective height as a consequence of the appearing surface potential. In the direct tunneling regime the shape of the barrier is trapezoidal and the analytic expression of the

potential energy is given by:

$$qV(x) = \Phi_B - q\frac{V_I}{X_I}x \tag{1.19}$$

The origin of the spatial x axis is chosen at the semiconductor-insulator interface where the height of the potential energy barrier is labeled as Φ_B: V_I and X_I are the voltage drop and the thickness of the insulator respectively. The total transmission probability is given by the product of the single probabilities for an electron to tunnel across each rectangular barrier of width dx.

$$T = \exp\left(-2\int_0^{X_I}\frac{\sqrt{2m_I^\star\left(\Phi_B - q\frac{V_I}{X_I}x - E\right)}}{\hbar}dx\right) \tag{1.20}$$

The solution of the integral leads to the result:

$$T_{DT} = \exp\left(-\frac{B\,(\Phi_B - E)^{3/2}X_I}{V_I}\right)\exp\left(\frac{B\,(\Phi_B - E)^{3/2}X_I}{V_I}\left(1 - \frac{qV_I}{\Phi_B - E}\right)\right) \tag{1.21}$$

where a constant $B = \frac{4}{3}\frac{\sqrt{2m_I^\star}}{q\hbar}$ is defined.

In the case of Fowler-Nordheim tunneling the energy barrier is triangular; the calculation of the transmission probability is performed similarly but the effective thickness $X_{I,eff}$ of the barrier is lower. It is found by inserting equation 1.19 in the expression of the kinetic energy which is then set to zero: $E - qV(x) = 0$.

$$X_{I,eff} = -\frac{(\Phi_B - E)\,X_I}{qV_I} \tag{1.22}$$

Substituting this expression in the upper limit of integral 1.20 and solving, the total transmission probability in the case of triangular barrier reduces to:

$$T_{FN} = \exp\left(-\frac{B\,(\Phi_B - E)^{3/2}X_I}{V_I}\right) \tag{1.23}$$

Equations 1.21 and 1.23 clearly show the exponential dependence of the transmission probabilities on the thickness of the oxide: for practical applications such strong dependence imposes very thin oxide layers. The considerable effects of the applied voltage can also be highlighted. The voltage drop across the insulator V_I is directly related to the applied potential V_{BIAS}. Their difference simply equals a constant $V_I - V_{BIAS} = \left(\Phi_{Pt} - \chi_{Si}\right)$. This last relation also predicts the effect of the

metal work function on the transmission current: it shifts the applied voltage and consequently, the IV characteristics of the MIS structure.

As a consequence of the fact that the second exponential of equation 1.21 is usually much lower than 1, the tunneling probability in the case of Fowler-Nordheim tunneling is much higher than in the case of direct tunneling, for this reason the Fowler-Nordheim tunneling generates the highest currents; this is particularly true when the focus of interest is the emission current. Because of the necessity to exceed the metal work function the range of applied bias is usually higher than the threshold voltage V_{FN} and only the Fowler-Nordheim tunneling takes place.

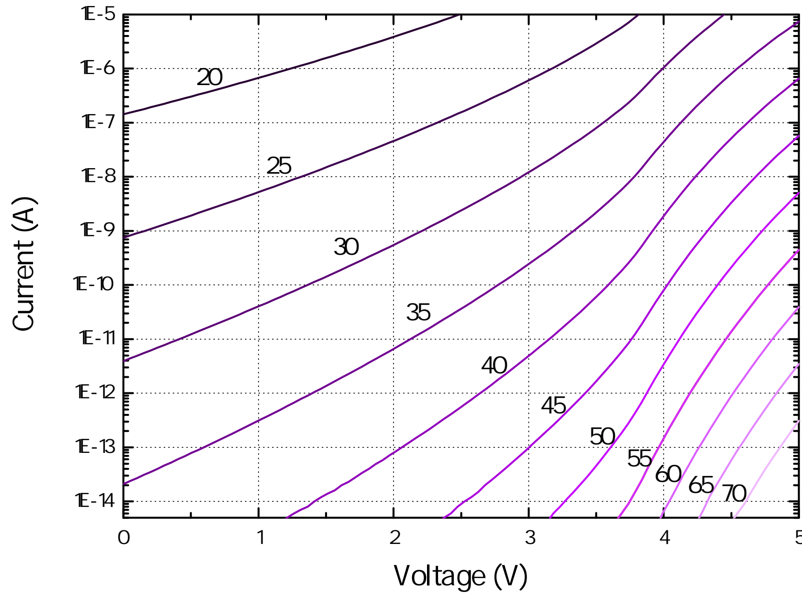

Figure 1.5: *Theoretical IV curves as calculated from the model for various thicknesses of the oxide. The thickness is shown on the left of each curve.*

Figure 1.5 shows the IV curves for various insulator thicknesses as predicted by the Tsu-Esaki formula of equation 1.12 after the expressions for the transmission function and for the supply function have been inserted. The following parameters have been chosen: $\Psi_{Au} = 4.8eV$, a donor concentration of $N_D = 10^{19} cm^{-3}$, an effective mass in the insulator $m_I^\star = 0.3 m_e$, where m_e is the electron mass, and an active area for the device of $A = 1 cm^2$. It has to be notice that the results are extremely dependent on many parameters, for instance both the transmission function and the supply function are exponential; for this reason, a quantitative agreement between

the model and the measured currents is rather difficult to be achieved. Some of the approximations are also rather strong, efforts have been spent trying to eliminate some of them: considering the correction due to the band bending of the MIS structure and the consequent surface potential, the correction related to the image charge potential in the insulator; finally, implementing a self-consistent method for describing the current from the quantized states originated by the potential well at the semiconductor-insulator interface.

1.1.5 Emission current

Once the electrons have tunneled across the insulator and have reached the insulator-metal interface, they need to pass through the metal layer in order also to reach the surface of the device and be emitted. Emission will only occur if the energy of the arriving electrons is higher than the work function. This is a measure of the energy which is needed to overcome the image charge potential. Just after the tunneling, the electron energy referred to the Fermi level of the metal is equal to the sum of the thermal energy they owned before the tunneling and of the energy due to the bias voltage $E - E_F = eV_{BIAS} + E_{th}$: avoiding the breakdown of the oxide this can usually go up to 6 Volts. Nonetheless various kinds of interactions may cause the hot electrons to lose energy in the metal and gradually be thermalized: excitations of phonons or excitons are considered to be the most efficient in this low energy range. The probability for the electrons to be scattered is strongly dependent on the metal thickness L and can be expressed as a function of the electron mean free path starting from the probability distribution $f_\lambda(x)$ of the distance travelled between two scattering events x.

$$f_\lambda(x) = \frac{1}{\lambda} \exp\left(-\frac{x}{\lambda}\right) \tag{1.24}$$

where λ is the electron mean free path in the metal. The probability not to be scattered over a distance L becomes:

$$P(L) = 1 - \int_0^L \frac{1}{\lambda} \exp\left(-\frac{x}{\lambda}\right) dx = \exp\left(-\frac{L}{\lambda}\right) \tag{1.25}$$

Such exponential decay reflects on a crucial importance of the electron mean free path in the metal; nonetheless this is strongly dependent on the electron energy. In the low energy range of interest it is difficult to find reproducible experimental results or accurate theoretical predictions. Since typical values vary from 10 to 60 Å equation 1.25 restricts the metal thickness to the low nanometer scale.

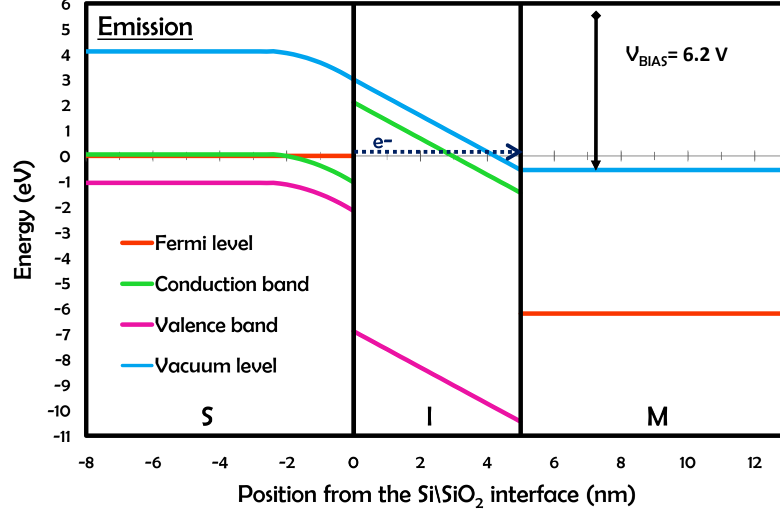

Figure 1.6: *A positive bias voltage is applied and it exceeds the work function of the metal* $V_{BIAS} > \Phi_{Pt}$. *After tunneling in the Fowler-Nordheim regime the energy of the electrons overcomes the vacuum level of the metal. If the electrons travel the all metal thickness without being scattered they will be emitted.*

In order to quantify the losses in the metal layer and compare the transmission current with emission, an emission efficiency is introduced:

$$\eta = \frac{I_E}{I_T + I_E} \tag{1.26}$$

where I_E and I_T are the emission and transmission currents: in this case the term transmission refers to the current passing through the device but not being emitted so that the total current is: $I = I_T + I_E$.

The efficiency measurements provide an approximated method for the estimation of the electron mean free path in the metal. The approximation consists in requiring that all the electrons being scattered in the metal, are not emitted. This is probably close to reality since the energy losses in a scattering event are expected to be very high [26]. Under this assumption the probability P(L) relates the emission current and the total current passing through the device:

$$\eta = \frac{I_E}{I_T + I_E} = K \exp\left(-\frac{L}{\lambda}\right) \tag{1.27}$$

where $K \leq 1$ is a proportionality constant taking into account other losses due to the scattering in the conduction band of the insulator or at the interface between the insulator and the metal: it can also take into account the presence of a second metal layer. If K is known the calculation of λ is straightforward and can be performed from one single measurement. In the other cases more measurements with various thicknesses are needed and the value of λ is estimated as the inverse slope of the linear fit on a logarithmic plot of the efficiency.

$$\ln \eta = \ln K - \frac{L}{\lambda} \tag{1.28}$$

1.2 Design of hot electron emitters

In order to successfully apply the theoretical principles of MIS structures a series of conditions must be fulfilled while designing real devices: the necessity of very thin tunnel barriers and very thin metal gate layers has already been mentioned. Other requirements are induced by the final purposes of this research. The need of reasonably cheap, easily reproducible devices leads to the choice of semiconductor technologies. This allowed the production of hot electron emitters on silicon wafers. A scheme of a wafer, containing 20 devices, is shown in figure 1.7.

On the other hand the idea of employing MIS devices in femtochemistry forced the choice of an ultra-large active area; this is required in order to be able to detect reactions on the surface since the amount of reactants is proportional to this area. Furthermore this choice enhances the emitted current which is limited by the rather low current density of the devices: to date the highest measured value is $J = 5\mu A cm^{-2}$. Nonetheless the realization of a high quality thin oxide, over such a large area, is particularly challenging. Consequently the presence of defects is quite common and affects the durability of the devices. It also limits the bias voltages which can be applied before causing the breakdown of the oxide. A square active area of 1 cm^2 was considered to be a good compromise; the term "ultra-large" is justified by the typical size of similar semiconductor devices: characteristic areas are thousands of times smaller. The lateral dimensions of a full device, taking into account the regions dedicated to the electrical contacts and the external thick oxide frame are 16×14 mm.

A description of the single layers constituting a hot electron emitter follows.

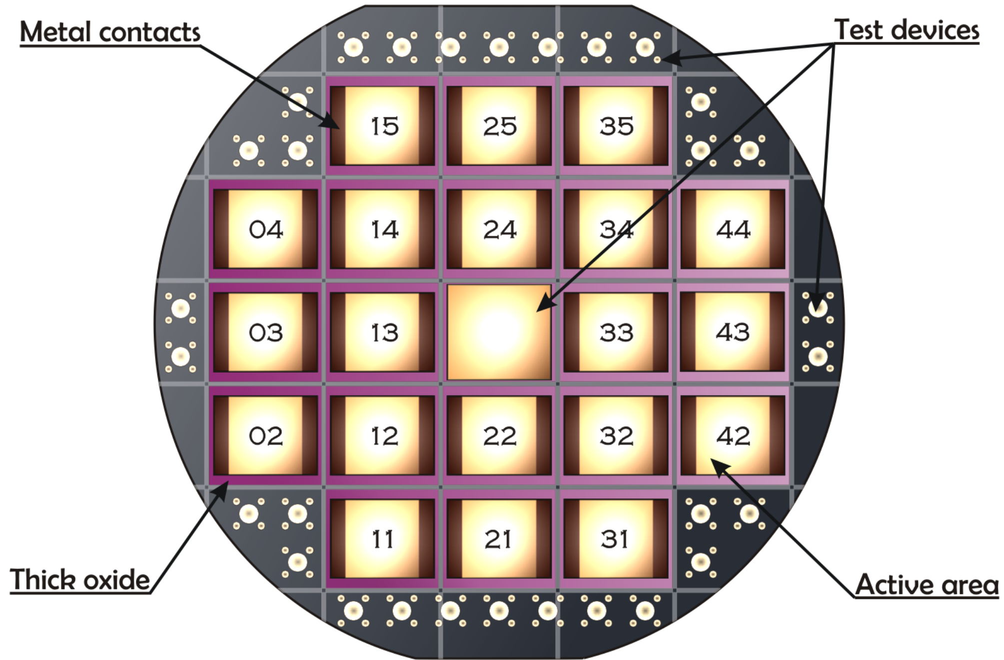

Figure 1.7: *A typical wafer with some of its features. Twenty devices of active area* A = 1cm^2 *are surrounded by smaller devices sometimes used for characterization.*

1.2.1 Substrate

The totality of the hot electron emitters described in this thesis possesses a silicon highly n-doped substrate. Since its thickness is 525 µm, it constitutes the main volume of the devices and is responsible for their physical rigidity. Further details about the choice of silicon wafers are found in section 1.3. The high quality of these standard wafers together with the high concentration of donors ensures the good conductivity of the substrate and a negligible voltage drop across the silicon itself. Furthermore the considerably high concentration of carriers enhances the tunneling current.

1.2.2 Thin oxide

The thin oxide layer represents the central part of the MIS structure and the tunnel barrier for the electrons moving from the semiconductor to the metal gate. Because of this central role the properties of the thin oxide crucially affect the electrical properties of the all device, governing both their current density and their durability. Therefore the high quality of the oxide is essential, especially when considering its ultra-large 1 cm^2 area which multiplies the probability of defects. Par-

ticular attention was given to the definition of the fabrication technique: the final choice was directed toward the thermal grown in an ultra-clean furnace 1.16.

In section 1.1 the exponential dependence of the tunneling probability on the oxide thickness was derived: equations 1.21 and 1.23. Such expressions lead to the necessity of tunnel barriers in the very low nanometer range. Nevertheless the requirement of low breakdown probability imposes a lower limit to the thickness for a given applied bias voltage: in fact the thin oxide is not able to sustain excessively high electric field. On the other hand particular applications may require electrons with certain fixed energies, hence a particular applied voltage. According to these considerations a compromise needs to be found. Thicknesses in the range between 3 and 7 nanometers were previously tested [14]: most of the devices fabricated and studied during this project were fabricated with a target thin oxide thickness of 5.5 nm which was found to exhibit good results.

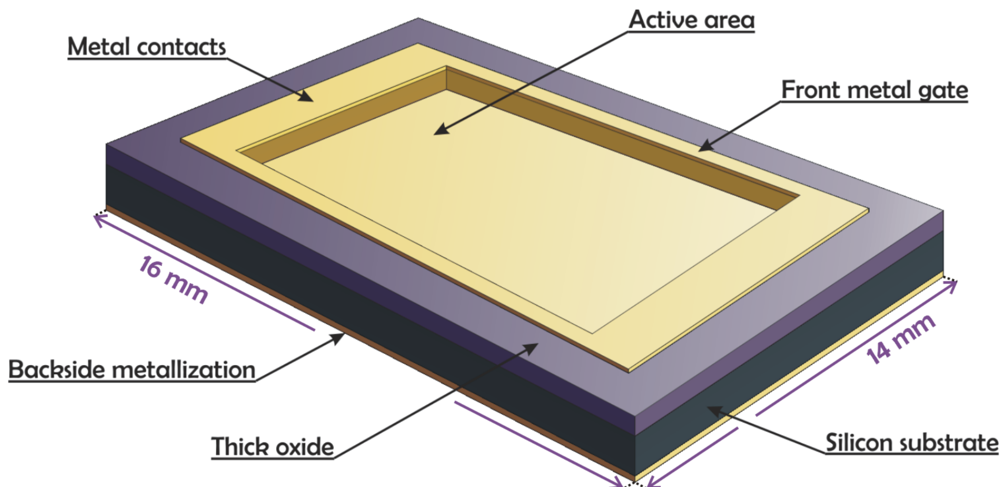

Figure 1.8: *Sketch of a single device with its components.*

1.2.3 Metal gate

The metal gate serves several functions; because of its multiple roles this is also the most variable part of the MIS devices since it needs to fulfill different requirements depending on the application. During the fabrication through Physical Vapor Deposition (PVD) the need of flexibility is satisfied by the evaporator itself which operates on each single wafer separately and allows an easy and fast deposition of various metals with various thicknesses.

The first purpose of the metal gate is to establish electrical contact between the measuring instruments and the front of the device. In this sense it also permits to

apply a bias voltage across the tunnel barrier. Both these functions would lead to the choice of rather thick metal layers: the electrical contacts would be simplified and the voltage drop on the active area minimized. Thick metal layers constituted of 10 nm of titanium (Ti) or cromium (Cr) as wetting layers and 100 nm of gold (Au) are often deposited for a general electrical characterization.

Nonetheless both the application in surface chemistry and in electron emission requires the electrons not to be scattered inside the metal and to reach the surface. This necessity obliges to scale down the metal thickness according to equation 1.25. For these applications a reasonable value is 5 up to 20 nm: still usually providing good electrical contact and negligible voltage drops.

The choice of the metal is also taken in order to meet specific needs. Clean weakly reacting surfaces are necessary for surface chemistry in order to detect the effects of hot electrons in enhancing the reactivity: hence the selection of noble metals as gold (Au) or platinum (Pt). A strong oxidation of the surface is believed to play a negative role on the emission as well. This is probably one of the reasons why the best emitters produced so far possess gold metal gates although their emission at a given applied voltage is limited by the high work function of gold: $W_{Au} = 5.1 - 5.47 eV$ [18]. Another reason is the rather high value of the inelastic mean free path of low energy electrons in gold: $\lambda_{Au} \approx 50\,Å$ [27, 28]. During the development of this project, the possibility of enhancing the emission current by choosing other materials with high inelastic mean free path and lower work functions suggested the investigation of new materials.

1.2.4 Thick oxide

The main function of the thick oxide layer is to allow both mechanical and electrical contacts to the device. These contacts are typically achieved by using a couple of metallic clips pressing onto the metal surface on the front of the devices. Usually, if the metal layer is thicker than 20 nm, good contacts can be obtained easily, even on the active area of the device where the thick oxide is absent: the mechanical stress induced by the clips does not damage the device. Nonetheless thin metal layers are required in order to exhibit a significant emission current: thicknesses lower than 10 nm are often chosen. In these conditions mechanical stresses can seriously affect the properties of the emitters and in particular the quality of the tunnel barrier. The thick oxide, with a typical thickness of 0.75 μm, prevents the clips from pressing directly onto the active area. The importance of having good electrical contacts on both the right and left side of the active area is understood

when considering the voltage drop across such thin metal layers.

1.2.5 Backside metal

In order to ensure good electrical contact between the n-doped silicon substrate and the measuring instruments a thick metallic layer is deposited on the backside of the wafers. A first 10 nm wetting layer of chromium (Cr) or titanium (Ti) enables a thicker 100 nm gold (Au) layer to stick to the back of the devices.

1.3 Fabrication sequence

The purpose of this section is to provide a description of the processes involved in the fabrication of the MIS devices and their realization in the cleanroom facilities at Danchip. Originally, the sequence of these processes was designed by Professor Ole Hansen: further improvements were later found by PhD students Lasse Thomsen, Gunver Nielsen and Robert Jensen. They were also directly responsible for the production of some MIS devices, other devices have been produced with their collaboration and supervision. The steps reported here refer to the final and to date the most reliable sequence.

1. **Silicon wafer.** Highly doped 4 inch silicon (Si) wafers constitute the semiconductor 525 μm thick substrate of MIS devices. One side polished wafers, with (100) crystal plane exposed, have been chosen. They are n-doped with antimony (Sb): a concentration of donors of $N_D = 3 \times 10^{18} cm^{-3}$ results in a sheet resistance $\leq 0.025 \Omega cm$ as reported by the manufacturer (Okmetic, Finland).

2. **Thick oxide formation.** A 750 nm thick oxide layer is growth by wet thermal oxidation in a phosphor drive-in furnace at 1000 °C for 180 min under a pressure of 1 bar H_2O. Wafers are then annealed in nitrogen (N_2) for 20 min.

3. **Positive masking with resist.** The wafers are covered by a 1.5 μm sacrificial AZ resist, prebaked at 90 °C for 90 s and exposed to UV. A positive mask connected by hard contact defines the active areas of the emitters which will be back etched. Development for 60 s in Sodium hydroxide (NaOH), rinsing in de-ionized (DI) water and hard baking at 120 °C for 60 s follow.

4. **Back etching of the oxide.** The wafers are back etched in 5 % buffered hydrofluoric acid (bHF) for 9 min. The time is calculated considering an approximate etching rate of 80 $nm min^{-1}$. Since it is essential to completely remove this

low quality oxide from the active area, after this time the wafers are visually inspected in order to check their hydrophobicity: silicon dioxide (SiO_2) is hydrophilic while clean silicon (Si) is hydrophobic. The wafers are rinsed in DI water.

5. Photo resist strip. In order to remove the residual resist the wafers dipped in an acetone bath for 15 min and exposed to ultrasounds. Acetone dissolves the resist. The wafers are rinsed in DI water.

6. Thin tunnel oxide formation. The thin oxide growth is of critical importance for the properties of the emitters. For this reason standard RCA cleaning is performed immediately before the deposition minimizing the natural oxide formation on the silicon surface. The oxide is grown in an ultra-clean furnace at 800 °C for 40 min under a pressure of 1 bar oxygen (O_2). The typical target thickness is 50 nm, but it can be modified by tuning the exposition time in the furnace. The wafers are post-annealed in nitrogen (N_2) for 20 min.

7. Backside metallization. The naturally formed silicon dioxide on the backside of the wafers is stripped away with 5 % hydrofluoric acid (HF). In order to ensure good electrical contact to the silicon substrate, a titanium (Ti), or chromium (Cr), wetting layer and a gold (Au) layer are deposited by Physcal Vapor Deposition (PVD). Typical thicknesses are 10 nm for the wetting layer and 100 nm for the gold one.

8. Deposition of the front metal gate. Physical Vapor Deposition (PVD) is used for depositing the metal layers on the front of the wafers. An aluminum (Al) shadow mask avoids electrical contact between different devices. The metals and the thicknesses involved in this last step of the fabrication vary according to the applications of the devices. A 10 nm thick titanium (Ti) wetting layer and a 100 nm thick gold (Au) is normally used for electrical characterization, on the other hand emitters require much thinner metal layers. A Quartz Crystal Microbalance (QCM) measures the amount of evaporated metals and calculates their deposition rate: this usually varies between 1 Ås^{-1} and 10 Ås^{-1}. The thickness of the metal layers is set by regulating the deposition time. This method and possible errors in the calibration of the microbalance may lead to a rather high uncertainty on the effective deposited thicknesses. In some cases as previously studied by PhD student Lasse Thomsen, these errors may be of the order of the 20 %.

9. Optional wafer dicing. When the fabrication process is finished it may be necessary to separate the single devices. This separation is performed by scribing the wafers with a diamond tip along the crystal directions of silicon. A small stress is then manually placed on the wafer in order to break it along these directions.

Typically these fabrication processes are carried out on a full batch of 25 wafers: in particular both the thick and the thin oxides are grown in furnaces containing all the 25 wafers at the same time. This usually allows them to exhibit similar electrical properties, nevertheless the thickness of the oxides is affected by uncertainty. Because of this reason an ellipsometer is normally used for measuring the oxide thickness. Since a deviation of 4 % is rather common, if necessary they are adjusted by slow etching the oxide in dilute hydrofluoric acid. The metal deposition is carried out on each single wafer separately.

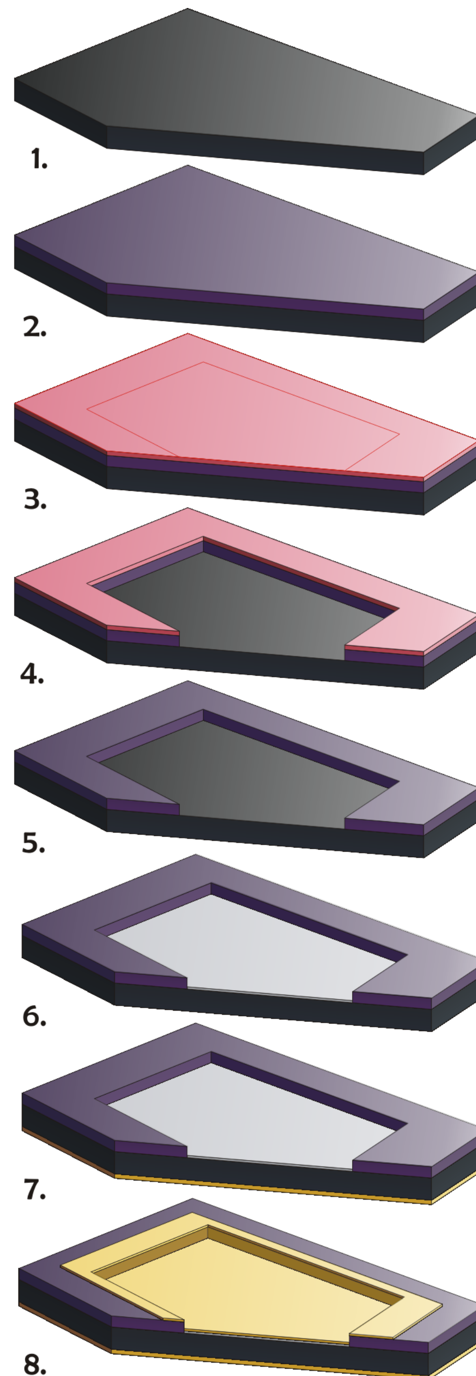

Figure 1.9: *The various steps of the fabrication sequence are shown. 1) A clean silicon wafer is chosen. 2) A thick oxide layer is grown. 3) A resist layer defines a positive mask. 4) The thick oxide is etched away from the active area. 5) The resist is stripped away. 6) The high quality thin oxide is grown. 7) Titanium and gold are deposited on the backside. 8) The front metal gate is deposited through Physical Vapor Deposition (PVD).*

Chapter 2

Electrical characterization

In the previous chapter a theoretical treatment of the MIS devices was provided; shortly the first experimental results will be presented. In particular the fundamental methods for the electrical characterization of hot electron emitters will be introduced: namely the current-voltage characteristic (IV curves) and the emission-voltage measurements. A description of the experimental setup is given together with some considerations about the problems involved in such measurements. A comparison between the theory and the experimental data will demonstrate the suitability of the model: at the same time some of its limits will be underlined.

2.1 Introduction to the measurement techniques

The current-voltage characteristic represents the principal and easiest tool for the determination of the quality of the devices. It allows to check both the tunneling nature of the current or the presence of undesired leakage currents. It also provides the first information about the durability of the devices since many different causes may lead to the oxide breakdown for very low voltages. In order to take IV measurements various consecutive bias voltages are applied as a step function, the current values are acquired at a particular time after each step. The importance of this time delay is due to the high capacitance of the device and to the resulting charging-discharging currents. Typically time delays of the order of 500 ms were chosen: usually this time is also sufficient to avoid the transient currents due to the internal capacitance of the instruments. In general the necessity of high quality measurements always corresponds to the necessity of slow measurements but this is in contrast with the progressive deterioration of the devices and the time evolution of their electrical behaviour when a bias voltage is applied: this can often be

fast as it will be investigated in chapter 6. A compromise between the accuracy of the measurements and the need of preserving the devices must be found.

Efforts have been made in order to always couple IV curves with emission measurements. At each voltage step, after the measurement of the transmission current, the emission is measured. The resulting curve, emission as a function of the bias voltage, can easily be compared to the current-voltage characteristic and permits the immediate determination of the previously defined emission efficiency 1.26, which is also a function of the voltage. In relation to the purposes of this thesis the relevance of the emission curves is natural and obvious.

Although emission is measured both in vacuum conditions and in air or gas pressure, this chapter will mainly focus on experiments in ultra high vacuum, unless differently stated. The reason of this choice is due to the particular transport of the electrons in air and to the resulting transmission function. The possibility of measuring in air was important to facilitate the characterization of the devices since the vacuum techniques require much longer times: it was also advantageous for a qualitative comparison of different MIS devices and different materials. Furthermore, despite the unknown form of this transmission function describing the transport under gas pressure, some of its features can be successfully predicted. Chapter 3 and 4 will specifically consider this problem.

2.2 Experimental setup

In order to perform the electrical characterization of hot electron emitters various configurations and instruments have been adopted. Figure 2.1 shows the most common connections: two different ammeters separately measure the transmission current and the emission. The total current passing through the device can be directly achieved as the sum of the two, nonetheless the low efficiencies of hot electron emitters cause the total current to be almost equal to the transmission one: for most of the practical matters they can be exchanged leading to negligible errors. In the circuit one voltage supply applies a variable bias voltage across the device while the second one applies a positive voltage V_C to a metal collector. The purpose of this metal plate is to work as an anode generating an electric field between the surface of the device, where the electrons are emitted and the collector itself. The electrons are accelerated towards the anode and enter the metal plate allowing the measurement of the emission current.

In order to measure IV characteristic and emission curves the positive voltage

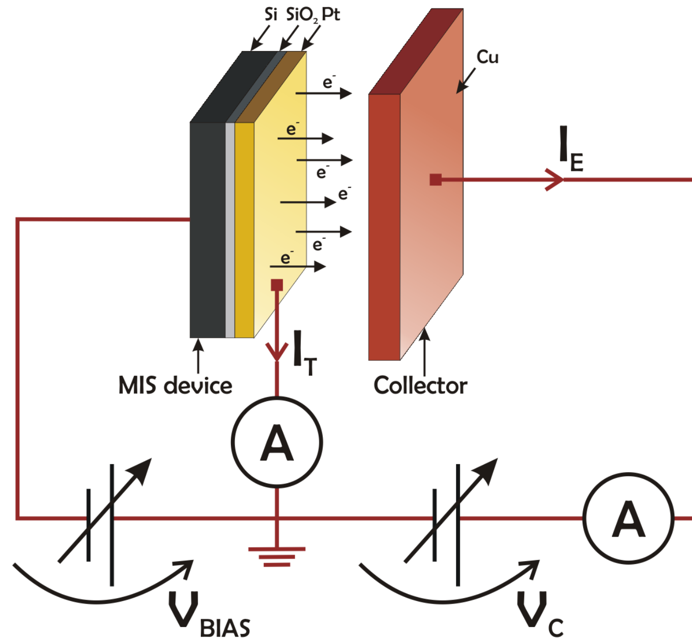

Figure 2.1: *Scheme of the most common connections for measuring both IV and emission curves. The electrical instruments are connected to the system in three points: the back of the device, the front of the device and the collector. A voltage supply is responsible of the bias voltage* V_{BIAS} *across the MIS structure while a second voltage supply applies a positive voltage* V_C *to the anode. At each voltage step after a certain time delay two ammeters measure the transmission and the emission currents: respectively* I_T *and* I_E.

applied to the collector is kept constant and usually equal to $V_C = 20V$: other kind of measurements needed a variable collector voltage. The role of the collector voltage and of the electric field it generates, which is not crucial under vacuum conditions when the electrons propagate ballistically between the two metal surfaces, is much more relevant under gas pressures and will be better discussed in the following chapters. A similar argument concerns the geometry of the collector with respect to the emitter: typically the metal plate is a few millimeters larger than the active area of the device and completely covers it so that the number of emitted electrons escaping the collector is minimized. For the same reason the distance between the two is usually set to $d = 0.5mm$. In ultra high vacuum (UHV) these conditions certainly enable the measurement of a current which is very close to the real total emitted current. Under gas pressures where the electrons are scattered by molecules all these parameters must be carefully checked and more rigid rules must be followed.

The contacts between the cables and the various components of the device are

also important in order to get reliable measurements: for instance in order to limit the voltage drop on the thin metal gate. Various holders were designed with the common objective to simplify the connections and protect the devices from mechanical stresses: every time further particular requirements had to be met. A more accurate description of the employed holders is postponed to appendix C. A significant attention was given to the reduction of the electrical noise. Depending on the measurement and on the current of interest shielding and guarding procedures were applied. In the case of measurements under UHV the walls of the chamber represent already a good shield which, if connected properly, may reduce the noise due to capacitive and magnetic coupling. A copper box designed for the same purpose contains the holder, the device and the collector when measuring in air. Most of the cables used are also shielded.

2.3 Current-voltage characteristics

The first experimental data presented in this thesis are targeted at giving a general description of real IV curves. Most of the measurements of this project were taken on devices belonging to batch 26 according to the internal classification of samples; the expected oxide thickness for this batch is 55 Å which is in agreement with most of the ellipsometry measurements. Various metal layers have been deposited on the wafers but they will always be mentioned in the following descriptions together with their thickness expressed in Å.

A double metal layer of titanium (Ti) and gold (Au) represents the most common combination and deserves a note. So far the best emitters produced have been made with gold, both considering the intensity of the emission currents and the durability of the devices. The titanium wetting layer is essential in order to establish good contacts: the gold alone is too noble to stably stick to the silicon dioxide. On the other hand the presence of two layers may introduce a further degree of freedom in the electrical behaviour of the MIS devices. Its effects will play a particular role on the efficiency of the devices, a topic that will be treated later in chapter 5.

2.3.1 Reproducibility of IV curves

The IV curves of figure 2.2 refer to batch 26 and in particular to different devices of the same wafer number 6: metal layers are titanium and gold with thicknesses 7 and 100 Å respectively. The exponential dependence of the current on the ap-

plied bias voltage is clearly seen: in every IV curve the current ranges between the nano-amper regime to the milli-amper one which increases the difficulties of noise reduction on the all range. Being more interested in the high voltage regime where emission occurs the high quality of the curves in the lower regime is not always considered as crucial. In principle the structure of devices belonging to the same wafer

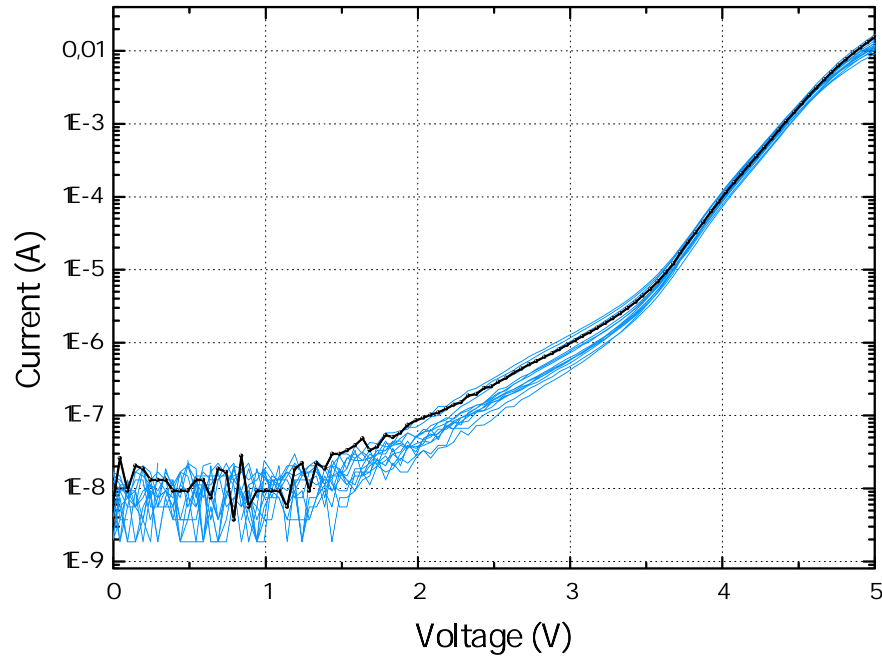

Figure 2.2: *Various IV curves from different devices of the same wafer (Wafer 6 from batch 26) are shown. The metal layers are titanium and gold. Despite the noise at low voltages the reproducibility of the curves is evident. One of the curves has been plotted with darker colors in order to better identify the shape. The increasing slope of the curve at* $V_{BIAS} \approx 3.5V$ *on a logarithmic plot is a signal of the Fowler-Nordheim tunneling becoming the dominant transport mechanism.*

is exactly the same: this is not true if different wafers of the same batch are considered since the deposited metal layers are different. Different metals affect not only the emission but the tunneling itself, thus also the IV curves. Despite the variability due the unavoidable uncertainty of the fabrication processes the plotted curves are a proof of the reproducibility of the current-voltage characteristics of hot electron emitters. Differences may be especially noticed in the low voltage range where in general the influence of direct tunneling is combined with complementary effects like leakage currents and noise. Normally, these secondary effects do not compro-

mise the curves in the higher voltage range where the Fowler-Nordheim tunneling predominates and the currents are sufficiently high to mask the other undesired currents. Possible differences in this range are more probably due to the deviance of the thickness of the oxide layers which was especially investigated by the PhD student Lasse Thomsen in his PhD thesis. Measures at the ellipsometer of the average thickness of various devices on the same wafer gave an uncertainty of 4 Å. Both the average thickness of the oxide and its roughness over the all active area produce noticeable deviations of the curves. The dependence of the tunneling current on the thickness of the insulator is in fact exponential as predicted in section 1.1.4.

2.3.2 Effects of the work function

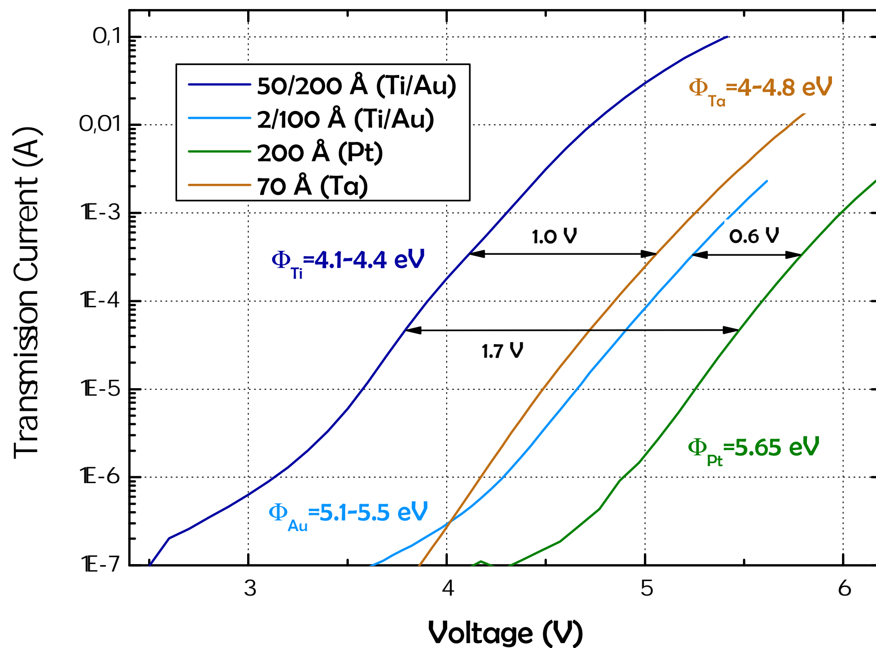

Figure 2.3: *Four IV curves from different devices of batch 26 are plotted. The metal combinations are illustrated in the legend with the thicknesses in angstroms. In the high current range where the Fowler Nordheim tunneling dominates the voltage shift due to the different work functions is evident and in agreement with the predictions of 1.1. The amplitude of this shift is also in rather good agreement with the values of the work functions.*

In section 1.1.4 the tunneling probability through the oxide was found to be strongly dependent on three quantities: some effects of the exponential depen-

dence with respect to the bias voltage and to the inverse of the insulator thickness were shown in the previous paragraph. The influence of the metal work function was also predicted: a voltage shift of the probability and of the resulting IV curves is expected. Figure 2.3 illustrates this behaviour. In order for the IV curves to be comparable the oxide thicknesses must be the same, that is why the chosen wafers all belong to batch 26; this requirement forbids the comparison with other materials deposited on wafers from other batches.

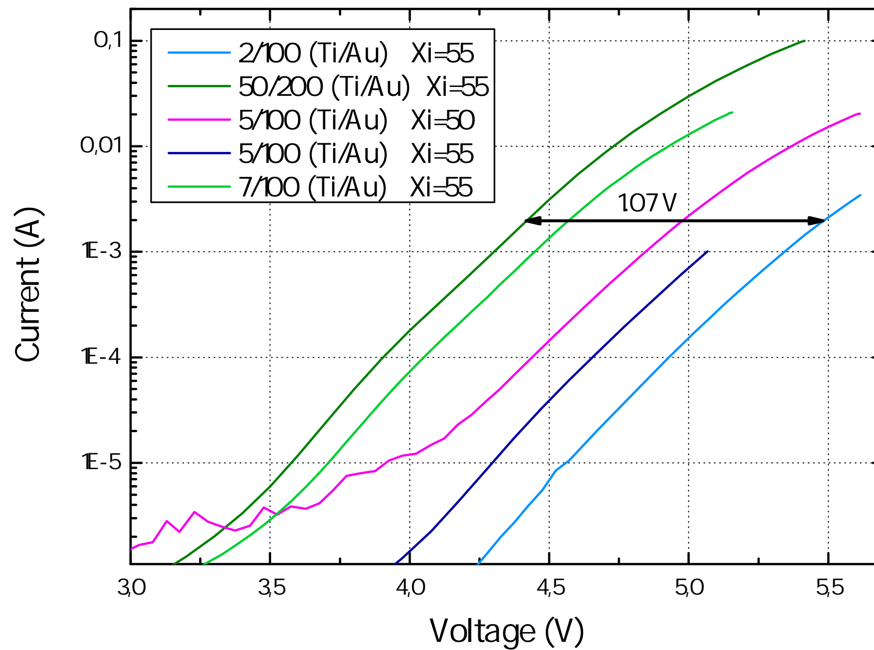

Figure 2.4: *Various IV curves from devices with titanium and gold as metals are shown. The pink curve refers to a device from batch 21 while all the others refer to batch 26. All the thicknesses of metals and oxides are reported in the legend: angstrom is the unit of measure. The thicker the titanium wetting layer the higher the work function and the lower the current. It is believed that this trend is related to the progressive relaxation of the titanium work function toward the one of gold when the thickness of titanium becomes very low.*

The displacement of the IV characteristics in the Fowler-Nordheim regime is clearly noticed and in discrete agreement with the values of the work functions known from literature. It must be noticed that the value of the work function to be considered is the one at the insulator-metal interface, namely the distance between the Fermi level of the metal and the vacuum level in this region. In the case

of a double metal layer, as for titanium and gold, the value of such work function depends on the thickness of the wetting layer. For a thickness of 50 Å this is expected to be almost equal to the normal work function of titanium. When it is much thinner, the effective work function is an intermediate value between Φ_{Ti} and Φ_{Au} since discontinuities of the vacuum level are not allowed and a minimum relaxation distance is expected. A 2 Å wetting layer results in a work function that is probably similar to the one of gold. Furthermore such thin wetting layer is probably not uniform over the all interface and a direct contact between gold and silicon dioxide can be present in various parts of the active area.

Further evidence for such relaxation of the work function is achieved considering other thicknesses of the titanium wetting layers, such analysis is performed in figure 2.4. Although the relative uncertainty on the deposited thicknesses of metals is rather high for such thin titanium layers, as already described in section 1.3, a general trend is certainly observed. It also seems that the main variation in the effective work function occurs between 5 and 7 Å which is consequently expected to be the scale of this relaxation length.

2.3.3 Fowler plot

The features of the current-voltage characteristics investigated so far are all proof of the tunneling nature of the current. In order to compare the shape of the measured IV curves with the model of chapter 1 more accurately, some of the curves already presented in this section have been inserted in a Fowler plot.

Various papers [29, 30] document the possibility of approximating the current density in the Fowler-Nordheim regime with the expression:

$$J_{FN} = A\epsilon_I^2 \exp -\frac{B}{\epsilon_I} \tag{2.1}$$

where ϵ_I labels the electric field in the insulator and is equal to: $\epsilon_I = \frac{V_I}{X_I}$. The two constants A and B are given by:

$$A = \frac{q^3}{16\pi^2\hbar}\frac{m_S^\star}{\Phi_B m_I^\star}, \qquad B = \frac{4}{3}\frac{\sqrt{2m_I^\star}}{q\hbar}\Phi_B^{3/2} \tag{2.2}$$

In a Fowler plot the current density is divided by the square of the potential difference across the insulator and the natural logarithm of this quantity is plotted as a function of the reciprocal of the voltage $1/V_I$. In formula, from equation 2.1

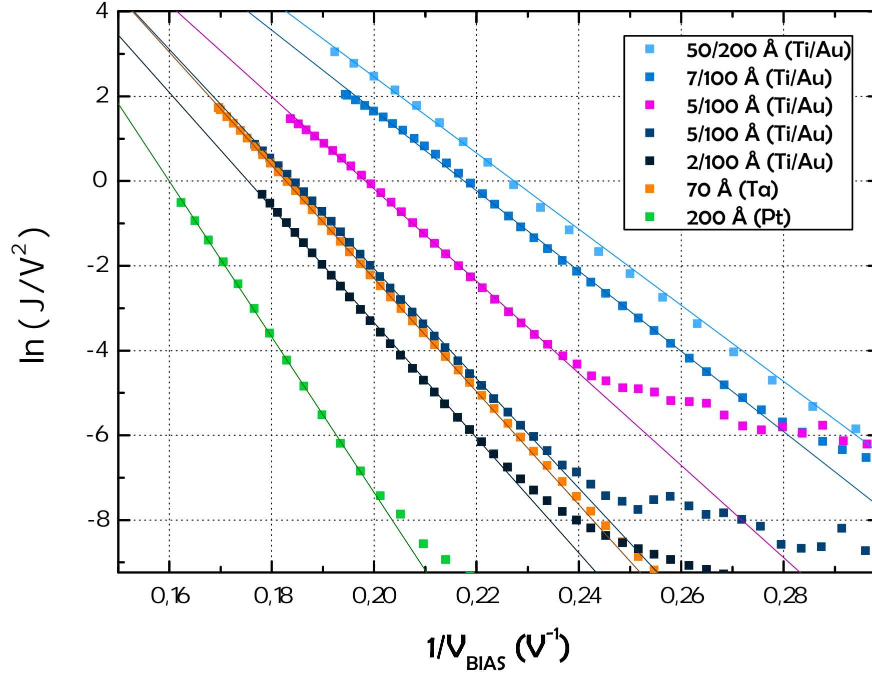

Figure 2.5: *The IV characteristics from figure 2.3 and 2.4 are inserted in a Fowler plot. The metal layers are labeled in the legend with their thicknesses in angstrom. The experimental data have been fitted with lines in order to show the tunneling nature of the current. Such linear behaviour supports the Fowler-Nordheim model of tunneling for voltages above* V_{FN}*, or on the x-axis for values below* V_{FN}^{-1}*. Reasonable values of the work functions,* $\Phi_{Au} = 5.1$, $\Phi_{Ti} = 4.33$, $\Phi_{Ta} = 4.8$, $\Phi_{Pt} = 5.65$ *produce the following inverse voltages:* $V_{FN,Au}^{-1} = 0.24$, $V_{FN,Ti}^{-1} = 0.29$, $V_{FN,Ta}^{-1} = 0.26$ *and* $V_{FN,Pt}^{-1} = 0.21$*. Effectively, the linear trends approximately appear below these values.*

after defining $A' = \frac{A}{X_I^2}$ and $B' = B \cdot X$:

$$\ln \frac{J_{FN}}{V_I^2} = \ln A' - \frac{B'}{V_I} \tag{2.3}$$

which predicts that, if the Fowler-Nordheim tunneling is responsible for the IV curves, they should appear as straight lines of slope $-B'$ and offset $\ln A'$. In figure 2.5 a Fowler plot generates rather linear relationships above the typical threshold voltages of the Fowler-Nordheim regime: $V_{FN} = \Phi_{Pt} - \chi_{SiO_2}$. This is a strong evidence of the Fowler-Nordheim tunneling being the dominant transmission mechanism

in the hot electron emitters. The expected numerical values of the two constants A' and B' and the values derived from the linear fits in the figure are in agreement within the 20 %: beyond the uncertainty on the values of both the effective masses in the insulator and in the semiconductor, this deviance can be due to the different effective potential barriers when the surface potential is considered.

2.4 Emission curves

The development of this section will proceed parallel with the previous one, first a general description of emission curves will be given, then some quantitative aspects will be considered. In particular an analysis of the efficiencies will be performed since general objective of this project is to enhance the emission of these devices. When measured together as described before 2.2 iv curves and emission curves from a device of batch 26 and platinum (Pt) as gate metal appear as in figure 2.6. The first consideration concerns the large difference on the scale of currents. With the typical bias voltages needed for emission the transmission currents are usually in the milliampere regime while the emission, in this case, barely reaches one nano-ampere. The efficiency, typically measured at standard fixed voltages, is equal to $\eta = 5 \times 10^{-8}$ at $V_{BIAS} = 6V$ and it is also extremely low. Although this device does not produce a particularly high emission current only devices from a few wafers could reach an emission in the microampere regime, and only with both titanium and gold layers. A better description of the influence of metal layers on the emission current is contained in chapter 5 where some strategies for improving the efficiency of hot electron emitters are also presented.

In figure 2.6 the emission current appears above $V_{BIAS} = 5.5V$, this is in rather good agreement with the known values of platinum work function: $\Phi_{Pt} = 5.65eV$. In general emission curves provide a good estimation of the work function of the emitting metal. Nonetheless it must be underlined that contaminants may seriously affect the work function of not perfectly clean surfaces, furthermore, the level of the background noise masks part of the emission. On the other hand the theory of MIS devices describes the broadening of the tunneling electron energy: the Fermi distribution in the conduction band of the semiconductor predicts the presence of electrons a few K_bT higher in energy than the applied bias. These electrons which also have a higher tunneling probability may shift the apparent work function of the metal. The combination of all these effects may lead to errors in the estimation: typically, this argument applies for gold (Au) whose work function

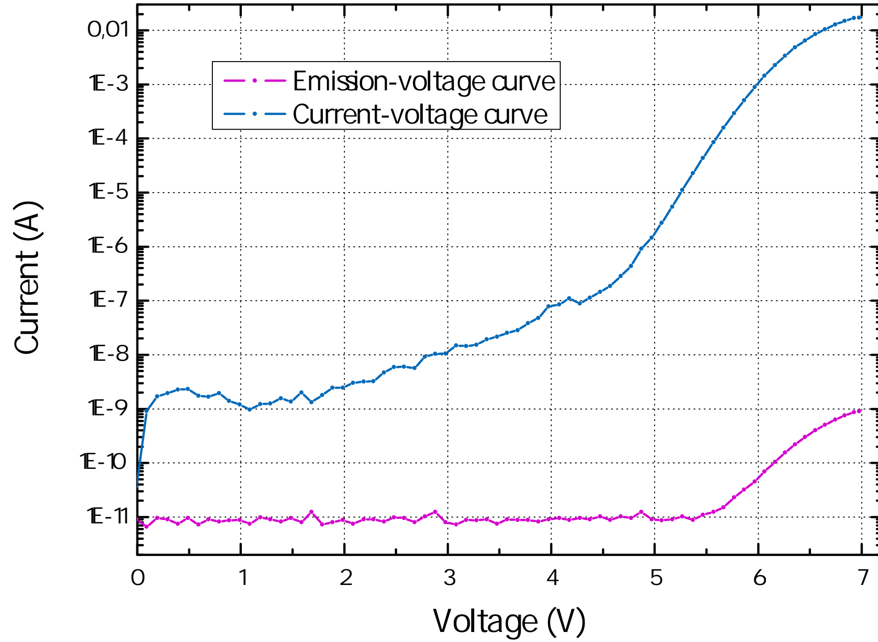

Figure 2.6: *A typical IV curve accompanied by the correspondent emission curve. The device has a platinum metal layer. The emission current is dramatically lower and only reaches* 1 nA*: the consequent low efficiency at* $V_{BIAS} = 6V$ *is equal to* $\eta = 5 \times 10^{-8}$*. The emission starts increasing at a voltage* $V_{BIAS} = 5.5V$ *in good agreement with the work function of platinum:* $\Phi_{Pt} = 5.65eV$.

roughly measured from emission curves ranges between $4.5eV$ to $5.1eV$, in general disagreement with the values known from literature: $\Phi_{Au} = 5.1 - 5.47eV$ [18]. This shift is probably mainly related to carbon (C) impurities or other kind of contaminants: similar results have been reported in literature [31].

2.4.1 Reproducibility of emission curves

In the previous section 2.3.1 the reproducibility of several IV curves from different devices of the same wafer was investigated. The emission currents from the same devices are shown in figure 2.7. The measurements were taken in air: this may probably result in a higher variability from one measurement to the other since more variables play a role on the collected current, for instance an imperfect alignment with the collector could increase the loss current. Effectively the differences among the curves are evident, the value of the emission varies of one order of magnitude at an applied voltage $V_{BIAS} = 5V$. The estimation of the work func-

tion would lead to an uncertainty of $0.1eV$, the value $\Phi_{Au} \approx 4.5eV$ is far from the one expected for gold. Various articles report the dependence of the work function of gold on contaminants. [32, 31] Beyond the already mentioned reasons, other explanations can be the uncertainty on the metal thickness or the voltage drop on the metal film. A thicker metal layer results in an exponentially lower current as stated in equation 1.27.

Concerning the efficiencies, a comparison between these curves and their correspondent IV characteristics 2.2 produced an average value $\eta = 3 \times 10^{-7}$ at $V_{BIAS} = 5V$: it is interesting to notice that this value is already much higher than the one measured for platinum, even if these curves refer to measurements in air. The following paragraphs will better discuss efficiency trends.

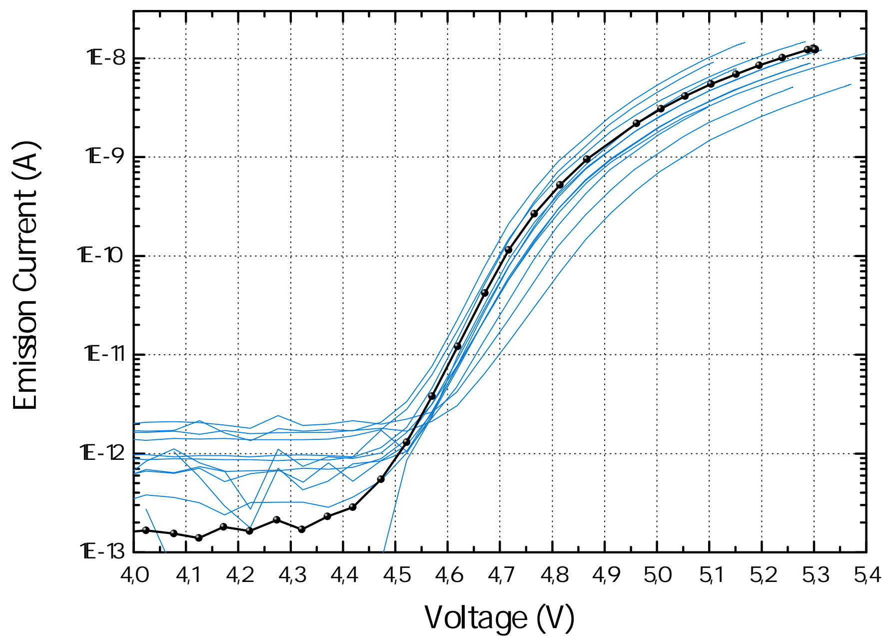

Figure 2.7: *The emission curves from the same devices described in section 2.3.1 and figure 2.2 are plotted. Although all these curves follow a general trend the variability is higher than in the case of IV curves. More variables play a role on the final emission. One of the curves has been plotted in black in order to better identify the shape.*

Chapter 3

Emission under gas pressure

Although the emission curves taken in air are less accurate and reliable than the ones taken in vacuum the measurements under air pressure have represented a relevant opportunity for this project. The advantages of measuring in air are several: first it is possible to test the devices without cutting a wafer. A PMMA plate was designed in order to make contact with a single device of the wafer by pressing on it. A thin gold layer deposited on the plate constituted the collector and still allowed the alignment on the device thanks to its partial transparency. The possibility of measuring on a whole wafer is important since the operation of dicing may sometimes be critical if the diamond tip is not sharp enough, damages may be induced in any case. In general it is easier and safer for the devices to work on full wafers. Secondly the amount of time saved analyzing devices in air is considerably lower: the UHV chamber employed can hold one device in a high pressure chamber and a second device in the mass spectrometer, as a result a test of a full wafer could take several days. Finally various experiments suggested the possibility that the durability of the devices in air and particularly in presence of oxygen is enhanced. Under this hypothesis which will be presented in chapter 6 in relation to the deterioration in time of the emitters, the measurements in air may have produced more stable results. These considerations as well as the others that will follow in this chapter till the end of this thesis particularly refer to the devices with titanium (Ti) and gold (Au) metal layers. These are the devices with the highest emission and durability, thus they were chosen for most of the experiments and as the most promising emitters. This chapter tries to estimate the differences between the measurements in vacuum and those in air or gas pressure. Especially the attenuation of the current and the modifications in the shape of the emission curves. In this thesis when referring to vacuum, the pressures are usually of the order of $p = 10^{-9}\ torr$, which

is the lowest pressure that could be reached using a turbo pump in a UHV chamber that was not previously baked. As a consequence of the fact that the devices were usually tested in air before, there was no reason for requiring lower pressures: the surface of the device certainly contains contaminants. Furthermore this pressure is low enough for ensuring the ballistic propagation of the electrons.

Before proceeding a consideration concerning the experimental setup for measuring emission needs to be made. As already anticipated in section 2.1 the importance of the collector voltage whose value does not vary much the measured emission in vacuum is critical under gas pressure. The transmission probability for the electrons to be transferred to the anode is dependent on the electric field in between; this theme will be treated in chapter 4. Furthermore, in presence of a gas, a high collector voltage may accelerate the electrons to the point of providing enough energy to ionize the gas molecules [33, 34, 35]. This is also the working principle of a mass spectrometer for revealing the presence of gases. Although the energy distribution of electrons after a big number of collisions is so broad that the ionizing probability will never be zero, this probability can be extremely reduced by limiting the collector voltage. Therefore it is rather important to keep the collector voltage below the ionizing potential of air molecules. The following table reports the ionizing energies of the main air components: the data are taken from the article [33].

Table 3.1: The ionization energies of air molecules from [33]. Only the value for CO_2 is taken from [36].

Gas molecule	Ionization energy (eV)
N_2	16.00
O_2	14.20
H_2	15.95
CO_2	14.01
He	24.59
Ne	21.56
Ar	15.76

3.1 Comparison of the results in UHV and in air

A first big difference between the measurements taken in air and the ones taken in vacuum concerns the shape of the emission curves. Theoretically there is no rea-

son why the IV curves should change in the two cases. This statement is actually wrong as it will described later in chapter 6, where the differences in the IV characteristics will be related to the effect of oxygen on the durability of the devices. Therefore this section will be confined to a description of the emission curves. Two of them, taken in air and in vacuum on a device with titanium (Ti) and gold (Au), are shown in figure.

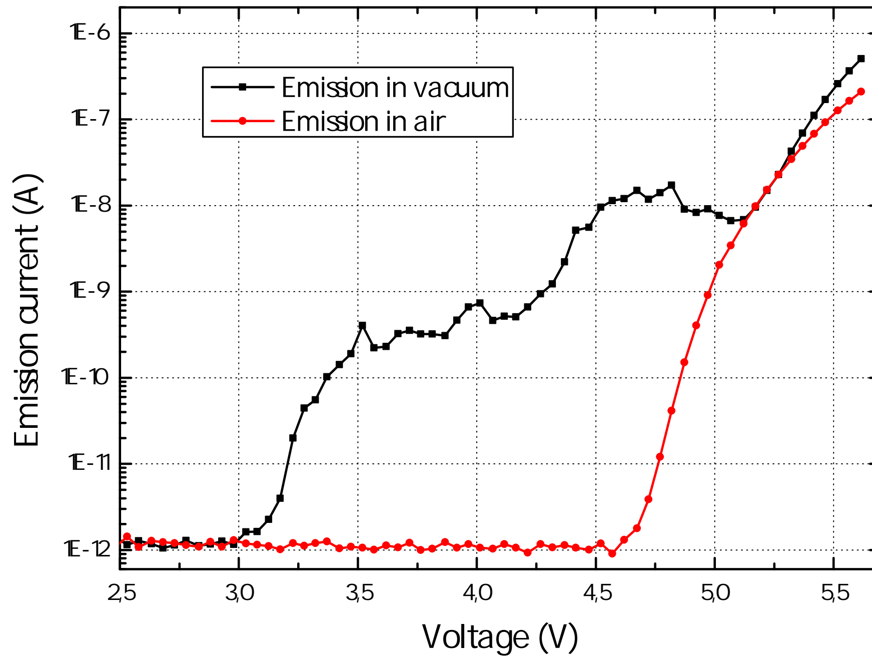

Figure 3.1: *Two emission curves measured in air or in vacuum are plotted. Under vacuum conditions and after a very few measurements a secondary emission of electrons occurs at relatively low voltages. The origin of this low voltage emission* $I_{E,low}$ *is not completely understood but it is considered to be related to a modification of the metal layer on the insulator and consequently to a deterioration of the device. At higher voltages the primary emission current still dominates with its peculiar shape.*

According to the theory of chapter 1 the devices should not emit under a threshold voltage which is equal to the work function of the metal gate. Despite the uncertainty on the value of the work function for some materials this phenomenon has always been observed in air. In vacuum this is not always true: very often and with increased probability after a certain amount of measurements, an emission current is also measured at lower voltages: usually starting from $V_{BIAS} \approx 2.5V$. This

value is much lower than the work function of all the metals used.

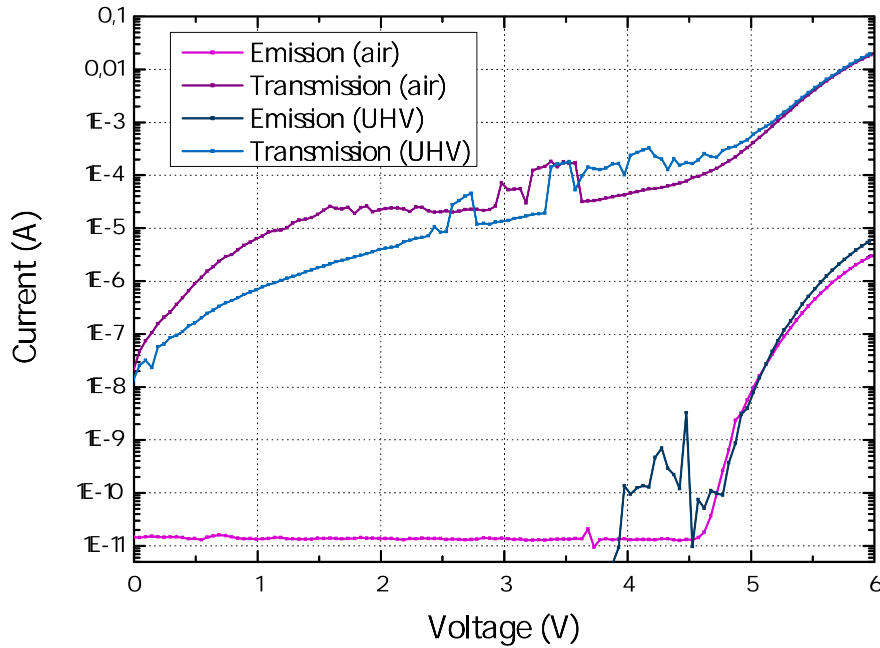

Figure 3.2: *Two emission curves measured in air or in vacuum are plotted with the correspondent IV curves. Beyond the already mentioned emission at low voltages which starts growing already in the first measurement in vacuum, the different shape of the emission curves can be noticed. At higher bias voltages the attenuation due to the scattering events with the air molecules is stronger.*

This current, appearing at low bias voltages, $I_{E,low}$ has no fixed shape in the emission curves. Nonetheless it usually increases with further measurements and it is considered as an effect of the deterioration of the device in the metal layer. The intensity usually reaches $1nA$ which is rather high if compared with the usual emission currents at higher voltages; above the work function of gold $V_{BIAS} > \Phi_{Au}$ the expected emission current $I_{E,high}$ still dominates. This is also due to the fact that $I_{E,low}$ usually seems to decrease just before. This decrease is suggested by the emission curves but the only proof is provided by the comparison with the emission curves when no current at low voltages appears. In the other cases there is no way of separating the two currents: $I_E = I_{E,low} + I_{E,high}$.

The origin of $I_{E,low}$ is not completely known, the fact that this current can only be measured above a certain voltage and is emitted supports the idea of a tunneling current. It can be thought that pin holes in the gold layer justify this emission:

they would expose titanium (Ti) or silicon dioxide (SiO_2) at the interface with vacuum and electrons could be directly emitted from these materials. This hypothesis would explain the fact that $I_{E,low}$ is not seen in air since oxygen could simply oxidize the parts of the device uncovered by gold. It also probably explains the intensity of the current because with no gold layer even a very small area of the device could produce a high current, since the attenuation due to scattering is much smaller. However it is in contrast with the band diagram of the MIS structure: the vacuum level of silicon dioxide or titanium is lower than for gold but still too high for producing a current at $V_{BIAS} \approx 2.5$V. Other contaminants could explain the presence of an even lower work function.

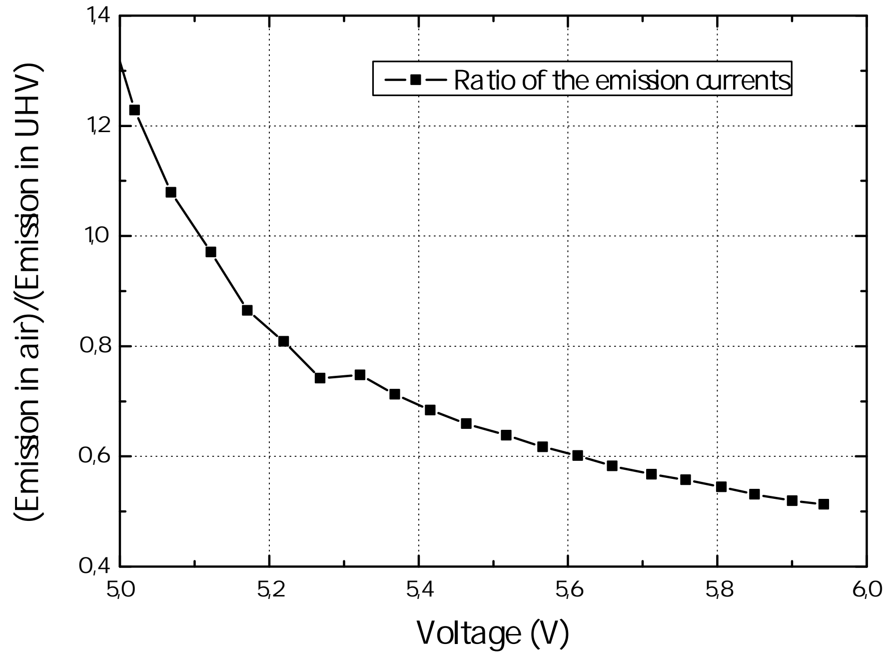

Figure 3.3: *From the curves of figure 3.2 the ratio between the emission current measured in air and the one measured in vacuum is plotted. The voltage range has been chosen from 5 V to 6 V since at lower voltages the low values of the emission would just generate noise. For higher voltages and higher kinetic energies of the emitted electrons the transmission probability decreases till a ratio of about* 1/2. *The ratios bigger than 1 at low voltages must probably be due to a small offset between the two measurements or to a small ionization of the air molecules.*

Apart from $I_{E,low}$, a comparison between the emission currents at high bias

voltage shows other interesting features. Figure 3.2 illustrates two typical emission curves in vacuum and in air: the low level of $I_{E,low}$ allows a more quantitative comparison. The current in vacuum is higher as expected but the attenuation due to the collisions with the molecules of air is not dramatical. Furthermore this attenuation is dependent on the applied bias voltage; this means that it is dependent on the kinetic energy of the emitted electrons. The nature of this dependence is one of the topics of chapter 4, here the ratio between the measured current and the total current emitted in vacuum is plotted in order to have an idea of how the transmission in air affects the experimental results: figure 3.3.

3.2 Pressures of Argon

A deeper study of the dependence of the emission on the gas pressure has been performed in the high pressure chamber of the UHV setup. Here emission curves have been taken while varying the pressure of argon (Ar). The choice of this gas is due to its inertness, furthermore it is a monoatomic gas which could simplify a description of the collisions with electrons from a microscopic point of view. The argon pressure was measured by different pressure gauges, each working in a different pressure range: one going up to $1mbar$, another one up to $10mbar$, the last one up to $1bar$. At each pressure step an IV characteristic and an emission curve were measured. Finally values of emission for a fixed applied voltage have been plotted as a function of the pressure. In order to be sure of the reliability of these measurements, the pressure was increased to $1bar$ first and later decreased to vacuum again.

Figure 3.4 refers to the emission measured when a constant collector voltage $V_C = 12V$ was applied. According to table 3.1 this value is low enough to limit the argon ionization. The intensity of the electric field between the surface of the device and the collector can be easily calculated knowing that the distance between the metals is $d = 0.3mm$: $\varepsilon = V_C/d = 400V/cm$. The emission always decreases for higher pressures but as already noticed before the variation is limited; also such attenuation is stronger when the applied bias voltage is higher which means that the current of electrons with higher kinetic energy is more affected by the presence of the gas. This was already mentioned in the previous section. A better understanding of the particular shape of these curves can be achieved in chapter 4 where the problem of the transport mechanism through the gas is assessed.

The same measurement was performed a second time on the same device but

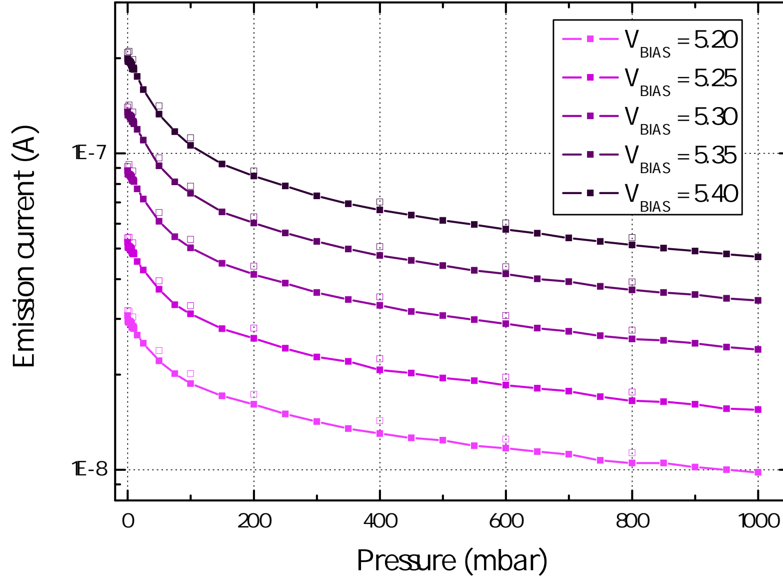

Figure 3.4: *Emission current as a function of the argon pressure in the high pressure cell of the UHV chamber. The low collector voltage* $V_C = 12V$ *produces a negligible current due to ionization. First the pressure was increased from vacuum up to 1 bar, then it was decreased. The empty squares refer to the measurements taken while decreasing the pressure. Different gradations of purple refer to different applied voltages. An attenuation due to the scattering events occurring in the gas phase is observed. Previous experiments, performed in the high pressure range* $p > 0.2bar$, *lead to the supposition of an exponential decrease which would appear as a line on a logarithmic plot. Reaching lower pressures the trend clearly looks different. It is worth noticing that for higher bias voltages and for the consequently higher kinetic energies of the electrons the attenuation is stronger: a factor of* $1/3$ *for* $V_{BIAS} = 5.2V$ *and about* $1/6$ *for* $V_{BIAS} = 5.4V$.

with a different electric field. A collector voltage of $V_C = 100V$ was applied in order to effectively notice the expected ionization in the gas: $\varepsilon = V_C/d \approx 3300V/cm$. The values of the pressure were also modified in order to better describe the features of the curves. Figure 3.5 shows a peak in the current for values of pressure between 30 and 40 $mbar$. In this point the emission is much higher than with a lower electric field, this is a clear evidence of the argon ionization: about one order of magnitude higher. The probable reaction is given by:

$$e^- + Ar \rightarrow 2e^- + Ar^+ \quad (3.1)$$

these ions will be accelerated in opposite directions by the electric field increasing the total current. The presence of a peak is due to the balance between the mean free path of electrons in the gas and the probability of collisions with gas molecules. For very low pressures most of the electrons will travel a sufficient distance for reaching the ionization energy before being scattered, but because of the low pressure the probability of colliding will be small, thus the lower current. On the other hand when the pressure is too high the mean free path of the electrons will be too short for gaining such energy and ionization will also be rare. The possibility of having a current that is higher than in vacuum, even at atmospheric pressure, is particularly important since it can affect the measurements in an originally unexpected way.

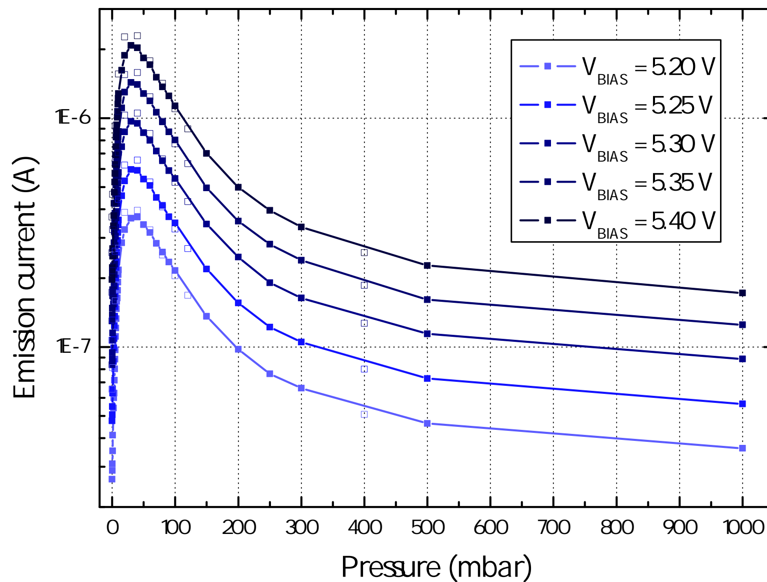

Figure 3.5: *Emission current as a function of the argon pressure in the high pressure cell of the UHV chamber. The measurement was carried out with the same procedure as in figure 3.4 and on the same device. Only the collector voltage is varied* $V_C = 100V$ *and some of the chosen values of the pressure. Such high voltage allows a partial ionization of the argon gas: the generated ions increase the measured current and are responsible for the observed peak. This represents the optimum coupling between the mean free path of the electrons and the probability of colliding with molecules.*

Chapter 4

Model for transport of electrons under air pressure

The current chapter was conceived with the ambitious purpose of describing qualitatively and possibly quantitatively the transport of electrons in air or other gas pressures. The importance of this study may be understood in correlation with the analysis of chapter 3 where emission curves taken in air have been presented. These curves provided essential information for this project and similar measurements will still be important for future characterization; this is probably true for a further development of hot electron emitters, but emission curves and spectra are also an important investigation tool for hot electron femtochemistry at surfaces (HEFatS). They inform about the current of electrons reaching the metal surface without being scattered and allow to measure their energy distribution: both these quantities must be known for an estimation of the reaction rates.

Nonetheless, every kind of measurement taken in air can only give qualitative information as far as the transmission function which relates the measured current and the total emitted current is totally unknown. Although this chapter is not able to give a closed expression of this transmission function, some of its important features will be derived and a model for the transport of the electrons from the surface of the metal gate to the collector will be theorized. In the end of the chapter, a comparison between the model and experimental data is presented.

The first measurements of emission in air have been surprising since the mean free path of electrons in air is known from literature [37, 38] and is of the order of $\lambda = 200nm$. The distance between the surface of the device and the collector is more than three orders of magnitude bigger: usually $d = 0.5mm$. This is a clear

evidence of the electron transport not to be ballistic in air; for this reason, the possibility of obtaining currents which do not differ dramatically from the real currents measured in vacuum is intriguing. Collisions with molecules must occur and still a current may be established.

During the derivations that follow, a particular attention will be addressed to four quantities, these are the main variables playing a role during the transport: namely the distance device-collector d, the electric field $\varepsilon = \frac{V_C}{d}$, the pressure p and the bias voltage V_{BIAS}. These are also the parameters that can be varied in order to take measurements comparable with the model. In the model the bias voltage V_{BIAS} will not be directly used but the kinetic energy of the electrons E_K and particularly their mean kinetic energy $\overline{E_K}$. Theoretically a direct relationship exists between the bias voltage and this mean energy; a first approximation might be $\overline{E_K} = V_{BIAS} - \Phi_{metal}$ where the kinetic energy is referred to the vacuum level, nonetheless a better estimation is achieved from the model of chapter 1 or even better from a measurement of the energy spectrum of the emitted electrons. Such measurements have been previously taken by PhD student Lasse Thomsen and Gunver Nielsen.

In the most general case the transmission function is expected to be dependent on all four variables:

$$T(d,\varepsilon,p,V_{BIAS}) = \frac{I_{trans.}(d,\varepsilon,p,V_{BIAS})}{I_E} \tag{4.1}$$

where I_E is the total emitted current and $I_{trans.}$ the transmitted measured current: appendix A provides a summary of all the symbols of this chapter and of this thesis in general.

4.1 Idea of the model

The central thread of the model consists in the description of the motion of electrons in a gas phase under the effect of a constant and uniform electric field ε. Such description relies on the fact that when such a field is applied, after a transient, a steady state will be reached and the electrons will move into the gas phase at a certain drift velocity w. This kind of problem has already been addressed before in literature and rather good results have been achieved. Nonetheless what needs to be understood here is that the knowledge of this transport mechanism is not sufficient for the purposes of this chapter. Even the most accurate model governing the motion of electrons in such a system does not allow to estimate the relationship

between emitted current and the measured one. The results of this first model will be inserted with some modifications due to the peculiarities and to the particular boundary conditions of the system device-collector into a second model which is totally original of this thesis.

This second model introduces the possibility of electron losses since only this phenomenon may explain the difference between $I_{meas.}$ and the total current I and estimates these losses through a statistical analysis of the motion. Although a certain amount of electrons is lost due to geometrical effects, the experimental setup and the holders are designed in order to minimize these losses: therefore in this treatment it will be considered as a secondary effect. Also the current due to ionization, as a consequence of the rather small collector voltages considered in this section and the rather high pressures, is considered to be very low [33]. The mechanism of backscattering is considered as the main responsible for these electron losses: the collisions in the gas phase will randomize the directions of the moving electrons producing a non-zero probability to reach the surface of the metal gate and here to be reabsorbed in the device. These back-scattered current I_{back} will then increase the current of typical IV curves: nonetheless the low efficiencies of hot electron emitters 2.4 do not allow to measure this rise. Considering all these losses the total emitted current can be written as:

$$I = I_{meas.} + I_{back} + I_{geom.} + I_{ions} \approx I_{meas.} + I_{back} \tag{4.2}$$

4.2 Theory of slow electron motion in gases

In literature, various studies of the motion of slow electrons in air have been performed: initially because of their importance in applications related to the ionosphere and to the propagation of radio-waves in this region of the atmosphere [39]. The distribution of the collisional frequencies with molecules influences the absorption of radio-waves traversing the ionosphere hence the interest of researchers. More in general the description of electron diffusion in gases is of great relevance in plasma physics even if in this case the energy range will be sufficiently low to neglect ionization. The method adopted here is originally due to Townsend in the year (1928) [40], and later modified by Huxley and Zaazou (1949) [41].

4.2.1 Electron energies and Townsend factor

The terms *slow electrons* deserve a note before proceeding. The maximum energy of the emitted electrons is known with rather good accuracy since the distribution of electron energies above the level of the applied bias voltage is only due to the Fermi distribution in the semiconductor multiplied by the tunneling probability: the result is an energy distribution which does not extend over a few K_bT beyond the applied bias. If this energy is referred to the vacuum level the work function of the metal needs to be subtracted. Considering a maximum applied bias of $V_{BIAS} = 6V$ and the work function of gold to be $\Phi_{Au} = 4.9$, a reasonable value due to the probable impurities on the surface and in agreement with experimental results, the electron energy may exceed the value $E_K = V_{BIAS} - \Phi_{Au} = 1.1eV$ of a few $K_bT = 0.026eV$.

The mean electron energy will be lower than this maximum value, and the ratio between this mean energy and the thermal energy $E_{th} = \frac{3}{2}k_bT$ will be lower than $k_T = \frac{\overline{E_K}}{E_{th}} \leq 28$: this factor k_T quantifying the excitation of the electrons with respect to the thermal equilibrium is referred to as the Townsend factor. Depending on the considered parameters and especially on the electric field ε and on the pressure p the combined effect of energy gain due to acceleration and energy loss due to collisions will vary the Townsend factor. According to literature [39], the range on pressures and electric fields considered here will produce values: $k_T < 80 \Rightarrow \overline{E_K} < 2eV$ and the electrons will be much slower than how they could be in vacuum when subjected to typical collector voltages $V_C \approx 10 - 200V$. Furthermore for the purposes of this chapter it is of great importance to limit the Townsend factor: if it increases too much the average energy of the electrons becomes sufficient for ionizing the gas molecules, this phenomenon was shown in chapter 3.2. In this case equation 4.2 must be modified adding the currents due to ionization and this is not desirable since it introduces a further degree of freedom.

4.2.2 Drift velocity in steady state

When a constant and uniform electric field is applied to a gas in excess of electrons these will move according to the combined effect of deterministic acceleration and statistical collisions: after a transient as apparent from literature [40, 42, 43] and from the results of similar models, for instance the Drude model, a steady state is reached. By definition in this regime all the mean quantities as mean energy $\overline{E_{K,s}}$, mean velocity $\overline{v_s}$ or drift velocity w are constant: the subscript 's' here refers to *steady state*. As a consequence of the electric field the electron mean energy

exceeds the thermal energy of the surrounding environment and the Townsend factor $k_{T,s} > 1$. The numerical value is also characteristic of the particular steady state: as reported in the cited articles it is a function of the ratio ε/p a quantity that, from now on, will represent the main variable of the system since it determines the steady state.

The next question the model tries to answer relates to the energy distribution of the electrons in such steady state. If this distribution is always the same and is known, then the mean velocity $\overline{v_s}$ can be directly related to the mean energy of the electrons $\overline{E_{K,s}}$ and as a consequence, to $k_{T,s}$. Various distributions have been suggested, the first possibility is to employ the Maxwell distribution of velocities, another one is known as Druyvesteyn distribution and should give better results when $k_{T,s}$ is significantly above the equilibrium value of 1 [44, 45, 46].

$$f_{Maxwell}(v) = 4\pi \left(\frac{3m}{4\pi\overline{E_K}}\right)^{(3/2)} v^2 \exp\left(-\frac{3mv^2}{4\overline{E_K}}\right) \tag{4.3}$$

While the Druyvesteyn distribution:

$$f_{Druyvesteyn}(v) = 0.735 \left(\frac{m^3 v^4}{\overline{E_K}^3}\right)^{(1/2)} \exp\left(-\frac{0.137 m^2 v^4}{\overline{E_K}^2}\right) \tag{4.4}$$

In order to relate the drift velocity of the steady state to the mean velocity, an assumption needs to be made. This is a rather well accepted assumption and consists in assuming isotropic scattering events in the collisions with molecules. It is probable that real scattering events, mainly of electrostatic nature, are not completely isotropic but the large amount of collisions in the range of interesting ε/p randomize the directions of electrons so fast that the assumption leads to good approximations. Under this assumption simple mechanical and geometrical considerations lead to the relationship [40, 47]:

$$w = \frac{2e}{3m}\varepsilon\lambda\overline{v^{-1}}_s \tag{4.5}$$

where λ is the mean free path of electrons in air and $\overline{v^{-1}}_s$ is the expectation value of the inverse of the velocity which can be derived once the velocity distribution has been chosen. Defining ν as the collision frequency $\overline{v} = \lambda\nu$, the previous expression becomes:

$$w = \frac{2e}{3m}\left(\frac{\varepsilon}{p}\right)\left(\frac{p}{\nu}\right)\left(\overline{v^{-1}}_s\,\overline{v}_s\right) \tag{4.6}$$

where the right side of the equation has been multiplied and divided by the pres-

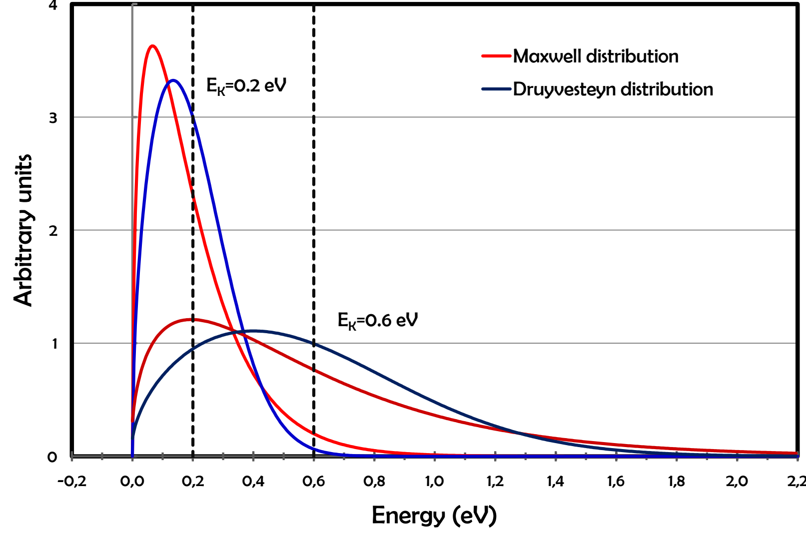

Figure 4.1: *A comparison between the Maxwell distribution and the Druyvestein distribution with two different values of the mean kinetic energy. The Druyvestein distribution predicts a larger amount of electrons at high energies: the peak of the distribution is also closer to the mean value.*

sure p. The product $\overline{v_s^{-1}}\ \overline{v_s}$ is a property of the velocity distribution; in the Maxwell distribution the single expressions of these two factors are:

$$\overline{v} = \frac{2}{\sqrt{\pi}}\left(\frac{2K_BT}{m}\right)^{1/2}, \qquad \overline{v^{-1}} = \frac{2}{\sqrt{\pi}}\left(\frac{2K_BT}{m}\right)^{-1/2} \tag{4.7}$$

and the consequent product: $(\overline{v^{-1}}\ \overline{v})_{Maxwell} = \frac{4}{\pi} = 1.27$, to be compared to the one produced by the Druyvesteyn distribution, $(\overline{v^{-1}}\ \overline{v})_{Druyvesteyn} = 1.18$. Once this constant has been inserted, equation 4.6 can be rearranged in order to express the ratio $\frac{\nu}{p}$ as a function of ε/p and w.

$$\frac{\nu}{p} = \frac{2e}{3m}\left(\frac{\varepsilon}{p}\right)\frac{1}{w}\left(\overline{v^{-1}}_s\ \overline{v}_s\right) \tag{4.8}$$

This formula is useful for the calculation of the collision frequency ν when the drift velocity is known; being a property of the steady state w is also a function of the ratio ε/p, nonetheless its shape is complex and there is no closed expression over the

all ranges of ε/p. On the other hand the drift velocity can be easily measured with different experiments [41, 42]; the common procedure is to put the experimental results into equation 4.8 or a fit of these results on a limited range, empirical formulae have also been proposed. A similar argument concerns the relationship between $k_{\mathrm{T},s}$ and ε/p.

Both $k_{\mathrm{T},s}$ and the collision frequency, or its inverse $\tau = \nu^{-1}$ namely the mean time between collisions, will be needed for the second part of the model: for this purpose the choice of w and $k_{\mathrm{T},s}$ will be deferred to section 4.2.4.

4.2.3 Energy loss per collision

In order to apply this first model another quantity is necessary, this is the energy loss per collision. The steady state described so far is a dynamic equilibrium where the electrons in each collision may gain or lose energy exchanging it with the gas molecules. If the electric field varies, the mean energy of the electrons will evolve toward a new steady state: for instance, if it is turned off, statistically, the losses will exceed the gains and the mean energy will decrease until the thermal energy is reached. At the generic steady state the losses and gains due to collisions are compensated by the energy furnished by the electric field. This state of equilibrium is expressed as:

$$\overline{\mathrm{E}_{\mathrm{K},loss}} = \overline{\mathrm{E}_{\mathrm{K},gain}} \quad \Rightarrow \quad \nu\Delta\mathrm{E} = e\varepsilon w \tag{4.9}$$

where $\Delta\mathrm{E}$ is the exchanged energy per collision while the expression on the right is the power due to the electric field. If the direction of the electric field is assumed to be conserved, namely in the same direction as the drift velocity, the term on the right will always be positive: the electric field gives a positive contribution to the energy. On the other hand this means that at steady state the collisions will always provide a net negative contribution; for this reason $\Delta\mathrm{E}$ is referred to as energy loss per collision. By combining the last expression with equation 4.5 the energy loss also becomes a function of w.

$$\Delta\mathrm{E} = \frac{3}{2}\frac{m}{\left(\overline{v^{-1}}_s\,\overline{v}_s\right)}w^2 \tag{4.10}$$

and it will be found after the choice of w. From equation 4.10 is apparent that when the system is farther from the thermal equilibrium and the drift velocity is higher, the energy losses will also be higher. This is reasonable since a system far from the equilibrium is expected to relax faster while the losses for a system approaching the

equilibrium must vanish. Because of these reasons a natural expression governing the energy losses was thought:

$$\Delta E = G\left(\overline{E_{K,s}} - E_{th}\right) \tag{4.11}$$

where the losses are simply proportional to the distance from the equilibrium: G is an unknown constant. The fraction of energy lost in a collision is written as: $\eta_c = \frac{\Delta E}{\overline{E_{K,s}}}$ it represents the efficiency of each collision in reducing the energy. This definition leads to:

$$\eta_c \overline{E_{K,s}} = G\left(\overline{E_{K,s}} - E_{th}\right) \tag{4.12}$$

Finally, rewriting this efficiency κ as a function of the Townsend factor:

$$\eta_c = G\left(1 - \frac{1}{k_{T,s}}\right) \tag{4.13}$$

In literature various experiments reported good agreement with this equation: particularly for values $k_{T,s} < 40$ [41]. Its importance is understood in relation to the behaviour of η_c for considerably high values of $k_{T,s}$: it approaches a constant value equal to G. This behaviour is effectively observed for $20 < k_{T,s} < 40$ and provides a rather reliable method for the estimation of G.

4.2.4 Assumptions and modifications

In order to employ this theory in the description of the hot electron motion between the surface of a device and a collector, a few but important modifications need to be made. Furthermore reasonable relationships representing $k_{T,s}$ and w as a function of ε/p must be assumed. Some of these approximations may be rather strong but at this stage necessary in order to get results.

The main reason why the model cannot be directly used is due to the mean energy of the electrons emitted and to their energy distribution. Since the mean energy for a fixed device depends only on the applied bias voltage, this energy $\overline{E_K}$ will differ from the mean energy $\overline{E_{K,s}}$ of the steady state described so far. In other words just after the electron emission, the system is not in a steady state but it will evolve in that direction. Not only the mean energy is different but also the energy distribution: initially this is definitely out of equilibrium, nevertheless its shape is known from the model of chapter 1 or, more accurately, it can be measured as PhD students Lasse Thomsen and Gunver Nielsen have done.

The progressive evolution of the shape of this distribution towards the typi-

cal distribution of the steady state is complex and will not be considered here: the mean energy loss must be considered instead and for this purpose the electron distribution will be assumed to be always equal to the Druyvesteyn distribution. The Druyvesteyn distribution was formulated in order to describe systems being out of equilibrium especially in an electric field, furthermore for the same mean values of energy it predicts a larger amount of electrons at high energy and the peak of the distribution is also closer to the mean value. For these reasons the Druyvesteyn distribution better approximates the initial conditions of the emitted electrons. Figure 4.2 summarizes the energy conditions of the system showing the typical energy distribution of the hot electrons and comparing it with the distribution of the steady state and the distribution of energies at thermal equilibrium. The evolution of the

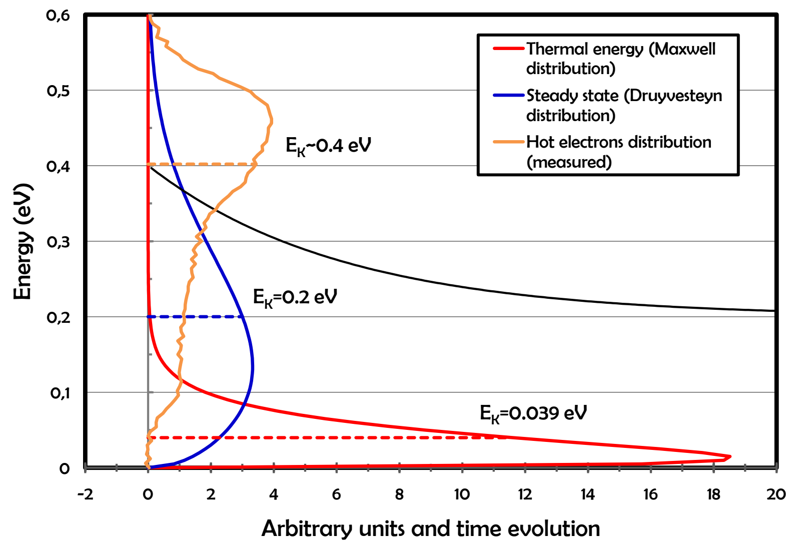

Figure 4.2: *The distribution of the energies of hot electrons just after being emitted is shown. A spectrum with a mean kinetic energy of* $\overline{\mathrm{E_K}} \approx 0.4\mathrm{eV}$ *is chosen. Due to collisions this distribution will evolve in time towards the energy distribution of the steady state which is here assumed to be a Druyvestein distribution at a mean kinetic energy* $\overline{\mathrm{E_K}} = 0.2\mathrm{eV}$. *The typical Maxwell distribution at the thermal equilibrium is also shown. The black line describes the exponential decay of the initial mean kinetic energy towards the steady state when equation 4.15 is valid.*

electron mean energy $\overline{\mathrm{E_K}}$ needs to be considered in more detail. Equation 4.11 is still valid when $k_T < 40$: this is not strictly the case in all the performed experiments

but it is still true if the considered pressures are not too low. A better description of the experimental results and of their characterizing quantities, k_T and ε/p is postponed to section 4.4. Even if equation 4.11 is still valid, equation 4.9 describing the energy balance in steady state is surely not. Initially the losses must differ from the gains in order to progressively shift the mean energy of the electrons towards the steady state. The energy gain per collision still needs to be estimated. Rigorously the right side of 4.10 is only valid in steady state since w itself, as defined here, is a property of the steady state. An idea is to choose an effective drift velocity w_{eff} which depends on the distance from the steady state $\overline{E_K} - \overline{E_{K,s}}$. Such quantity needs to fulfill two requirements:

$$\begin{cases} min(w, w') \leq w_{eff} \leq max(w, w') \\ \lim_{\overline{E_K} \to \overline{E_{K,s}}} w_{eff} = w \end{cases} \tag{4.14}$$

where w' is the drift velocity if the electrons were already in steady state when emitted at the energy $\overline{E_{K,s}}$. The first condition forces the state of the system to be an intermediate state between the initial one and the final steady state. The second condition describes the steady state: when the mean energy approaches $\overline{E_{K,s}}$, the effective drift velocity must approach the drift velocity of the steady state ensuring an equal balance of gains and losses. The assumption here is to simply choose $w_{eff} = w$ which is expected to be close to reality when the distance $\overline{E_K} - \overline{E_{K,s}}$ is small. With this choice equations 4.10 and 4.11 are still valid and the energy gain is simply the same as if the system has already reached the final steady state. With this choice the result of the energy balance is:

$$\Delta\overline{E_K} = \overline{E_{K,gain}} - \overline{E_{K,loss}} = G\left(\overline{E_{K,s}} - E_{th}\right) - G\left(\overline{E_K} - E_{th}\right) = -G\left(\overline{E_K} - \overline{E_{K,s}}\right) \tag{4.15}$$

As a consequence of the fact that the mean difference in kinetic energy for a collision $\Delta\overline{E_K}$ is proportional to the distance in energy from the steady state, the succession of collisions will vary the mean energy following an exponential decay, asymptotically reaching the steady state.

Now that all the necessary quantities have been found, the last objective of this first model is the choice of a reasonable expression for $k_{T,s}$ and w_s. Since various other approximations have already been made and it would be preferable to conserve part of the physical meaning in these formulae, a direct fit of previous experimental results is avoided. In 1949 Huxley and Zaazou [41] found good agreement

between experiments and the following equations:

$$k_{T,s} = \frac{1 + \left[1 + \frac{1.54\times10^{-4}}{G}\left(\frac{\varepsilon}{p}\right)^2\right]^{1/2}}{2}, \qquad w = \frac{5000\left(\frac{\varepsilon}{p}\right)}{\left(k_{T,s}\right)^{1/2}} \tag{4.16}$$

The derivation of these expressions employs equation 4.13 so that the agreement is also limited by the range of validity: $k_T < 40$. The value of the constant was estimated by Huxley and Zaazou as: $G = 1.3 \times 10^{-3}$. On the left of equation 4.2.4 the trend of $k_{T,s}$ is almost linear but it approaches the value of 1 and therefore the equilibrium, when ε/p is very small. On the right, the meaning of the formula

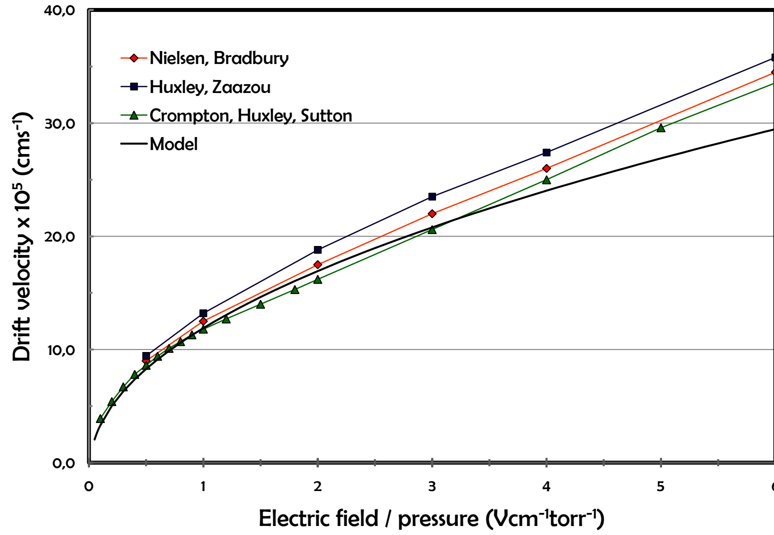

Figure 4.3: *The experimental results from three papers of Nielsen and Bradbury [42], Huxley and Zaazou [41], Crompton, Huxley and Sutton [47] are compared with the model of equation 4.2.4, also proposed by Huxley and Zaazou. The agreement is rather good in the range* $\varepsilon/p < 2.5 V cm^{-1} torr^{-1}$ *which approximately corresponds to a Townsend factor* $k_T < 40$.

for the drift velocity is rather intuitive: the proportionality with respect to the electric field could be expected in similarity with other models, for instance with the Drude model in metals. Both the pressure and the mean velocity of the electrons play an opposite role: they will enhance the randomizing effect of collisions to the prejudice of the drift velocity. The expression on the right was also independently

derived by Compton [48] with one difference: the constant is assumed equal to $G = 2.66m/M$ where M is the mass of the colliding molecules. In this way equation 4.2.4 could take into account the presence of different gases, nonetheless this choice of G did not seem to reproduce the experiments, especially for diatomic gases. In order to provide an idea of the level of approximation figure 4.3 shows the drift velocity as a function of ε/p: some experimental results, from the already mentioned articles, are plotted and compared with equation 4.2.4.

4.3 Model for the electron transmission probability in gases

In the previous section a model for the electron diffusion in a gas phase has been introduced. This lead to the estimation of typical macroscopic quantities describing the motion: the collision frequency ν (equation 4.8) and the Townsend factor $k_{T,s}$ (equation 4.2.4) as a function of the ratio ε/p, the mean energy loss per collision $\Delta\overline{E_K}$ as a function of the electron energy (equation 4.15).

The necessity of a second model is due to the fact that, in order to describe the percentage of emitted current reaching the collector, some microscopic phenomena need to be considered and boundary conditions must be implemented. Various approximations will be made, sometimes strong, but the necessity of simplifying the problem and the good qualitative results described in the next section justify such choice. The theoretical principles of these section have been applied in order to run *matlab* simulations and predict the transmission current.

4.3.1 Idea of the model

The basic idea of the model is to describe the spatial distribution of the electrons in the region of space between the surface of the device and the surface of the collector. This distribution varies as a consequence of the collisions and of the electric field accelerating the electrons and propagates in space. The parameters introduced in the expression of the transmission function 4.1 will play a fundamental role in the evolution of the distribution towards the collector or towards the surface of the device. After a certain amount of collisions the total amount of transmitted electrons can be found.

The first fundamental consideration will help focalize the sense of this strategy. A wordless assumption in the model of the previous section was the low electron density in the gas; this allowed to neglect the interactions among electrons. On the other hand the interactions with the molecules have been modeled as colli-

sions, meaning that the interaction is of impulsive kind. This means that the time scale of the interaction is assumed to be much smaller than the time between collisions. All these assumptions have two main consequences. The former is that the motion of the electron between two collisional events is ballistic: its trajectory can be simply derived from Newton's law. The latter consists of a strong simplification of the problem: the transport can be treated as a single electron problem. The previously mentioned spatial distribution of the electrons will simply be a single electron probability distribution function $f(x)$. The transmission function $\mathrm{T}(d,\varepsilon,p,\mathrm{V_{BIAS}})$ is simply equal to the single electron transmission probability.

The practical simulations will not directly predict T because the transmission probability is estimated as a function of the initial electron energy $\mathrm{E}_{k,0}$ and not of the applied bias voltage $\mathrm{V_{BIAS}}$. Therefore it will appear as $\mathrm{P}(d,\varepsilon,p,\mathrm{E}_{k,0})$. The derivation of the transmission function is then easily performed if the emission spectrum of energy is known $\mathrm{S_{V_{BIAS}}}(\mathrm{E}_{k,0})$: the probability must be weighted with respect to the normalized energy distribution:

$$\mathrm{T}(d,\varepsilon,p,\mathrm{V_{BIAS}}) = \int_0^\infty \mathrm{P}(d,\varepsilon,p,\mathrm{E}_{k,0})\mathrm{S_{V_{BIAS}}}(\mathrm{E}_{k,0})\, d\mathrm{E}_{k,0} \tag{4.17}$$

Here the energy $\mathrm{E}_{k,0}$ is the kinetic energy of an electron exiting the metal where the zero of the energy is taken at infinite distance from the metal surface where the effects of the image potential vanish: namely the vacuum level.

4.3.2 Classical electron motion between collisions

In order to describe the classical motion of the electron between the two metal plates, a coordinate system must be chosen: choosing the x axis to be orthogonal to the plates this region of space is delimited by: $0 < x < d$ where the origin of the axis corresponds to the metal surface of the device. As discussed in the previous paragraph, in the time interval between two collisions the motion is ballistic; since the system is conservative a potential energy can be defined and the kinetic energy is known. The lagrangian formalism allows a direct derivation of the equation of motion:

$$\frac{d\left(\frac{\partial \mathscr{L}}{\partial \dot{q}_i}\right)}{dt} - \frac{\partial \mathscr{L}}{\partial q_i} = 0 \tag{4.18}$$

where the lagrangian is defined as the difference of kinetic and potential energy, $\mathscr{L}(q,\dot{q}) = \mathrm{E}_k(q,\dot{q}) - \mathrm{U}(q,\dot{q})$ and q_i are the coordinates of the system. In this notation: $\mathrm{E}_k = \frac{1}{2}m(\dot{x}^2+\dot{y}^2+\dot{z}^2)$. The definition of the potential energy between the

two plates is less obvious: the main contribute is given by the presence of the applied electric field, nonetheless in order to describe more accurately the behaviour of the electrons when they are very close to the metal surfaces the image charge potential is also considered. Since the effect of the image charge is included in the

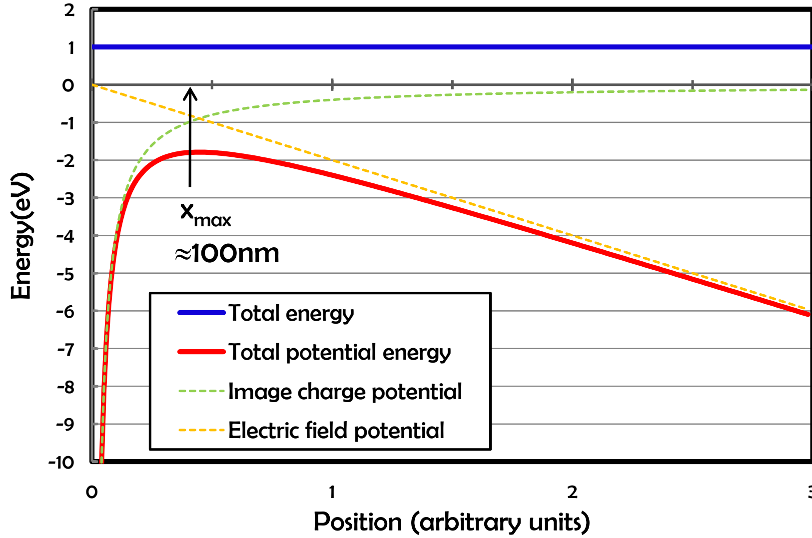

Figure 4.4: *A diagram of the energies involved in the system is shown. The effects of the image potential have been magnified in order to better visualize them. The zero of the energy is represented by the vacuum level inside the metal. The total energy of the electron exiting the metal is represented by the blue line, typically about* 1eV *above the vacuum level. The total potential energy is also shown in red: this is given by the sum of two terms, one for the image charge potential the other one related to the applied electric field. The fast vanishing image charge potential originates a maximum of potential energy at a position of about* $100nm$.

value of the work function, a first possibility is to consider the image charge potential as a potential barrier whose height is the work function itself. This is normally done when the motion of the electrons in proximity of the metal is not crucial. The choice here is different: the image charge potential is explicitly considered as the electrostatic attraction between two particles of opposite charge. Therefore the total potential energy referred to the vacuum level is given by

$$U(x) = -q\varepsilon x - \frac{1}{16\pi\epsilon_0}\frac{q^2}{x} - \frac{1}{16\pi\epsilon_0}\frac{q^2}{(d-x)} \tag{4.19}$$

where the image charge potential energy has been considered at both metal plates and the dielectric constant of air has been approximated with the one of vacuum: figure 4.4 helps with the visualization of the relevant energies. With these expressions the lagrangian equation of motion 4.18 becomes:

$$\ddot{x} = -\frac{1}{m}\frac{d\mathrm{U}(x)}{dx} = \frac{1}{m}\left(q\varepsilon - \frac{1}{16\pi\epsilon_0}\frac{q^2}{x^2} + \frac{1}{16\pi\epsilon_0}\frac{q^2}{(d-x)^2}\right) = a(x) \tag{4.20}$$

A differential equation whose resolution is not obvious since the acceleration a is not constant and uniform. In the other directions y and z there is no acceleration as expected. Integrating equation 4.20 in time twice, the trajectory of the electron can be written as:

$$x(t) = x_0 + v_{x,0}t + \int_0^t \left(\int_0^t a(x(t))\,dt\right) dt \tag{4.21}$$

with the initial position and velocity along the x axis respectively introduced as x_0 and $v_{x,0}$. It has to be noticed that at the initial time $t = 0$, the x component of the velocity $v_{x,0}$ is limited by the initial kinetic energy: $\left|v_{x,0}\right| < \sqrt{(2\mathrm{E}_k(x_0))/m}$. This relation can also be written as:

$$v_{x,0} = \upsilon\sqrt{\frac{2\mathrm{E}_k(x_0)}{m}}, \qquad -1 < \upsilon < 1 \tag{4.22}$$

The sign of the number υ defines the direction of the initial velocity, its modulus describes the portion of the total velocity being aligned with the x axis.

As a consequence of the fact that 4.21 is only valid between two scattering events, the collisions may be now introduced in the following way: x_0 will now represent the generic initial position of an electron after the i-th collision, it will be labeled as $x_0 \to x_i$ in order to specify the order of collision. The final position, when a new scattering event occurs, becomes $x(t) \to x_{i+1}$: this will also be the initial position for the following propagation. The velocity $v_{x,0}$ according to equation 4.22 is related to the initial kinetic energy which now is written $\mathrm{E}_k(x_0) \to \mathrm{E}_k(x_i)$. The time t is the time between two scattering events.

In order to solve the double integral an assumption is made: if the distance traveled between two collisions is small enough, much smaller than the distance needed for observing a considerable variation of the acceleration $a(x)$ then the acceleration can be considered constant between one collision and the following one. The value of the acceleration is assumed to be equal to the initial one: $a(x) \to a(x_i)$. Such assumption is suggested by expression 4.20 which shows that the dependence

of the acceleration on the position only appears in the extremely narrow regions where the image potential can be felt; this means that this assumption is very close to reality if not too close to the boundaries of the system: in this regions the potential energy produces a fast varying diverging acceleration. With these considerations and combining equations 4.21 and 4.22 the equation of motion between collisions becomes:

$$x_{i+1} = x_i + \upsilon\sqrt{\frac{2\mathrm{E}_k(x_i)}{m}}\,t + \frac{1}{2}a(x_i)\,t^2 \tag{4.23}$$

4.3.3 Probability distribution functions

Once the equation of motion has been defined the idea of the model is to substitute the main variables of equation 4.23 with the correspondent probability distribution functions. This paragraph describes the passage from the deterministic treatment conducted till now to a statistical one. Once the other distributions are defined, knowing the spacial distribution of the electron after the generic i-th collision which will be named $f_{x,i}$, it will be possible to determine the spatial distribution at the succeeding collision $f_{x,i+1}$. With this method and with the typical initial conditions of the system of interest the evolution of such distribution can be followed: starting from the device it will move towards the collector: the portion of the total area reaching the collector will represent the transmission probability. Referring to equation 4.23 the following distributions are defined: f_t represents the distribution of the time between two scattering events, f_υ expresses the transversal relative portion of the velocity and is related to the probability of assuming a certain direction after each collision.

The expression of f_t is chosen to be described by an exponential distribution, which describes the time between events in a Poisson process. This choice is rather common and already employed in other diffusion problems as in the Drude model.

$$f_t(t) = \frac{1}{\tau}\exp -\frac{t}{\tau}, \qquad t \in [0, +\infty) \tag{4.24}$$

where τ is the mean time between scattering events and can be derived from equation 4.8 as function of ε/p. Under the assumption of isotropic collisions f_υ describes the x-component of a vector of unitary length which assumes the all directions in space with equal probability. Its distribution is defined as Wigner semicir-

cle distribution and is given by:

$$f_\upsilon(\upsilon) = \frac{2}{\pi}\sqrt{1-\upsilon^2}, \qquad \upsilon \in [-1,1] \tag{4.25}$$

Before proceeding the last undefined term of equation 4.23, namely the kinetic energy deserves deeper considerations. There are various possibilities for choosing its expression: one alternative is to assume a particular energy distribution, for instance the measured distribution of the emitted electrons or the distribution of the steady state already taken as the Druyvestein distribution. After each collision the mean kinetic energy would change of a quantity defined by equation 4.15 and in this way it would evolve towards the steady state. Nevertheless a similar choice would completely neglect the spatial dependence of the energy: this can be easily understood considering the very fast increase of potential energy when the electron encounters the image potential just after exiting the metal and the consequent strong decrease of the kinetic energy. Furthermore the relative energy loss per collision with respect to the energy of the steady state is defined by the constant $G = 1.3 \times 10^{-3}$ which is rather small and the energy of the electron after a number of collisions of the order of $G^{-1} \approx 770$ is correlated with the initial one. As it will be apparent later, within the range of electric field of interest, the traveled distance of the electron is mainly due to the term $\upsilon t\sqrt{(2E_k(x_i))/m}$, with typical values for the mean time between collision $\tau \approx 1ps$ and typical velocities $\sqrt{(2E_k(x_i))/m} \approx 10^5 ms^{-1}$, the traveled distance per collision is $10^{-7}m$. Such quantity within a number of collisions ≈ 770, assuming a totally random walk, originates a total traveled distance of the order of $10^{-7}m \times \sqrt{770} \approx = 3 \times 10^{-6}m$. This displacement is easily able to produce very high changes on the kinetic energy of the electrons since the image charge potential varies on a very short scale $\approx 10^{-7}m$. For this reason and for the importance to accurately describe the first collisions, those mainly responsible for backscattering, the kinetic energy is chosen as a deterministic function of the position; this is typical of conservative systems. The energy losses are then introduced being also a function of the position since they are proportional to the local distance in energy from the energy of the steady state. The spacial dependence of the kinetic energy is defined as $E_{k,0}(x) = E_0 - U(x)$ which is also the kinetic energy of the electrons before collisions. Introducing the energy losses of equation 4.15 the kinetic energy after an arbitrary number $i+1$ of collisions can be related with the kinetic energy after collision i. The generic element

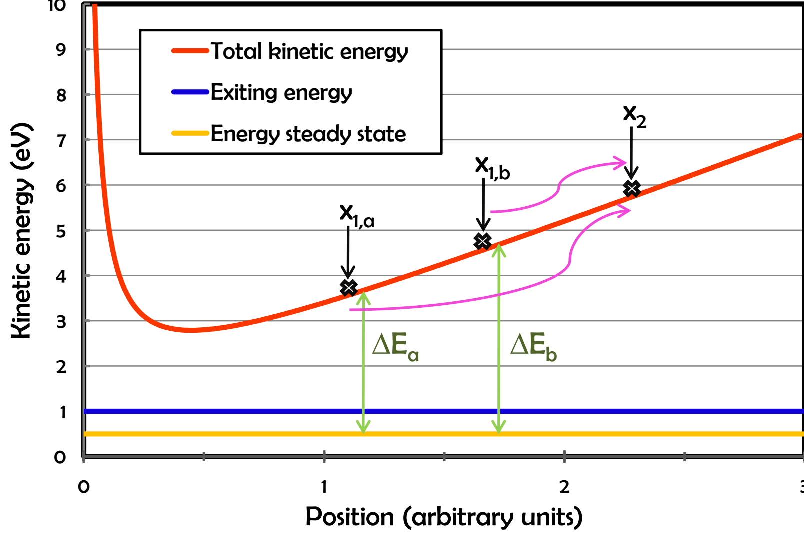

Figure 4.5: *The blue line represents the total energy of the electrons when they escape the metal: namely* $E_{k,0}$*. Their initial kinetic energy is also shown in red: this is achieved as* $E_k(x) = E_{k,0} - U(x)$*. The yellow line represents the energy of the steady state which is the average energy of the electrons after an infinite number of collisions. Before colliding the electron moves on the x-axis and varies its kinetic energy as in a conservative system, according to the red line. If it collides at the position* $x_{1,a}$ *it will lose an amount of energy which is proportional to* ΔE_a*. Its new energy is still a deterministic function of the position. On the other hand this is not true when it reaches the location of the second collision, assumed to be* x_2*. In this position the energy of the electron is now unknown, because the electron could also be arriving from another position, for instance* $x_{1,b}$*: in this case the electron would have lost a higher energy, proportional to* ΔE_b*. The model, instead, loses memory of the electron pathway and considers the kinetic energy as a pure function of the position and of the collision number* i*, which introduces the energy losses through equation 4.26 and evolves the system toward the steady state.*

of the sequence is:

$$E_{k,i}(x_i) = \overline{E_{K,s}} + \left(E_{k,0}(x) - \overline{E_{K,s}}\right)(1-G)^i \tag{4.26}$$

after a large amount of collisions, of the order of $G^{-1} \approx 770$ the kinetic energy relaxes over the energy of the steady state $\overline{E_{K,s}}$ but till that moment the spacial distribution of energies is partially conserved. Equation 4.3.3 correlates the kinetic

energy after a generic number of collisions with the initial kinetic energy and therefore with the position, what is neglected here is the particular energy loss due to the all pathways of the electron for reaching the final position. In other words the system is assumed to be partially conservative. The energetic diagram of figure 4.5 may help understanding the energy loss mechanism.

4.3.4 Initial conditions

Now that all the terms of equation 4.23 have been defined, in order to start a simulation some initial conditions must be chosen. The choice of the initial spacial distribution is rather natural since the motion of the electrons is studied from the surface of a device which is set as the origin on the x axis. All the electrons are placed in the same position $x = 0$, a condition that can be expressed as a Dirac distribution.

$$f_{x,0}(x) = \delta(x), \qquad x \in [-\infty, +\infty] \tag{4.27}$$

The direction of the initial velocities differs from the expression 4.3.3 since they must be directed in the positive direction in order for the electron to be effectively emitted. Furthermore as a consequence of the fact that most of the emitted electrons are expected not to have been scattered inside the metal, their directions will rarely be parallel to the surface of the device. The perpendicular direction is preferable instead. The assumption here is to consider a Wigner semicircle distribution defined on the positive axis: equal to the previous one but with double amplitude. A correcting factor takes into account the stronger exponential attenuation the electrons suffer when they propagate through the metal for non-perpendicular trajectories.

$$f_{\upsilon,0}(\upsilon) = \frac{4}{\pi}\sqrt{1-\upsilon^2}\,\upsilon_0 \exp\left(-\frac{\mathrm{L}_{metal}}{\upsilon\lambda_{metal}}\right), \qquad \upsilon \in [-1, 1] \tag{4.28}$$

where L_{metal} is the thickness of the metal layer, λ_{metal} is the mean free path of the electron in the metal, υ_0 is a constant which must be added in order to normalize the all distribution.

4.3.5 Iterations and transmission probability

In order to derive the spatial distribution of the electron after the collision $f_{x,i+1}$ starting from the typical distributions of the collision i: $f_{x,i}(x_i)$, $f_\upsilon(\upsilon)$ and $f_t(t)$. The

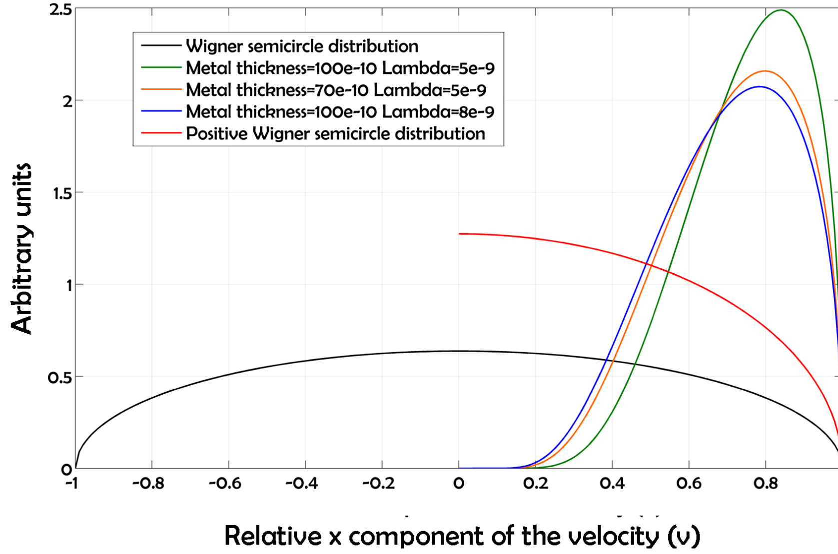

Figure 4.6: *The Wigner semicircle distribution is plotted. The black line refers to the standard semicircle distribution also defined on the negative axis and representing the isotropic collisions. The red line refers to the same distribution when only defined on the positive axis. Since this distribution would be unrealistic for the electrons escaping the metal a correction factor is added. For thinner metal layers the attenuation of the emitted current is lower and the differences due to the deviation of the electron trajectories from the perpendicular one is less strong. The same effect is seen when the mean free path of the electrons is increased.*

joint distribution of these three variables must be found. Since they are independent, the joint distribution is given by the product of the three.

$$\mathrm{F}(x_i, \upsilon, t) = f_{x,i}(x_i) f_\upsilon(\upsilon) f_t(t) \tag{4.29}$$

it is a function of three variables and describes the probabilities of all their possible combinations. The normalization of the three marginal distributions ensures the normalization of F:

$$\int_{-\infty}^{+\infty} \int_{-1}^{1} \int_{0}^{+\infty} \mathrm{F}(x_i, \upsilon, t)\, dx_i d\upsilon dt = 1 \tag{4.30}$$

As a consequence of the fact that for each choice of these three variables the final position x_{i+1} is given by the deterministic expression 4.23, the joint distribution may be also expressed as a function of x_{i+1} and other two variables arbitrarily

chosen among x_i,υ,t. The simplest choice is to express it as a function of x_{i+1},υ,t:

$$F(x_{i+1}, \upsilon, t) = f_{x,i}\,(x_i(x_{i+1}, \upsilon, t))\, f_{\upsilon}(\upsilon) f_t(t)\, |J(x_{i+1}, \upsilon, t)| \tag{4.31}$$

Where J is the Jacobian matrix describing the change of variables: υ and t are unchanged thus $J = \frac{\partial x_i}{\partial x_{i+1}}$ and it is also a function of x_{i+1},υ,t. Finally the marginal distribution of the variable x_{i+1} is achieved integrating the joint distribution over the other two variables.

$$f_{x,i+1}(x_{i+1}) = \int_{-1}^{1} \int_{0}^{+\infty} F(x_{i+1}, \upsilon, t)\, d\upsilon dt \tag{4.32}$$

This formula represented the central part of the matlab coding. It allows to effectively perform the iterations and to simulate the effect of collisions. The deterministic trajectory of the electron between collision is contained in the partial derivative of the Jacobian. An example of the evolution of the curves is shown in figure 4.7. In order to determine the transmission probability from the evolution of the spatial distribution of the electrons boundary conditions are added. After each collision the portion of the distribution $f_{x,i+1}$ extending inside the metal of the device, in the negative part of the x-axis is canceled. This part of the distribution represents the probability that after each collision the electrons have been backscattered into the metal. The assumption consists of neglecting the probability of double scattering events: first from the gas phase into the metal and later from the metal into the gas phase again. As already discussed in the previous chapters the energy lost in the scattering events in the metal is expected to be high and it should rarely allow the electrons to reach the vacuum level. The second boundary condition concerns the second metal surface, the one of the collector. Also in this case after each collision the portion of the spatial distribution extending beyond the position d is canceled and added to the total transmission probability.

4.4 Comparison with the experimental results

In this section the model described in the rest of the chapter will be compared with some of the experimental results. In chapter 3.1 and especially in figure 3.2 a different transmission probability was observed for different bias voltages or better for different kinetic energies of the emitted electrons. A higher transmission probability was found for the less energetic electrons emitted at lower bias voltages. This

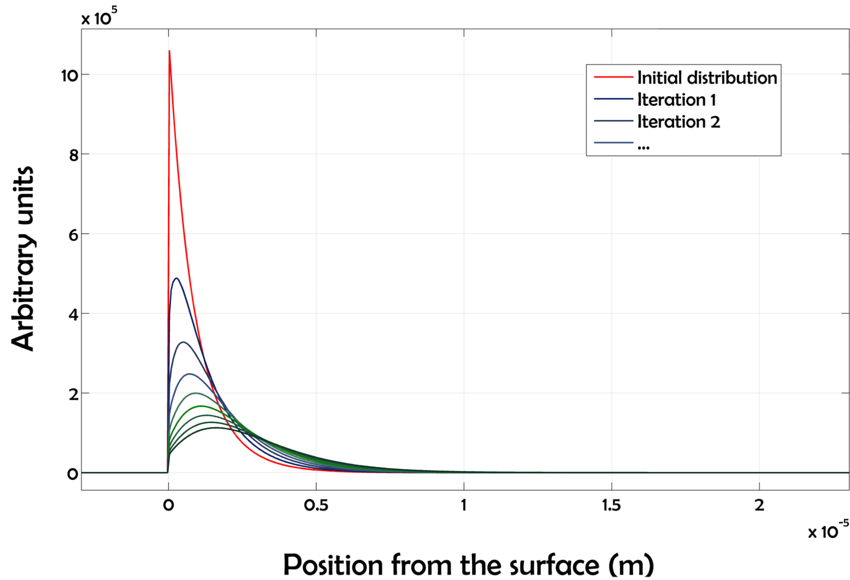

Figure 4.7: *The evolution of the electron distribution in the first iterations is illustrated. The red line refers to the distribution of electrons after exiting the metal, when they are subjected to the first collision. The other distributions refer to the eight following iterations. It has to be noticed that the evolution of the curves does not represent an evolution in time but only an evolution with respect to the number of collisions. The main variation from one iteration to the other one is due to the initial velocity of the electrons which spreads the distribution. The effects of the acceleration may be only noticed after a conspicuous amount of iterations. Nonetheless the suppression of the backscattered tails of the distribution, on the negative part of the x-axis, moves the average position far from the metal surface.*

could seem counterintuitive since such electrons own a lower kinetic energy.

4.4.1 Emission as a function of the electric field

A further investigation of such phenomenon was performed in a different experiment. The bias voltage applied across the device is kept constant while the collector voltage is varied. In this way the accelerating electric field is also varied and the results are compared with the model at the correspondent ε/p ratios: the distance from the device to the collector is equal to $d = 0.5mm$. The measurements were taken in air so that the pressure is constant and equal to $p \approx 1000mbar$. Under these conditions the applicability of the model proposed by Huxley and Zaazou in section 4.2.4 is expected to be valid: the calculation of the Townsend factor predicts values of $k_\mathrm{T} = 1$ for a zero electric field which is obvious since the electrons

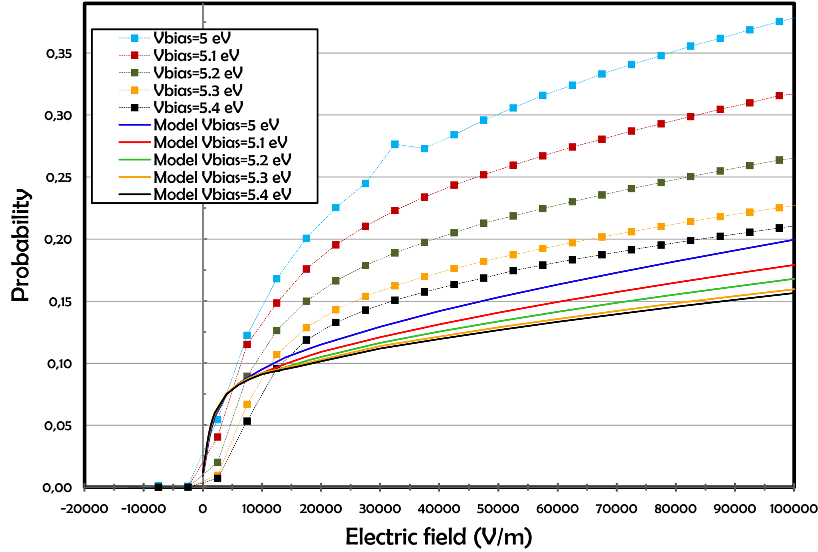

Figure 4.8: *Five measurements of emission as a function of the electric field are plotted. The values have been normalized with respect to the values of the emission current in vacuum at the same bias voltages; in this way they can be compared with the transmission probabilities estimated by the model. The five curves achieved from the simulations are also shown. The shape of the curves manifests similar trends: for low electric fields the probability increases fast. At higher values the slope reduces. Despite the model predicts in general lower probabilities a similar dependence on the applied bias voltage is observed. It is believed that the lower transmission probability for higher bias voltages is due to the higher velocities of the electrons which enhance the probability of being backscattered in the metal.*

will not be accelerated and at the steady state their mean energy will be the one of the thermal equilibrium. At the maximum electric field $\varepsilon = 100kV/m$ such factor becomes $k_T \approx 30$ according to equation 4.2.4, and the Townsend factor is still smaller than the assumed limit value of validity: $k_T < 40$.

In vacuum the dependence of the emission on the electric field is expected to be very low: this is effectively observed as far as the electric field do not become negative. Under atmospheric pressure the emission increases fast while passing from zero to about $10-20kV/m$, for higher voltages the slope of the curves reduces without a total saturation. The dependence on the voltage applied on the device can also be observed. As already mentioned before the lower the bias voltage the higher the transmission probability.

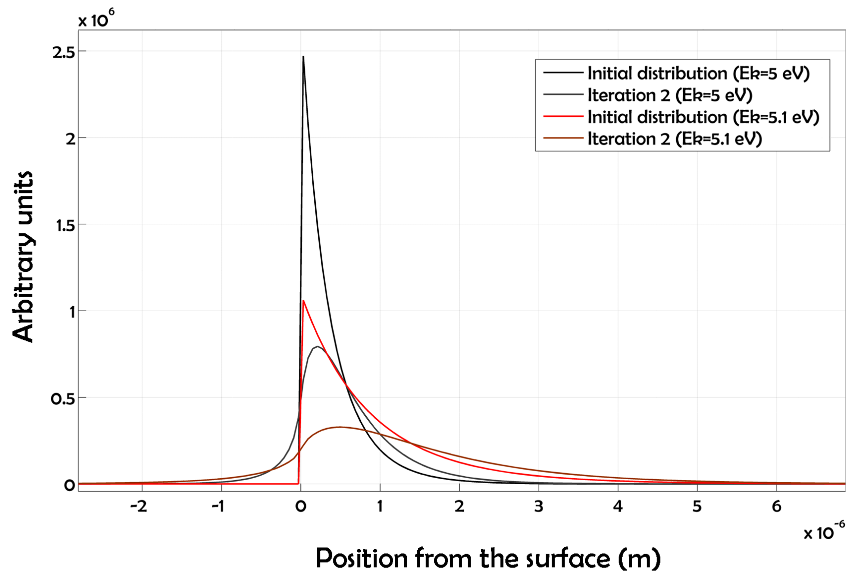

Figure 4.9: *Electron distributions from two different simulations. In the first one the initial kinetic energy of the electron with respect to the Fermi level in the metal is* 5eV*, in the second case it is* 5.1eV*. In both cases the initial distribution of the electrons and the distribution after 2 iterations are shown. When the kinetic energy is higher the distribution broadens faster and a bigger portion of it reaches the negative part of the x-axis. This means that the probability of backscattering will also be higher.*

In order for these curves to be comparable with the model, the currents have been normalized to the total emission current measured in vacuum on the same device at an electric field of $40kV/m$. A value that was proved to be largely enough for collecting the highest possible current in UHV. Figure 4.8 illustrates the comparison between the measured curves and the probabilities predicted by the model in the same range of electric fields and with the same pressure. Since the model predicts a certain probability given a certain value of kinetic energy and not directly from the applied bias voltage, a large amount of kinetic energies has been inserted in the model. Later the resulting probabilities have been transformed according to equation 4.17 where the spectra measured by PhD student Lasse Thomsen were used.

Although the results cannot be considered quantitative, good qualitative agreement is observed. The model underestimates the current of a factor of about 2. Nonetheless the shape of the curves resembles the measured ones. The passage between the initial rising regime and a successive saturation of the current is also

present and even sharper. This could be due to the losses due to geometry that may certainly affect the measurement at very low electric fields. Particularly the model predicts the dependence on the kinetic energy of the electrons and allows to understand the motivation for such behaviour.

The presence of a higher kinetic energy results in higher velocities; when deriving the equation of motion during collisions 4.23 it was already pointed out that as typical in diffusive problems the randomizing effect of the kinetic energy is stronger than the deterministic acceleration which always keep the same direction. When the electrons escape the metal higher energies result in a faster broadening of the spatial distribution. Therefore the probability of being scattered back into the metal before being moved away by the acceleration term is higher. Figure 4.9 shows two distributions from electrons at different energies after two iterations of the model.

4.4.2 Emission as a function of pressure

Another experiment which can be easily compared with the model consists in measuring the emission current as a function of the pressure. For this purpose the results obtained in chapter 3 varying the argon pressure will be used. These were taken at a constant collector voltage of $V_C = 12V$ at a distance of $d = 0.3mm$. Thus the electric field is constant and equal to $\varepsilon = 40kV/m$. The range of pressures was very broad: from UHV up to $1bar$. The value of the Townsend factor in this case becomes much higher than 40 for low pressures. For this reason the simulations have been performed in a range of pressures between $100mbar$ and $1bar$: for these values equation 4.2.4 predicts $k_T = 50$ and $k_T = 9$ respectively. The first value is higher than 40 but a comparison may still be interesting in order to observe the effective disagreement in this region. The measurements have been normalized with respect to the values of the current in UHV that in this case is already part of the measurement. A comparison with the probability predicted by the model with the same parameters is shown in figure 4.10.

Also in this case the model provides no quantitative agreement, the probabilities resulting from the simulation are remarkably lower. Nonetheless the shape of the curves is still similar apart from the behaviour in the low pressure range, in this region the rise of the probability is much slower than in the measurements. Instead, the dependence on the bias voltages is rather well described. Also in this case and for the reasons already described the transmission probability is enhanced for the less energetic electrons.

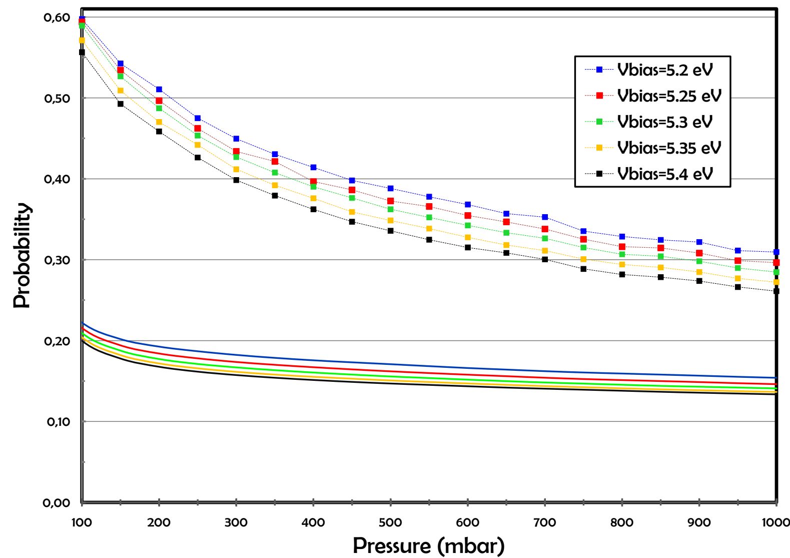

Figure 4.10: *The five measurements as a function of the pressure of argon already shown in figure 3.4 are plotted here after having been normalized with respect to their emission in vacuum. The predictions from the model are plotted with continuous lines. It estimates remarkably lower probabilities: more precisely a factor between 2 and 3. Nonetheless the shape of the curves still resembles the shape of the measured curves. In particular the dependence on the applied bias voltage is confirmed to be the same. Also in this measurement the probability is higher for lower kinetic energies. In the graph the condition* $k_T < 40$ *that was used for defining the model of section 4.2 is satisfied when the pressure is above* $200 mbar$.

4.4.3 Conclusions about the model

Summarizing, the model defined in the first sections of this chapter was able to describe qualitatively all the experimental evidences. A determination of a quantitative relationship between the emitted current and the measured current is still impossible. The high number of assumptions sometimes noticeably strong obviously lead to a high uncertainty: many different assumptions may be chosen and the model can be certainly improved.

Since the other kinds of electron losses have been ignored in the model the transmission probability would be expected to overestimate the current while here the opposite occurs. The reason of the low predicted currents must be found in the strong assumptions made; in particular the hypothesis of isotropic collisions,

probably good after a large number of collisions, may represent one explanation of these results which strongly depend on the very first scattering events. Non-isotropic collisions could force the electrons to reach a minimum distance from the metal surface before being backscattered in the metal: in fact their trajectory could need a minimum number of deviations before being inverted. At such distance the electric field would be much more efficient in determining their motion toward the anode, especially the effect of the image potential would be lower. Despite these limits and the possibilities of improvement, the presented method has the merit of providing an explanation for the observed increased transmission probability of low energy electrons. This is also a strong evidence of this kind of backscattering to represent one of the main kind of electron losses in the considered systems.

Chapter 5

Optimization of hot electron emitters

This chapter tackles the problem of hot electron emitters efficiency. Typically, as already shown in the previous chapters the emission curves are various orders of magnitude lower than the correspondent transmission curves. With the definition of efficiency provided in chapter 1:

$$\eta = \frac{I_E}{I_T + I_E} \tag{5.1}$$

the resulting efficiency rarely exceeds the value of 1×10^{-5} at $V_{BIAS} = 5V$. This is one of the main drawbacks compared to other kind of emitters together with the related low current density. For this reason various efforts have been made in order to enhance emission and efficiency. The most successful strategy concerned the devices that already manifest the higher emission currents, the devices with titanium (Ti) as wetting layer and gold (Au). The next paragraph is focused on the description of such structure. Other experiments related to the quest of new materials or to the work function lowering will follow.

5.1 Thickness of titanium wetting layers

As already mentioned before, the devices showing the highest efficiencies and emission currents have titanium and gold metal layers, hence the interest on this kind of metal gate. Although the presence of the titanium is necessary in order to achieve good contact between the gold and the rest of the MIS device, its presence introduces both problems in the characterization and undesired effects. Since the

titanium layer must be very thin in order to produce efficient devices, typical thicknesses are of the order of $L_{Ti} = 2-10$Å, the uncertainty on these values is very high. Therefore also the effects resulting from the titanium thicknesses can be hardly estimated.

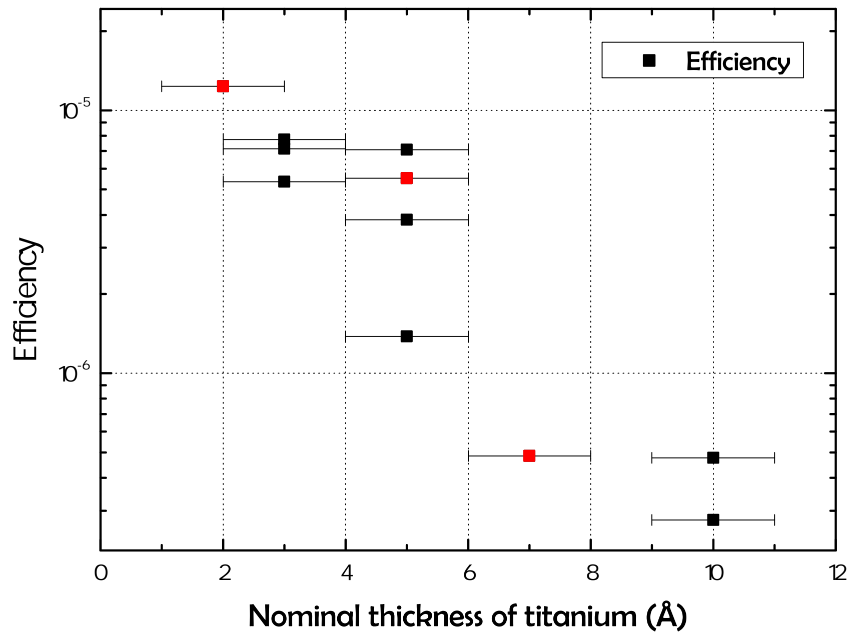

Figure 5.1: *The efficiencies measured on various devices with titanium and gold are plotted. The black data have been taken by PhD student Lasse Thomsen. The red data refer to measurements taken during this project. Since the devices of these last measurements had a* 100 *Å thick gold layer while for the others it was* $L_{Au} = 70$ *Å the red values have been normalized according to equation 5.2. Despite the large uncertainty due to the variability during the evaporation a clear trend can be identified: the titanium thickness must be minimized in order to achieve a high efficiency.*

Lasse Thomsen in his PhD thesis described the dependence of the efficiency on the titanium thickness. His data are shown in figure 5.1 together with some new data collected during this project. The old data have been achieved with various thicknesses of titanium and a constant thickness of gold: $L_{Au} = 70$Å. The new data have been measured on devices with a higher gold thickness, $L_{Au} = 100$Å. Nonetheless the effects of this difference can be predicted with a reasonably good accuracy since the mean free path of electrons in gold is rather well known both from liter-

ature and from experiments on hot electron devices: at 5eV a value of $\lambda_{Au} = 52\,\text{Å}$ is chosen [27, 28]. In order to compare the data the attenuation factor of equation 1.27 must be considered, the efficiencies are then related by:

$$\eta_{70} = \eta_{100} \exp\left(-\frac{70}{\lambda_{Au}}\right) \exp\left(+\frac{100}{\lambda_{Au}}\right) = 1.78 \times \eta_{100} \tag{5.2}$$

Such correcting factor produces much smaller effects than the ones due to the ti-

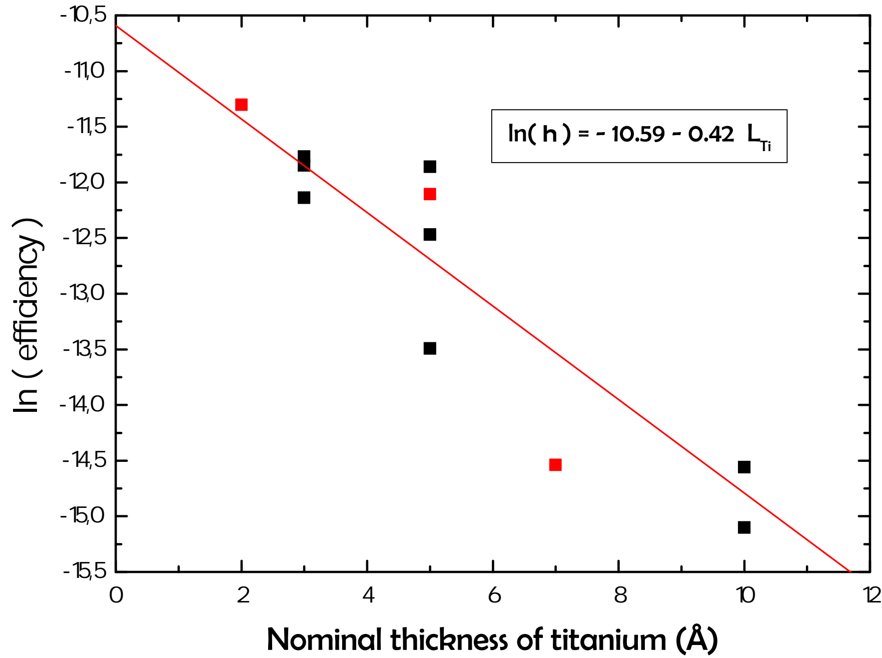

Figure 5.2: *The logarithms of the efficiencies in figure 5.1 are plotted as a function of the titanium thickness. Assuming that the only losses related to titanium are due to the thickness of this material, equation 5.4 allows an estimation of the electron mean free path in titanium. This is equal to the inverse of the slope of the linear fit shown:* $\lambda_{Ti} = 2.38\,\text{Å}$. *This value is too low and suggests the presence of scattering mechanisms related to the junction between titanium and gold.*

tanium as evident from figure 5.1, hence the possibility of a comparison. The presence of titanium dramatically reduces the emission efficiency leading to a drop of more than one order of magnitude while passing from $L_{Ti} = 2\,\text{Å}$ to $L_{Ti} = 10\,\text{Å}$. A wafer with a bigger titanium thickness, $L_{Ti} = 50\,\text{Å}$ did not even produce an observable emission above a background noise of $\approx 0.5pA$. This decrease is certainly due to the lower mean free path of electrons in the titanium layer. If the only effect of

the titanium layer on the emission current was to exponentially decrease the current with the thickness, the resulting efficiency would be:

$$\eta = K \exp\left(-\frac{L_{Ti}}{\lambda_{Ti}}\right) \exp\left(-\frac{L_{Au}}{\lambda_{Au}}\right) \tag{5.3}$$

passing to the natural logarithms it becomes:

$$\ln \eta = -\frac{L_{Ti}}{\lambda_{Ti}} - \frac{L_{Au}}{\lambda_{Au}} + \ln K \approx -\frac{L_{Ti}}{\lambda_{Ti}} - 1.34 + \ln K \tag{5.4}$$

With the choice $\lambda_{Au} = 52$ Å and the gold thickness $L_{Au} = 70$ Å while K takes into account other losses: mainly in the conduction band of the insulator. Therefore if the exponential attenuation of titanium and gold were the only effects of the metal layers on the efficiency a logarithmic plot would estimate the mean free path of low energy electrons in titanium. Nonetheless the logarithmic plot in figure 5.2 and the linear fit shown predict a titanium mean free path $\lambda_{Ti} \approx 2$ Å. Even with this high uncertainty this value is considered to be too low compared to other values expected from literature [49, 50] and some other phenomena should better explain the strong attenuation of the emission. The line intercepts the zero thickness axis at the value which is far from 1.34: this suggest that a large percentage of the electrons is scattered in the insulator before entering the metal.

From the previous considerations there is good evidence of the presence of other phenomena affecting the efficiency and particularly depending on the presence of titanium. A hypothesis consists in an enhanced scattering probability due to an electric scattering potential originated at the titanium gold interface, in the region where the different work functions meet each other.

5.2 Different materials

Theoretically, according to the description of hot electron emitters of chapter 1, every kind of metal should both permit the tunneling of electrons in the Fowler-Nordheim regime and also the emission of electrons. On the other hand different behaviours were predicted: these are mainly due to the value of the work function and to the mean free path of electrons. Focusing on the emission, the work function plays a fundamental role since it introduces a lower limit to the bias voltage needed to observe emission. The mean free path is also crucial since it causes an exponential decrease of the emitted current with respect to the metal thickness.

Therefore the possibility of freely choosing any kind of metal with the best com-

bination of work function and electron mean free path and consequently achieve a higher current was considered to be as a promising opportunity. Nevertheless the experiments demonstrated that there are many other variables playing a role on the functionality of the device which are not included in the theoretical model.

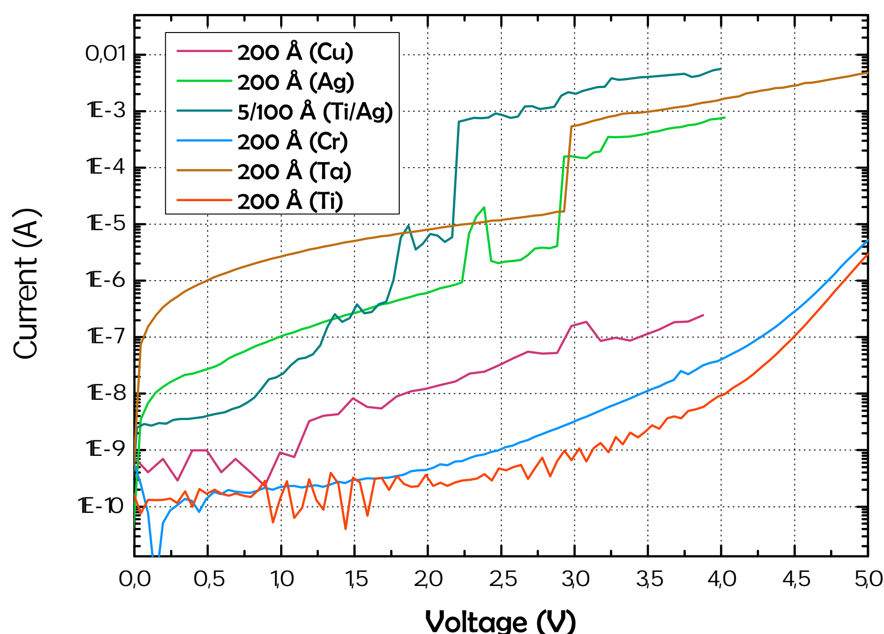

Figure 5.3: *Various IV curves from devices with different metal layers and belonging to different batches are illustrated. Of all these metals only titanium and chromium produced stable and durable devices. Most of the other materials deteriorate the oxide and cause the rapid breakdown: this is the reason why most of the curves are interrupted. For each metal the curves show typical breakdown voltages. Devices with tantalum were also breaking rather easily but the degradation of the oxide seemed to be slower and allowed to measure considerably high values of emission.*

The interest in employing hot electron devices in femtochemistry initially directed the choice towards the noble metals: despite the low efficiencies, platinum (Pt) and gold (Au) showed very good compatibility with the other components of the MIS structure and allowed a good characterization of the devices. Various other metals were tried both during this project and before but only a few of them lead to promising results. One of the variables can be effectively related to the reactivity of these metals: the surfaces of platinum and gold are rather clean even when exposed to air while various other metals will strongly oxidize. The formation of

an oxide layer on the surface of the devices may affect the emission enhancing the scattering probability, thus attenuating the current. The role of such thin oxide layer is probably comparable with the role of thin SiO_2 layer after the tunneling. In both cases the electrons, in order to be emitted, must propagate above the level of the conduction band of the oxide.

Nonetheless the main reason why most of the other metals did not allow to measure emission currents must be found elsewhere. Most of the metals seriously affect the electrical properties of the emitters inducing breakdown in the oxide. The physical principles determining whether a metal compromises such properties is still largely unknown.

In figure 5.3 some IV curves from devices with different metal layers are shown. Copper (Cu) and silver (Ag) layers were deposited because of the rather high mean free path and various similarities with gold. Silver is also noble compared to other transition metal, but both silver and copper always provoked breakdown. On the other hand titanium (Ti) and chrome (Cr), which are much more reactive, did not usually degrade the device and produced good IV curves but no emission, probably because of the low mean free path. Such reactive metals are expected to strongly bind to the silicon dioxide probably absorbing part of the oxygen and passivating. This phenomenon should enhance the durability of the device. Nevertheless aluminum (Al) was expected to manifest similar properties while it damaged the device in all previous measurements. Tantalum (Ta) was tried because of its work function: from literature it equals $\Phi_{Ta} = 4-4.8eV$ and a reasonably high mean free path. Emission was observed but sometimes breakdown occurred:the estimated work function was still high $\Phi_{Ta} = 4.9eV$ without noticeable improvements with respect to gold.

5.3 Work function lowering

The most promising technique for improving the efficiency of hot electron devices consists in lowering the work function of the metal surface. The idea is to deposit a very small amount of a metal with a low work function on top of the metal gate. The resulting work function is usually lower than the one of the first metal and in many cases close to the low work function of the metal on top. Typically one monolayer of metal is sufficient for ensuring such decrease. The advantage of this method, compared for instance with the simple deposition of a single metal, is dual; on one side the work function is lowered and only in proximity of the sur-

face. This is an advantage because a single metal with a lower work function would emit electrons at lower voltages but also its IV curve would be shifted. Thus the efficiency in this case would not be enhanced considerably. The second advantage relates to the possibility to combine a low work function with a long electron mean free path since there are no particular restrictions on the chosen metal gate.

Since the high values of the mean free path for gold and platinum are known and they also ensure a good durability of the MIS devices limiting the degradation of the oxide, the idea was to lower the work function of these two metals.

A first try was made by PhD students Lasse Thomsen and Gunver Nielsen: they tried to deposit Cesium (Cs) on a gold (Au) film. The choice was natural since alkaline metals are characterized by a very low work function: $\Phi_{Cs} = 2.14eV$ and $\Phi_{Na} = 2.36eV$. Furthermore they have successfully been used many times in literature [5, 51, 52] with this purpose. With the deposition of about one monolayer on a 70 Å thick gold film the work function shift was effectively observed and emission was measured for $V_{BIAS} > 2V$. Nonetheless the presence of such small amount of cesium was sufficient to compromise the oxide and also the IV curves were much higher in current. At a bias voltage of $V_{BIAS} = 3V$ an extremely high efficiency was measured $\eta = 0.08$, about four orders of magnitude higher than the typical values, but the breakdown of the device was reached shortly [53]. The influence of the cesium monolayer on the quality of the oxide is probably due to the presence of cesium at the insulator-metal interface, probably due to the diffusion of cesium through the gold layer. The possibility of cesium to alloy with gold is known from literature [54].

During this project a similar experiment was performed; because of the suspected high mobility of alkaline metals a silver (Ag) layer was deposited on platinum. Since the work function of silver is $\Phi_{Ag} = 4.5 - 4.7eV$ the expected work function was not extremely low: the idea was to lower the work function of platinum in a controlled way in order to demonstrate the potentialities of this technique without compromising the durability of the device. Furthermore the other properties of silver are particularly promising: the mean free path is expected to be high and the reactivity lower than most of the other transition metals [28, 49]. Some of the results obtained from this wafer are shown in figure 5.4 and compared with the IV and emission curves of a platinum film without silver. The measurements shown, being aimed at testing qualitatively the quality of the devices were taken in air.

Some devices effectively produced emission at $V_{BIAS} \approx 4.5V$ in agreement with the expected value of Φ_{Ag} and the emission was higher than for clean platinum.

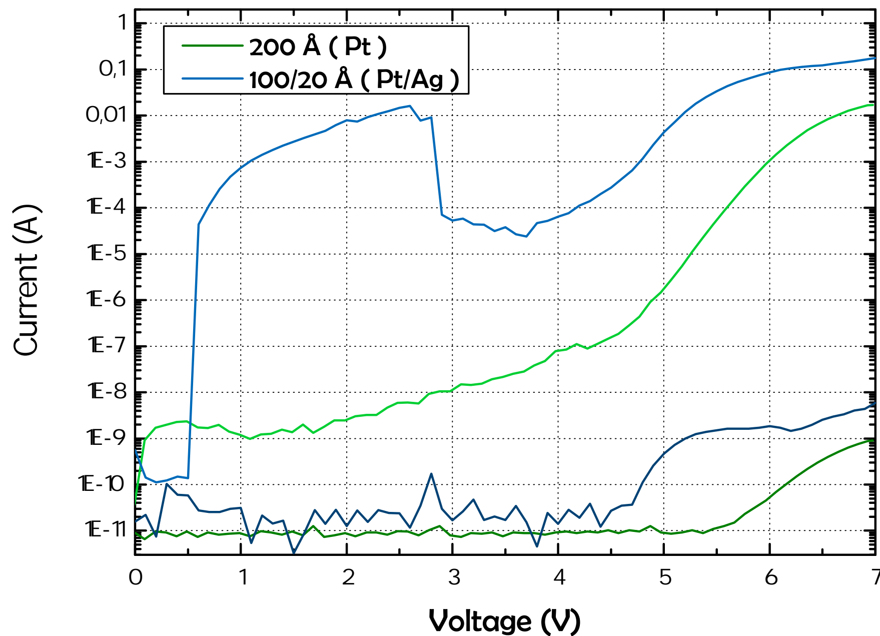

Figure 5.4: *Comparison between the IV curves and emission curves of devices with platinum. The green lines refer to* 200 Å *of clean platinum while the blue ones refer to* 100 Å *of platinum covered with* 20 Å *of silver. The colors are slightly darker for the emission curves. The higher emission current from the device with silver is evident at low voltages where the lower work function is in agreement with the values for silver* $\Phi_{Ag} = 4.5 - 4.7eV$. *At higher voltages the emission is still higher but it could be explained by the lower thickness of the metal layer. The transmission current is also much higher: such high currents may cause a noticeable voltage drop on the gate metal. This can be the explanation for the apparent saturation of the emission current just above* 1 *n*A. *The strange drop of the transmission current around* $V_{BIAS} \approx 3V$ *is a proof of the oxide to be damaged and probably corresponds to a conductive channel closing.*

However the success of this experiment is only partial: the IV curves are always much higher suggesting that silver also affected the oxide quality. In some cases it seemed to shift the IV curve to lower voltages, in other cases it simply caused breakdown.

Chapter 6

Time dependence of emission and durability

In order to be able to successfully employ the hot electron emitters in any kind of application, both concerning the possibility to enhance the surface reactivity and the possibility of replacing other kinds of emitters, the durability of the devices is essential. In the first case a long stable production of hot electrons is necessary in order to detect reactions at the surface, in the second case it is even more fundamental since most of the other electron sources are used for long times.

In chapter 5 examples of IV curves showing the breakdown of the oxide were already provided. Those were referred to particular metals which turned out to deteriorate the thin oxide layer. Nevertheless also the hot electron emitters made with platinum (Pt) or gold (Au), devices which are normally used in the experiments can be easily broken if high bias voltages are applied. The ultra-large area of the thin oxide threatens their resistance to voltages higher than about $V_{BIAS} > 6V$. Various studies have been directed towards the determination of the processes leading to the breakdown of silicon oxide, particularly the effect of hot electrons has been investigated [55, 56]. In general for these devices the breakdown is not sudden but it occurs gradually or typically in steps that are believed to correspond to subsequent activations of micro-conductive channels in the oxide. In this chapter the durability of the devices is investigated with a special reference to the prospect of employing them as the electron source of a mass spectrometer. This last opportunity will be then tested in the last chapter of this thesis.

6.1 Time evolution of the IV curves

This section aims at describing qualitatively how the electrical properties of the emitters evolve in time. As already mentioned most of the devices made with a titanium wetting layer and a gold film deposited on it do not break suddenly but in a progressive way. This feature has been clearly observed while measuring IV curves repeatedly. Figure 6.1 furnishes an example of this kind of measurement. After the first IV curve further measurements increase the current rapidly: in order

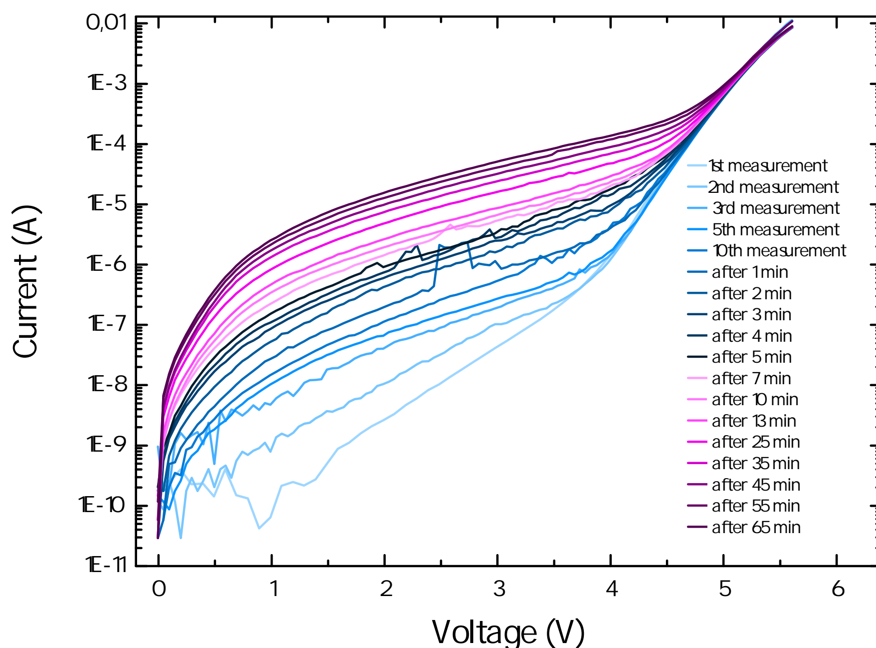

Figure 6.1: *Various IV curves were taken in air on the same device. The plot shows the evolution in time of these curves. After the tenth IV curve a bias voltage* V_{BIAS} = 5.2V *is applied for a certain amount of time between one IV curve and the succeeding one. In this way a faster deterioration of the oxide is induced. The time reported in the legend is the total application time of such potential. The transmission current continues increasing probably because of the activation of micro-conductive channels. This hypothesis is supported by the steps appearing sometimes in the IV curves: these would represent bigger channels which may randomly be opened or closed.*

to fasten this raise, after 10 IV curves a constant bias voltage is applied across the MIS structure for an increasing amount of time. At high voltages V_{BIAS} > 5V the tunneling current in the Fowler-Nordheim regime is still dominant after more than

one hour of applied bias and no big variations in the current may be observed. The stability of this current and the presence of emission for all these curves suggests that the two parallel transport mechanisms coexist: the tunneling current on one hand and a conductive mechanism on the other one. This conduction is believed to be due to micro-conductive channels opening through the oxide.

6.2 The repairing role of oxygen

In chapter 3 the unexpected shape of the emission curves appearing while measuring in vacuum was described. The presence of an emission current $I_{E,low}$ at bias voltages much lower than the work function of gold or titanium was found and not completely explained. It was suggested that such current should be a consequence of a modification in the structure of the device nearby the insulator-metal interface. Further elements which could facilitate the description of this phenomenon are obtained when the correspondent IV curves are also considered.

In figure 6.2 various emission curves have been plotted together with their IV characteristics. In vacuum after a very few measurements the emission current at low voltages $I_{E,low}$ starts to increase. This also happens at the same time and in the same range of voltages for the IV curves. The fact that these peculiar shape always appear at the same time in both measurements and that in both cases, even more strangely, it seems to decrease for higher voltages is an evidence of their correlation. Typically, after several measurements this hump in the transmitted current grows so much that the current exceeds the maximum current that can be supplied by one of the instruments in the experimental setup. The durability of the devices under vacuum appears to be lower.

Nonetheless when the devices are brought back to air both these phenomena disappear: as soon as they are removed from the UHV chamber the emission current $I_{E,min}$ vanishes together with the atypical part of the transmission current. This clearly suggests that the oxygen in air is able to repair the devices or at least to cancel the modifications that occurred in vacuum. This effect seems to need several hours for being completed since both the currents continue decreasing slowly for 20 hours. Especially the emission current that just after exposition to air was very similar to the emitted current above a bias voltage $V_{BIAS} > 5V$, slowly reaches the same intensity as before entering the UHV chamber. This is also probably the result of the oxidation of a certain portion of the surface of the device. Summarizing, even if the transport mechanism being responsible for the increased emission

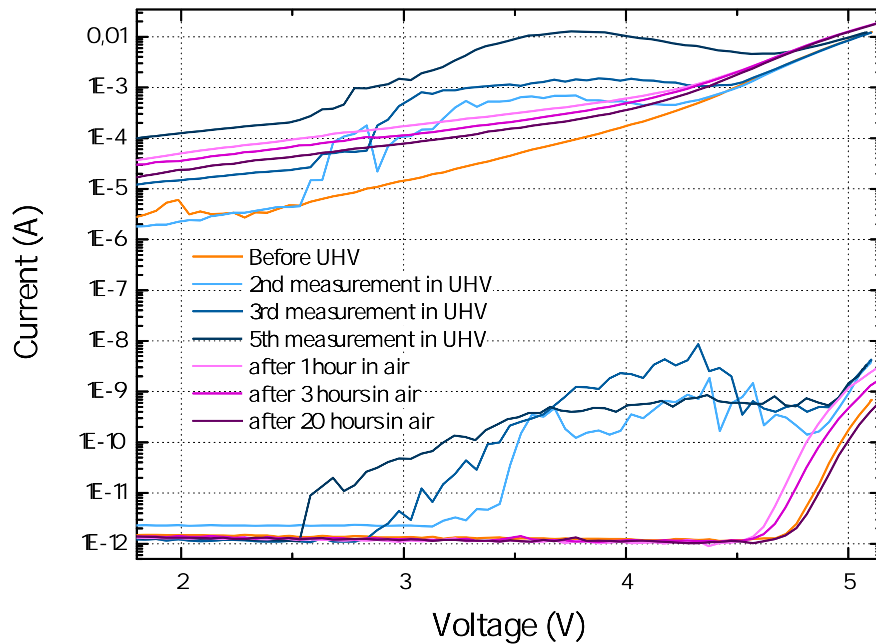

Figure 6.2: *The orange lines represent a normal IV curve and emission curve measured on a device in air. These two curves are used as a reference for studying the variations occurring in UHV. When the device is put under vacuum conditions subsequent measurements show an enhanced emission current. This is particularly evident in the low voltage range* $2.5\text{V} < V_{\text{BIAS}} < 4.5\text{V}$ *where no emission was seen in air. Almost in the same range of voltages also the transmission current increases. The reproducibility of this phenomenon on other devices and in the same range of voltages supports the idea that these currents are related and probably due to a tunneling mechanism. When put back into air the low voltage emission disappears and both currents start decreasing. A repairing effect due to the presence of oxygen is considered to be the explanation for such behaviour.*

and transmission currents in vacuum is not completely understood, the presence of oxygen seems to protect the device from deterioration.

6.3 Durability

In order to employ the MIS devices as electron emitters in any kind of application the capability to emit electrons without a complete breakdown of the oxide is not the only requirement. A rather stable and constant emission is also necessary, for this reason the time dependence of transmission and emission currents will now be investigated. In order to perform such analysis a constant bias voltage

has been applied across the devices: both the transmitted and emitted currents were measured at uniformly distributed intervals of time. The transmission current provides important information about the deterioration of the oxide. The first measurements were taken in air and the device lasted for various days even been subjected to $V_{BIAS} > 5.2V$. The total duration of each measurement was 20 hours: two curves from the same device but with different applied voltages are shown in figure 6.3. Apart from an initial transient which is often observed and lasts one or

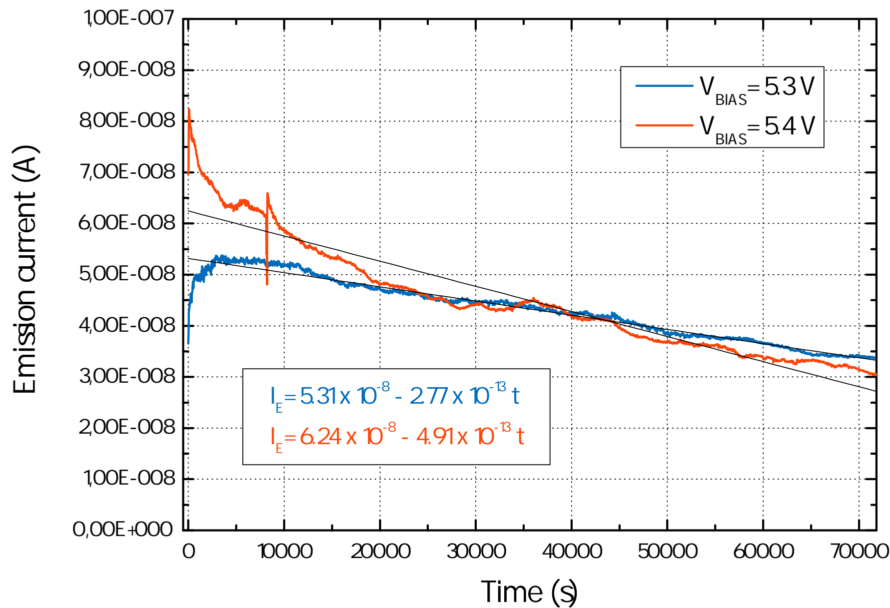

Figure 6.3: *The emission of a device, measured in air, is plotted as a function of time. The high durability of the device allows to take two measurements 20 hours long each. The first time a bias voltage of* 5.3V *is applied, the second time the voltage is higher:* $V_{BIAS} = 5.4V$. *The decrease of the current is not dramatic since they are lowered of a factor of about* 1/3 *during the first measurement and about* 3/7 *during the second one. Despite some noise, after a transient of about 2 hours the trend is rather linear and a fit is shown. Expressing the time in hours the decrement rates are:* $-1nA/h$ *at* $V_{BIAS} = 5.3V$ *and* $-1.8nA/h$ *at* $V_{BIAS} = 5.4V$. *As expected the higher the voltage the faster the deterioration. The relative decrement rate, which can be more interesting, leads to the same conclusions: respectively the values are* $-1.9\%/h$ *and* $-2.8\%/h$, *the calculation is made by dividing the previous rates by the initial values of the currents.*

two hours, the emission decreases at a rather constant rate: this is estimated in the figure through a linear fit. When the bias voltage is higher the modulus of the rate increases as expected. In figure 6.4 the analysis of the transmission is in agreement

with these results since the currents increase linearly demonstrating the degradation of the oxide: also in this case the rate is higher for larger V_{BIAS}. If the two

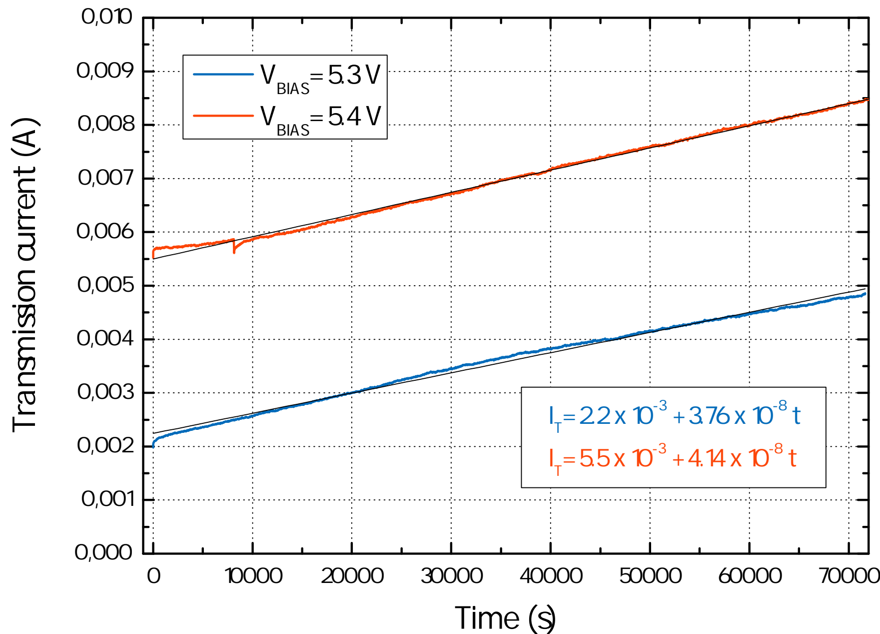

Figure 6.4: *The transmission currents corresponding to the measurements of figure 6.3 are shown with a linear fit. The increment rate is very stable as pointed out by the good linearity of the curves. The deterioration is faster for higher bias voltages as stated by the increment rates:* $+0.13 mA/h$ *at* $V_{BIAS} = 5.3V$ *and* $+0.15 mA/h$ *at* $V_{BIAS} = 5.4V$.

transport mechanisms, the tunneling and the conductance induced by activated micro-channels, are effectively independent and they occur in parallel, then the linearity of the curves could suggest a constant decrease of the portion of the active area interested by tunneling. The rest of the active area would be responsible for the transmission current.

As described in the previous section the effect of oxygen in air may be important for the durability of the devices; therefore in order to have a real estimate of the amount of time the devices will be able to emit in a mass spectrometer, the measurements of figures 6.3 and 6.4 should be also taken in UHV. The comparison could give important information about the effective role of oxygen. Here one measurement in vacuum is presented, nonetheless the presence of a higher current passing through the device makes the comparison difficult: other, more reliable

measurements, should be taken. As a matter of fact the high initial value and the fast increase caused the transmission current to reach a value close to $20mA$ about 3 hours before the end of the measurement. At such value one of the instruments of the experimental setup reaches the compliance limit, thus the unexpected shape of the curves. As apparent from figure 6.5 the emission current decreases slightly faster than in the previous measurements at the same applied voltage $V_{BIAS} = 5.3V$. Furthermore the transient time is bigger: only after 6 hours the decrease seems to become linear.

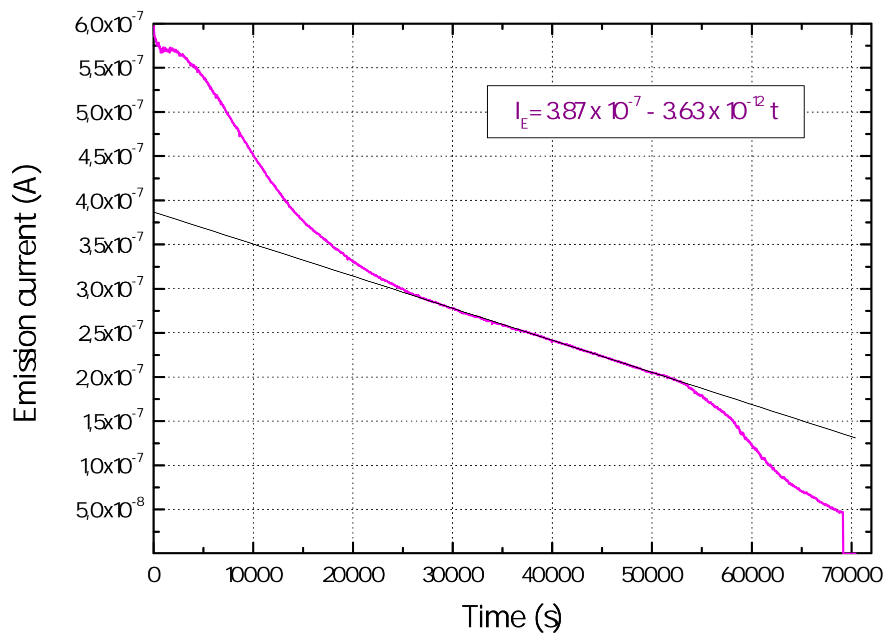

Figure 6.5: *The emission is measured as a function of time in UHV for a total duration of 20 hours. The applied bias voltage is* $V_{BIAS} = 5.3V$. *Initially the emission decreases fast until a linear behaviour is reached: this happens after about 6 hours. A linear fit in this region (between* 35000 *and* 52000 *seconds) predicts a decreasing rate of* $13.1nA/h$ *or a relative decreasing rate of* $-3.4\%/h$. *Althought these values considering the whole shape of the curve are considered to be a lower limit of the effective rate, a comparison with the results achieved in air 6.3 seems to support the hypothesis of a faster decay in UHV. Nonetheless the initial transmission current shown in figure 6.6 is very high: it can also be a reason for a faster deterioration of the device. The fast decay and the total drop of the emission current in the last hours of measurement is due to the transmission current reaching the compliance current of the circuit. Despite the uncertainties of the measurements on this device, the possibility of substaining a considerable current for several hours also in UHV is confirmed.*

The considerations concerning the transmission current are similar, also in this case the transient is very long, an almost linear shape is reached after 10 hours and in the first 3 hours the current decreases considerably. In figure 6.6 a fit of the linear part of the curve suggests an increasing rate much higher than before but the long transient makes this estimate unreliable. Even though these two measurements do not allow a quantitative determination of the variation of the currents as a function of time, they provide a good evidence of the possibility of having a relevant emission for several hours. They also justify the idea of testing the capability of hot electron emitters to substitute a filament in a mass spectrometer. The description of such experiment will be given in the next chapter.

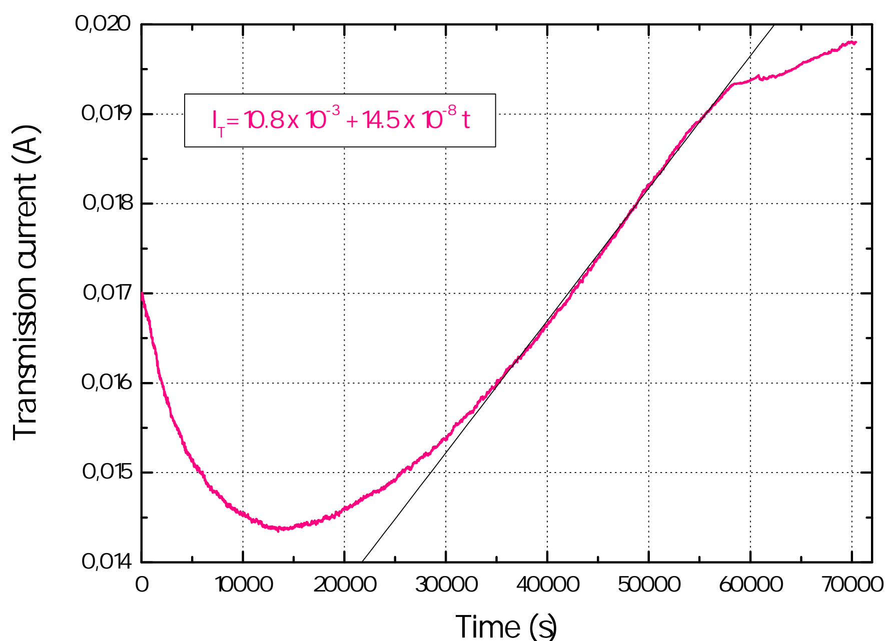

Figure 6.6: *The transmission current corresponding to the emission measurement of figure 6.5 is shown:* $\mathrm{V_{BIAS}} = 5.3\mathrm{V}$. *The current is particularly high as a consequence of a probable damaged oxide. For a long time after the beginning of the measurement the current decreases and only in a second moment after about 10 hours it approximates an increasing line which resembles the other measured trends as in figure 6.4. The saturation of the current in the last 3 hours of measurement is due to the transmission current reaching the compliance current of the instruments. The increasing rate in the same linear interval of figure 6.5, namely between* 35000 *and* 52000 *seconds, is estimated to be* $0.5m\mathrm{A}/h$, *considerably higher than in air.*

Chapter 7

Hot electron emitters for mass spectrometry

This last chapter provides a description of the first measurements of a mass spectrometer whose traditional electron source has been replaced with a hot electron emitter. As illustrated before in the rest of this thesis the best emitters fabricated till this moment were realized with a titanium (Ti) wetting layer and a gold (Au) thin film on it. For this reason the most promising device was chosen to be a device with 2 Å of titanium and 100 Å of gold: the correspondent IV curve and emission curve is shown in figure 7.1. In order to produce electrons in the mass spectrometer a constant bias voltage is applied, therefore the IV curve gives important information for the choice of such voltage. For this device emission was measured to exceed 1µA for $V_{BIAS} > 5.6$V. Beyond the values of the emission current it is important to choose a bias voltage which does not generate an excessively high transmission current: otherwise the deterioration of the device would be too fast.

In chapter 6 the time evolution of the currents was studied and demonstrated the possibility for the devices to run for many hours at a bias voltage $V_{BIAS} \approx 5.4$V. In order to achieve better spectra this bias voltage is chosen to be higher, typically $V_{BIAS} \approx 6.2$V, nonetheless there is still a good evidence for the devices to last a considerable amount of time. The time needed for achieving a spectrum is of the order of half a minute, thus the durability of the device should not represent a problem if a modest number of spectra are acquired. The current of electrons produced by a traditional filament in a mass spectrometer is usually of the order of $1-2m$A but this current can be lowered of about two orders of magnitude and the mass spec-

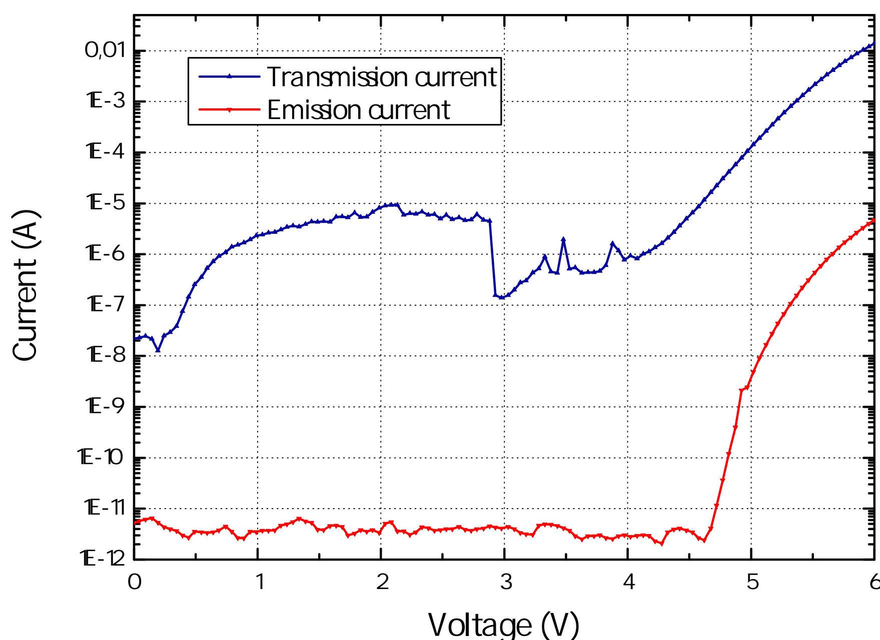

Figure 7.1: *IV characteristic and emission current of the device employed in the mass spectrometer. The emission current is particularly high and close to* 5µA *at* 6V*. At* V_{BIAS} = 6.2V *namely the voltage used for emitting electrons while measuring the spectra the emission is probably close to* 10µA.

trometer still works.

7.1 Preparation of the mass spectrometer

The operational principles of a mass spectrometer are shortly summarized; classically a current flows through a filament which heats up and emits electrons by thermionic effect. These electrons are accelerated by the positive voltage applied to an anode till they reach kinetic energies of the order of $E_K = 70-100eV$. At these energies the probability to ionize the gas molecules with collisions has a maximum. The ionized molecules inside the UHV chamber are then accelerated into a quadrupole analyzer by a high voltage of about $16-20kV$. The quadrupole analyzer consists of four rods used for applying radio frequency electric field. The trajectories of the ions are deflected as a function of the ratio M/e: where M is the mass of the ion and e is the electron charge. By tuning the electric field the transferred ions can be selected allowing to distinguish between the correspondent molecules of

the chamber. A Second Electron Multiplier (SEM) amplifies the ion currents which are finally measured by a detector.

In order to acquire a spectrum with a hot electron emitter source some countermeasures had to be taken. In order to place the device in proximity of the traditional filaments, in a position that allows the electrons to be accelerated by the anode, the mass spectrometer was modified by Professor Martin Johansson. A holder was placed just in front of the anode so that the electrons emitted from the surface of the device can be directly accelerated. At the same time the mass spectrometer can be run with a normal filament. A comparison between the spectra obtained from the two sources can be easily performed. Nonetheless the security controls of the mass spectrometer forbid to take measurements if the filament is not emitting, hence the necessity to skirt the obstacle. Three terminals of the mass spectrometer, which normally apply a voltage across the filament and measure the emission current at the anode, were connected to another filament previously placed in a second chamber of the UHV setup. Such filament does not influence the measurements. Finally, in order to maximize the probability of ionization and to better compare the spectra with the two sources, the acceleration voltage needed to be adjusted. When the traditional filament is used the voltage at the anode is measured to be 105V while the filament is kept at a potential of 35V with respect to ground. Therefore also the potential of the surface of the device was shifted to 35V to ensure the same conditions and particularly the same acceleration voltage of 70V.

7.2 Experimental results

When the UHV chamber has not been baked and the internal pressure is measured to be $p = 9 \times 10^{-9} torr$, the mass distribution of molecules as measured by a mass spectrometer with the traditional filament appears as in figure 7.2. The position of the main peaks with the correspondent gases is summarized in table 7.1.

The first measurements with a hot electron emitter at $V_{BIAS} = 6.2V$ produced a similar result even though the signal is about two orders of magnitude lower. In figure 7.3 the shape of the spectrum is certainly recognized, nonetheless a more careful analysis would show relevant differences in the relative height of the peaks. This difference could be partially explained by the effect of the outgassing due to the high temperature of the filament. The remarkable amount of water and other molecules in a chamber which was not baked can magnify this effect.

Table 7.1: Position of the main peaks appearing in the acquired mass spectra. The masses are associated to the most probable molecules being present in the chamber.

Mass (amu)	Molecules
2	H_2
12	C
16	CH_4, CO_2
17	H_2O
18	H_2O
20	Ar
28	N_2, CO
32	O_2
40	Ar
44	CO_2

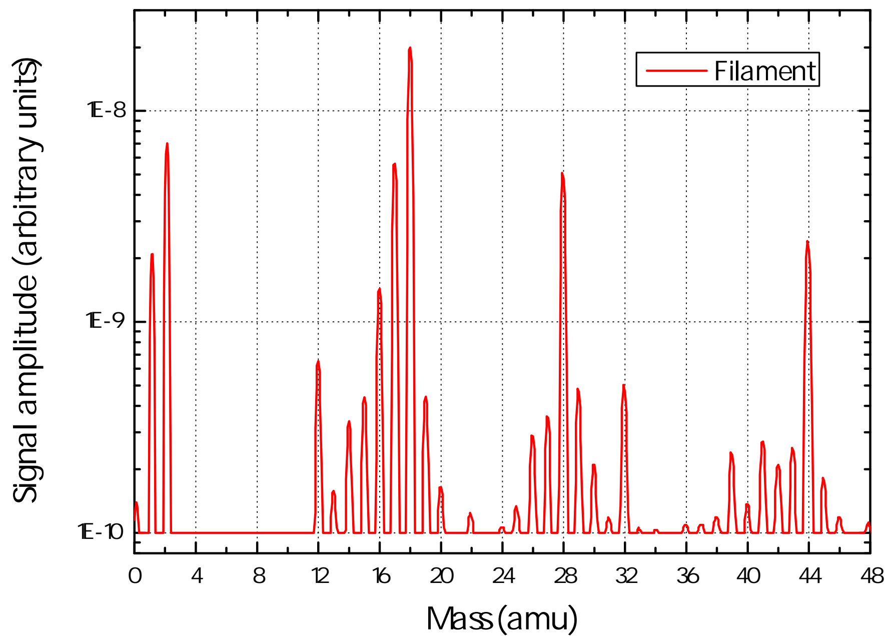

Figure 7.2: *An example of mass spectrum using a traditional filament. The main gases occupying the chamber can be deduced from table 7.1.*

In order to make a real comparison a fixed pressure of argon was dosed inside the chamber and the amplitudes of the measurements were normalized to the ref-

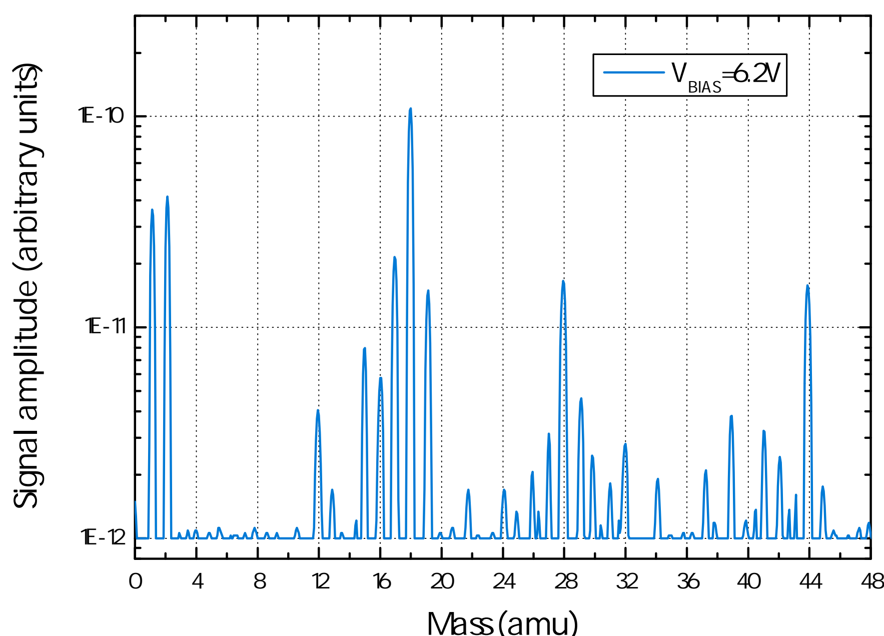

Figure 7.3: *A mass spectrum obtained with the hot electron emitter source. All the main features and peaks reflect the ones of a traditional spectrum, but the relative height of the peaks is different with respect to figure 7.2. Especially the peaks of hydrogen at* $\mathrm{M} = 2$*, of CO at* $\mathrm{M} = 28$*, of* CO_2 $\mathrm{M} = 16, 44$ *and of water* $\mathrm{M} = 17, 18$ *here seem to be lower with respect to the others. These gases desorb easily by increasing the temperature hence the hot filament could be the origin of this disagreement.*

erence value of the argon. Furthermore the emission current of the filament has been lowered to its minimum value, approximately $0.1\,m$A: the maximum current is about $1\,m$A. All this range of currents allows the mass spectrometer to operate well, however high currents produce a higher signal amplitude and a better signal to noise ratio. Since the interest here was not to measure the effective difference of noise but to compare the shape of the spectra using the two sources and the relative height of the peaks a lower current from the filament is preferable: a smaller current is closer to the low emission of the hot electron device and the comparison is simplified. Figure 7.4 shows the comparison of the results with the two sources.

The similarity of the two spectra is evident and proves the possibility of employing hot electron emitters in this kind of application. Focusing on the differences between the two spectra, the level of the background noise is higher for the hot electron emitter: this is a consequence of the lower signal. Nonetheless con-

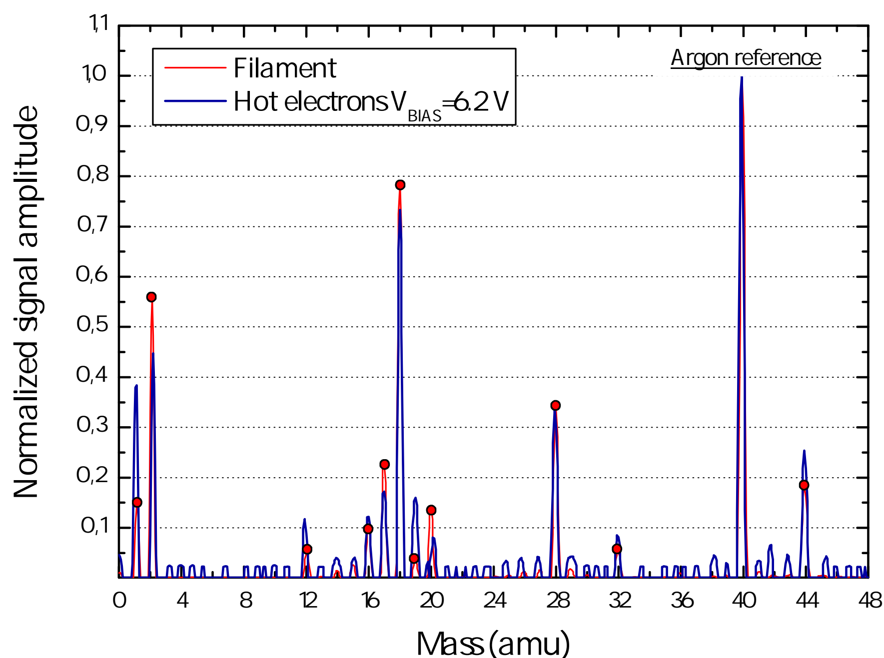

Figure 7.4: *A comparison of two spectra with a thermionic filament and with a hot electron emitter is presented. The two signal amplitudes are normalized with respect to the partial pressure of argon (*M = 40*amu) which was measured to be stable in subsequent measurements and set equal to 1. The mass spectrometer was run with the filament for more than half an hour before taking the measurements in order to further stabilize the height of the peaks. The red circles emphasize the position of the main peaks in the measurement with the filament. These peaks are higher for water (*M = 17, 18*amu) and hydrogen (*M = 2*amu) which could support the hypothesis of differences due to the outgassing caused by the filament. Nonetheless in this case a higher signal for the CO (*M = 28*amu) and* CO_2 *(*M = 16, 44*amu) would also be expected. The comparison shows a very similar partial pressure for the CO and a lower pressure for the* CO_2*. The level of noise is higher in the case of the hot electron emitter as a consequence of the smaller signal. The different intensity of the signal of the secondary peak of argon at* M = 20*amu can be due to the higher current density in the case of a hot filament, which could result in a higher probability of second ionization.*

cerning the height of the peaks both the signal of water and hydrogen are lower while various other molecules generate a stronger signal. If high temperature of the hot filament is effectively influencing the measurement the hot electron source should generally produce lower intensities. The fact that this is observed for water and hydrogen does not allow a certain conclusion.

Conclusion

During this project Metal-Insulator-Semiconductor structures were studied in relation to the possibility of creating hot electron emitters. The theoretical description of such heterostructures, which already constitutes the framework of common electrical devices as MOS transistors, was already well known from solid state physics. Nonetheless it was developed for the particular objective of achieving emission. This treatment introduced peculiar requirements for the design of real devices; these were fabricated in the cleanroom facilities of Danchip. During this thesis the electrical properties of the MIS devices were tested. The comparison with the theoretical results demonstrated a good qualitative agreement. Nonetheless a very accurate theoretical model can consider many more variables and phenomena as the quantum-size effect. Such investigation which was already attempted by Professor Ole Hansen and PhD student Lasse Thomsen provided an even better description of the system. A quantitative prediction of the currents is still difficult because of the extremely non-linear electrical behaviour of such structures and because of the unavoidable presence of fabrication defects. A lot of work may still be directed towards an even more accurate model.

The possibility of measuring emission currents under gas pressure and even in air at 1 bar represented an extremely useful tool for the characterization of the emitters. It allowed to take fast measurements on many different devices belonging to different wafers and obtain immediate information about the quality of the oxide, the breakdown voltages, the intensity of the currents and the efficiency. Starting from a previous theory by Townsend, a model was realized to describe the electron motion in a gas and the probability of electron transmission from the device to the anode of the experimental setup. The problem itself with the special conditions introduced by the hot electron devices and the measuring system was found to be particularly complex and interesting at the same time, since many variables play a role on the final measured current. Beyond the desire of achieving quantitative information while measuring emission in air, the model was useful for better

understanding the dynamics of electrons and ions in a gas; topics which can be applied to many other study fields and primarily to plasma physics. Such model was able to describe the qualitative trends of the transmission function when the accelerating electric field or the pressure is varied. Quantitative predictions would also require a further analysis of the ionization probability in the gas and of the consequent currents. The effects of the geometry of the experimental setup and especially of the combined system device-collector should also be precisely evaluated.

The devices produced with a titanium (Ti) wetting layer and a gold layer (Au) on top of it produced the highest emission currents and efficiencies. For a device with 2 Å of titanium (Ti) and 100 Å of gold (Au) these reached the values of 5μA and 3.4×10^{-4} respectively at 6V of applied bias voltage. Furthermore the considerably good durability of these devices allowed the application of the hot electron emitters as a new electron source in mass spectrometry. Nonetheless many aspects of these devices may be improved: especially the efficiency is still very low. Various methods for enhancing it were proposed and tested, others are being assessed for future devices. For this purpose the minimization of the thickness of the titanium wetting layer was proved to be essential, but it does not allow a further increase of the efficiency. The work function lowering is a promising strategy but till now it did not produce the expected results: higher emission and efficiencies are obtained to the prejudice of durability and oxide quality. A deep investigation of the breakdown mechanisms should be made in order to understand the reasons why most of the tested metal layers caused the deterioration of the oxide. Despite the complexity of this problem a broader knowledge of this effect could allow to find other metals having a low work function and simultaneously a better compatibility with the silicon dioxide. On the other hand efforts can be made in order to grow oxide layers of higher quality.

If these strategies are found not to produce considerable improvements other ideas are already under examination. Some of them could concern the realization of Metal-Insulator-Metal (MIM) structures or the substitution of the front gate metal with other kinds of conductive materials, for instance with graphene. MIM structures could be fabricated with aluminum oxide (Al_2O_3) which is known to posses very good insulating properties and is probably more resistant to the attack of other metals. Such oxide can be also grown layer by layer with extremely accurate techniques. The idea of graphene instead is related to its low sheet resistance. It could represent a good compromise between the necessity of applying a stable

bias voltage at the front of the device and the need of an extremely thin conductive layer, consequently an extremely low attenuation of the emission due to scattering events.

In the last chapter of the thesis the measurements acquired with a mass spectrometer whose electron source was substituted with a hot electron emitter were presented. An analysis of these spectra in relation to the ones measured with a normal thermionic filament showed that the results are comparable. As a consequence of the still lower emission current the hot electron devices produced amplitudes about two orders of magnitude lower when the filament is run at the maximum allowed power. About one order of magnitude when the emission current from the filament was minimized. Despite an accurate evaluation of the potentialities of the hot electron source would require a particular attention for reducing the residual gases of the chamber, this initial screening seemed promising. Gases like H_2O and H_2 whose presence can be easily due to outgassing were proved to exhibit significantly lower partial pressures. These evidences and the considerations provided in all this thesis prove the potentialities of MIS devices as hot electron emitters and justify the vivid interest in this project and more widely in this research.

Appendix A

List of symbols

$\mathrm{E_F}$**:** Fermi energy

$\mathrm{E_V}$**:** Valence vand

$\mathrm{E_C}$**:** Conduction band

$\mathrm{K_B}$**:** Boltzmann constant

$\mathrm{E_G}$**:** Energy gap

T**:** Absolute temperature

$\mathrm{N_D}$**:** Concentration of donors

n_i**:** Intrinsic concentration of carriers

q**:** Electron charge

m_e**:** Electron mass

$m^\star_{\mathrm{S}}$**:** Effective mass in the semiconductor

$m^\star_{\mathrm{I}}$**:** Effective mass in the insulator

g_{S}**:** Density of states in the semiconductor

g_I**:** Density of states in the insulator

f_S**:** Fermi distribution in the semiconductor

f_I**:** Fermi distribution in the insulator

V**:** Electron potential

U**:** Potential energy

E**:** Total energy

E_k**:** Kinetic energy

Φ_B**:** Height of the tunneling barrier

X_I**:** Insulator thickness

V_I**:** Voltage drop across the insulator

L**:** Metal thickness

Φ**:** Work function

χ**:** Electron affinity

T**:** Transmission probability

N**:** Supply function

η**:** Emission efficiency

I**:** Total current

I_E**:** Emission current

I_T**:** Transmission current

λ: Electron mean free path

V_{BIAS}: Bias voltage applied across the MIS structure

V_C: Collector voltage

d: Distance device-collector

p: Pressure

ε: Electric field

k_T: Townsend factor

f: Distribution functions

v: Electron velocity

m: Electron mass

ν: Collision frequency of the electrons

τ: Mean free time between collisions

w: Drift velocity

ΔE: Energy loss per collision

Appendix B

Hot electron surface chemistry

The research activity of this project takes part in a more general scientific background concerning the physical and chemical properties of surfaces and in particular the dynamics of catalytic processes. The current research at CINF is notably directed towards the study of heterogeneous metal catalysis where the interface between a metal and a gas phase is the site for catalytic events. This setting is also labeled femtochemistry because of the time scale which is involved: the atomic time scale, with the order of magnitude of femtoseconds. Although the physical concepts governing these phenomena have been quite well studied and understood, a new frontier of research is the realization of selective, non-thermal processes.

Traditionally, the purpose of theoretical and experimental catalysis has been focused on describing the interaction of adsorbates with surfaces by assuming the electronic configuration to be in the ground state at every step of the reaction pathway. This assumption relies on the fact that electrons equilibrate on a timescale orders of magnitude faster than the movement of the nuclei: this is known as the Born-Oppenheimer approximation [57]. Under this assumption reactions occur in the adiabatic limit without energy exchange with the surrounding environment. For various kind of reactions this point of view leads to an accurate description of the system and allows to estimate important parameters as the binging energies and the reaction rates.

For some classes of interactions at surfaces, however, the adiabatic picture is not appropriate. This is the case when other kinds of sources may directly exchange energy with the system. In literature there have been various attempts to activate reactions using excited carriers: these techniques are usually known with the acronym of HEFatS (Hot Electron Femtochemistry at Surfaces): examples are photocatalysis [58], Electron Stimulated Desorption [59], desorption induced by

Femtoseconds lasers [60] or by Scanning Tunneling Microscope (STM) probes [61]. More recently Metal-Insulator-Metal (MIM) tunneling device were proposed to be a promising source of hot electrons [2, 3]: studies about the possibility to apply MIM devices for electrochemistry and for the decomposition of relatively large molecules on surfaces have already been presented. This project is focused on Metal-Insulator-Semiconductor (MIS) devices instead: the hot electrons are generated by tunneling from the semiconductor substrate into the metal layer; if they reach the metal surface without energy losses they can interact with the adsorbates and promote desorption by directly injecting their energy into the reaction coordinate. The main advantage of such structures is related to the very narrow energy distribution concentrated around a mean energy equal to the applied bias voltage: in fact the energy is limited by the fast decay of the Fermi distribution at higher energies and by the exponential decrease of tunneling probability at lower energies. This narrow spectrum of energies is expected to represent the key for enhancing the selectivity on reactions, since a certain reaction coordinate can be preferred to the others; this is in contrast with classical energy sources, as the thermal energy, which accelerates reactions without any possibility of selectivity.

Theoretical approach. The interaction between hot electrons and an adsorbate may be explained through different processes: inelastic scattering, occupation of anti-bonding orbitals, creation of a temporary negative ion or more in general with a variation in time and space of the Potential Energy Surface (PES). The model may refer to two different regimes: Desorption Induced by Electronic Transitions (DIET) [62] and Desorption Induced by Multiple Electronic Transitions (DIMET) [63]. In the first case the desorption probability has a threshold, since the energy of a single hot electron needs to overcome the desorption energy and it is proportional to the electron flux at the surface. In the second case, a larger amount of electrons may contribute together to the reaction and no energy threshold is expected. Nonetheless this second situation requires a very high flux of electrons which is the case when the excitation is achieved with femtoseconds lasers. The low currents of MIS devices surely implies the DIET treatment. The theoretical group of the physical department, namely the Center for Atomic-scale Materials Design (CAMd), worked on the model for describing the interaction hot electron-adsorbate under DIET conditions. The estimation is based on results derived from Density Functional Theory (DFT): the traditional algorithm calculates the charge density of the ground state self-consistently. Such method relies on the assumption that the total energy of the nuclear system is a unique functional of the charge

density: this was demonstrated by Hohenberg and Kohn [64]. By comparing the total energy of selected geometric configurations important physical quantities as binding energies and forces can be achieved. The molecular PES can be then evaluated by mapping out the forces on a molecule as a function of the internal degrees of freedom, for instance the motion of the center of mass and the internal vibrational modes. Nevertheless Hohenberg and Kohn's proof is only valid for describing the ground state, while the description of DIET requires information about the excited states: for this reason a modified version of DFT, called linear expansion ΔSFC-DFT is employed [65]. A particular hot electron device, with silicon (Si),

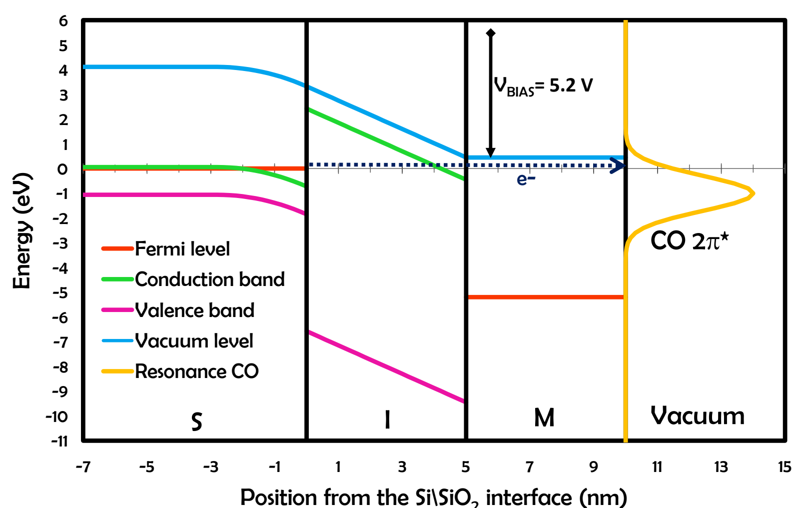

Figure B.1: *Typical energy bands in the MIS device when a bias voltage in the Fowler-Nordheim regime is applied. The metal surface is imagined to be covered by an adsorbate of CO and represents the reaction site. The tunneling electron may reach the metal surface and then be inelastically scattered on the resonance of the unoccupied* 2π *antibonding orbital catalyzing desorption.*

silicon dioxide (SiO_2) and platinum (Pt) has been studied; in fact the desorption of carbon oxide (CO) on the Pt(111) surface has been considered to be a promising candidate for observing the effects induced by hot electrons. The energy bands and the resonance of CO is shown in figure B.1. The 2π antibonding orbital can be partially occupied by hot electrons enhancing the desorption rate. From the PES of the ground state, of the excited states and assuming a given resonance shape, the

desorption probability can be calculated. Typical resonance width of the order of $1e$V produces a maximum probability close to 10^{-5}; the maximum occurs for an electron $0.6e$V higher in energy than the resonance of the 2π antibonding orbital which is positioned $3.9e$V above the Fermi level of the metal. The reason for the maximum to be higher than the resonance, suggesting a bias voltage $V_{BIAS} = 4.5e$V, is related to the minimization of the energy difference both between the energy of the incoming electron and the resonance and on the other hand the resonance and the energy of the outgoing electron [66]. So far the emission currents are still rather low and even the highest values of about 1μA only yield a hot electron event rate of $10ms^{-1}$, where the coverage has been assumed to be 1 monolayer with an adsorption site density of $10^{15}cm^{-2}$. Evidently, the main challenge is to maximize both the electron currents of hot electrons and the desorption probability in order to be able to clearly measure the enhanced desorption rate.

Appendix C

Measurement setup and holders

During the development of this project the extended knowledge concerning the behaviour of the hot electron emitters when subjected to different conditions and the interest in investigating some of their features imposed new requirements for the experimental setup. In particular the sample holder and the collector play a fundamental role in defining the accuracy of the measurements and the capability of observing particular properties rather then introducing strong limits in the measurements themselves.

Beyond the most obvious, but important, necessity of holding a device or a whole wafer and keeping it safe avoiding mechanical stresses the holder represents the coupling element between such devices and the measuring instruments. The structure of the holder and of its connections with the cables is fundamental for the noise confinement. The geometry of the collector and of the contacts with the sample may introduce systematic errors if not well designed. The necessity of measuring extremely low emission currents imposed other requirements. In order to lower the noise level and the leakage currents, shielding or guarding techniques were implemented. In the case of measurements in air a copper box was used to completely cover the measurement apparatus; in vacuum the UHV chamber itself provided the required shielding.

In the following paragraphs a better description of the mostly used holders is given, together with an explanation of the technical challanges they were expected to face and their particular features. Three different holders were employed for the electrical characterization.

Measurements in air on a full wafer. The main purpose of the measurements in air is to achieve fast results with the highest flexibility. An entire wafer is placed

on top of a cylindric metal holder which ensures the electrical connection to the backsides of the devices. The wafer is kept in a fixed position by a pump which induces vacuum and tightens them together: this improves the contact between metal layers and stabilizes the wafer. A PMMA plate contains the metal contacts to the front of the devices, in relief with respect to the other parts, and an anode for the collection of the emitted electrons: figure C.1. A micrometer screw is used to vertically move the PMMA plate and to press the metal contacts onto a single device. A measurement of the resistance between these two contacts is usually performed before taking other measurements: if both sides of the device are well connected such resistance approximates the resistance of the thin metal layer in front of the device, usually $20-100\Omega$. The plate can also be moved along the lateral directions through a couple of less accurate screws, they are used to align the metal contacts on a particular device of the wafer before pressing with the vertical screw establishing the electrical contact.

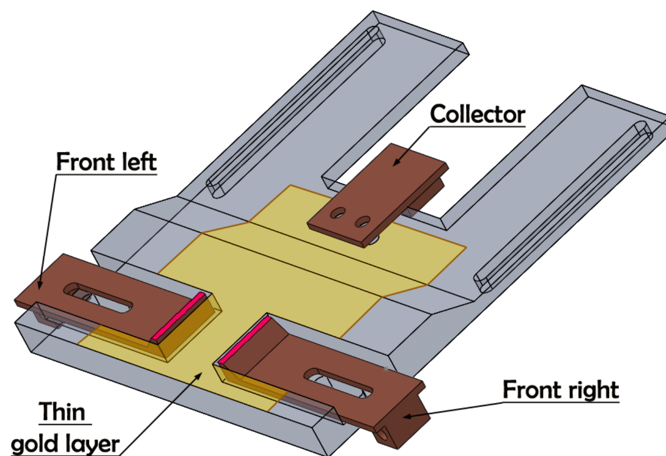

Figure C.1: *The PMMA plate as it was designed. Two lateral copper contacts are pressed onto the device: the two small surfaces in direct connection with it have been emphasized with pink. The collector is constituted by a gold semi-transparent layer deposited on PMMA: another copper piece allows the connection of this layer with the instruments.*

The reason for the choice of PMMA is related to the desire of having a transparent structure; in fact transparency is needed in order to be able to accurately align the plate on a single device. A thin gold layer ($\approx 15/10 nm$ of Au/Ti) is deposited on the PMMA plate in order to realize a conductive layer for the anode, maintaining a partial transparency. The distance between the active area and the anode depends on the shape and the thickness of the metal contacts on the plate, this can be var-

ied between 0.3mm and 1.2mm. This geometry, which is sketched in figure C.2,

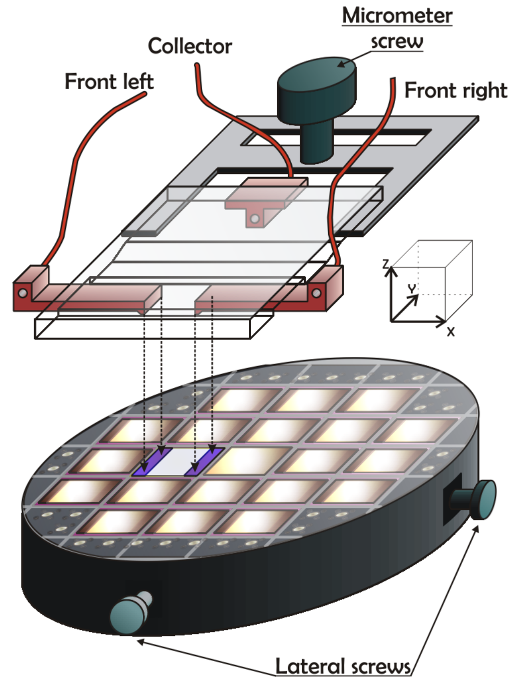

Figure C.2: *A sketch of the first setup is shown. The main objective is to provide good qualitative IV curves and emission curves in a short time. Measurements can be performed on an entire wafer selecting a single device simply by aligning it under the copper contacts of the PMMA plate. This particular device is marked with blue tonalities. Two lateral screws are used for this purpose while a vertical micrometer screw presses the PMMA plate onto the device.*

originates two main problems, both related to the relative position of the metal contacts. Since both the gold layer of the collector and the contacts to the front of the device are placed on the PMMA plate, very close to each other, it is important to accurately insulate the conductive parts. Despite the gold deposition threatens this insulation, the resistance was measured to exceed $10^{11}\Omega$: consequently the current between the contacts is negligible when typical collector voltages,$V_C \approx 30V$, are applied. The second problem was crucial instead, it concerns the position of the anode with respect to the active area of the device: if the PMMA plate is accurately aligned and connected to one device of a wafer, the collector layer completely covers the active area of the device. Nevertheless along the x direction of figure C.2, the extension of the collector is limited by the presence of the metal contacts to the front of the device and it only exceeds the length of the active area of about 1mm. On the other hand along the y direction the collector is much larger than the active area: about 2cm larger. This means that the geometrical losses, due to the diver-

gence of the electrons in the x direction during their diffusive motion in air, can be rather high. A different setup allows to minimize these geometrical losses at the cost of a lower flexibility: as it will be apparent in the next paragraph this will require to cut the wafer and measure on a single device.

Measurements in air for minimizing the geometrical losses. Every time the necessity to minimize the loss of emitted electrons, due to geometrical reasons, was important, as for all the measurements of chapter 4, this measurement scheme was preferred. A sketch of this second structure is presented in figure C.3. A sin-

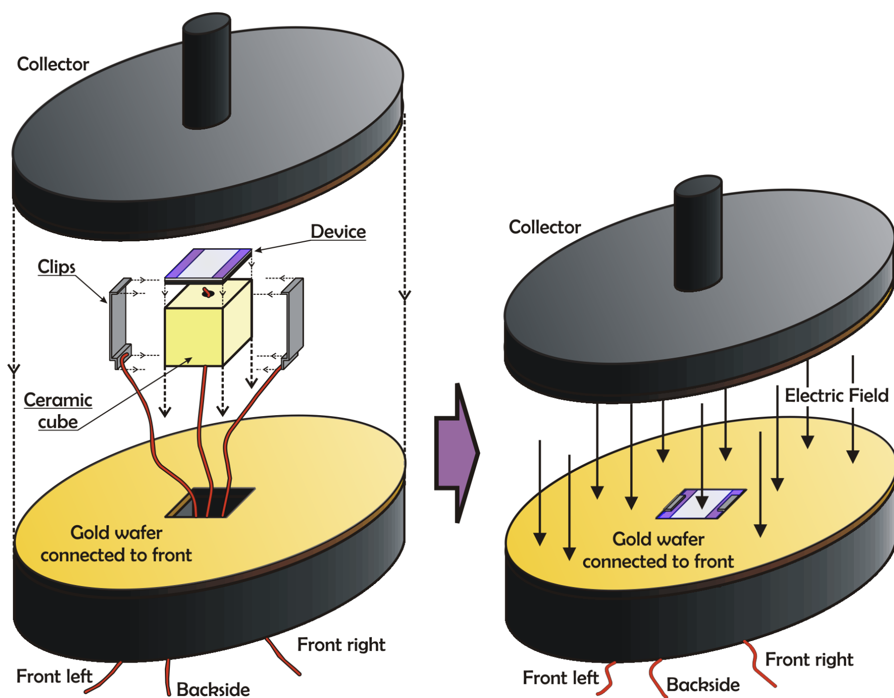

Figure C.3: *A sketch of the second kind of holder is illustrated. The main purpose of such structure is to avoid the geometrical losses of emitted electrons by producing a uniform electric field extended over a large area around the active area of the device. The figure on the left contains the various parts while the second one shows the full holder when already mounted.*

gle device is mounted on a ceramic cube and holden by two very thin metal clips, which also constitute the connection to the front of the device: in this case they are completely separated from the anode. A little hole in the ceramic cube allows a wire to establish the connection to the backside of the device. The collector is represented by a 4-inch wafer completely covered by gold, this is kept parallel to the active area. Their distance can be precisely tuned with a micrometer screw over a

rather large range: from 2 to 20mm. In order to generate a uniform electric field between the active area and the collector, the active area itself is surrounded by another gold covered 4-inch wafer. The device is inserted in a rectangular hole at the center of this second wafer whose surface is equipotential to the active area. These two wafers basically approximate the shape of a parallel plate capacitor producing a uniform electric field.

Measurements under Ultra High Vacuum. The particular features of UHV impose different requirements to the measurement setup. First, the confined dimensions of UHV chambers don't allow to easily design a system for measuring on a full wafer, therefore only single devices can be introduced. Furthermore the chamber was prepared in order to contain only two devices at the same time, one in the mass spectrometer where only a few IV curves were taken, and an other one in the particular holder described in this paragraph. The small size of the chamber does not permit to have very large collectors either, nonetheless the electron trajectories between the active area and the collector are supposed to be almost ballistic and the geometrical losses are still expected to be low. For the same reason, the intensity of the electric field is not expected to have crucial effects on the percentage of the collected electrons. The chosen geometry consists of a ceramic cylindric holder. The sample lies on a copper plate connected to the external part of the chamber through a conductive screw and a wire: this ensures the connection to the backside of the sample. Two other screws establish the connection to the front of the device thanks to a couple of flexible conductive clips. A gold covered copper plate is used as an anode in front of the active area in order to collect the emitted electrons. Its dimensions are slightly larger than the device on the x direction: about 2mm larger, and about 1cm larger on the y direction.

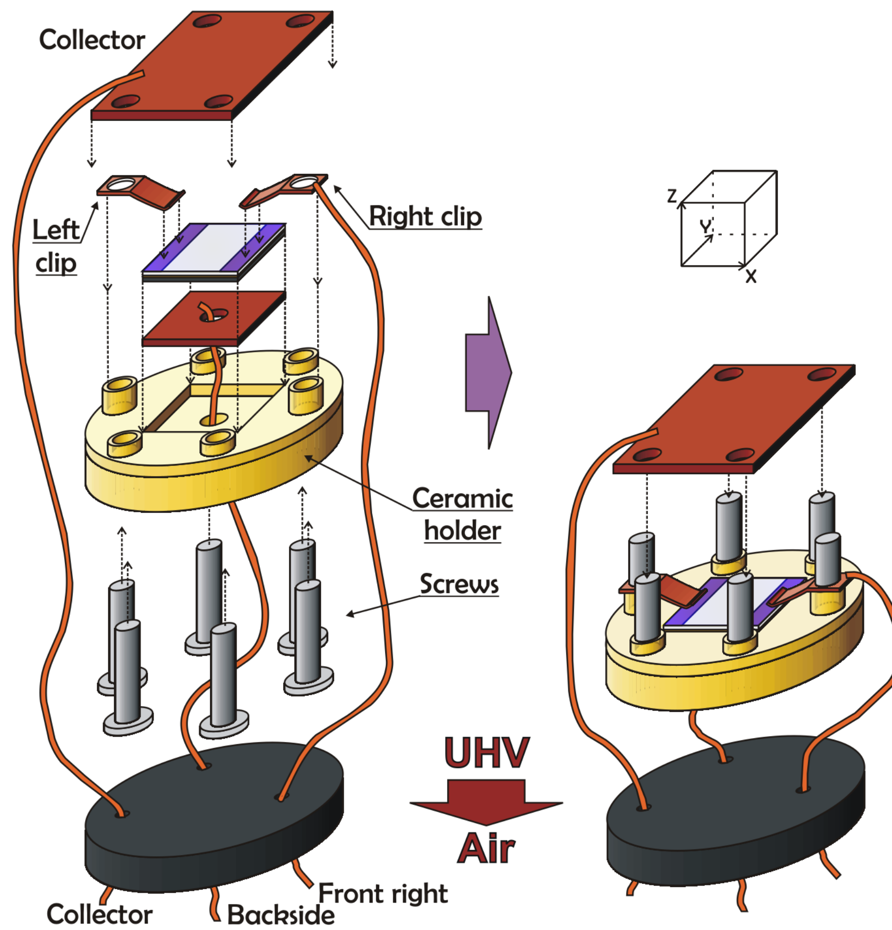

Figure C.4: *Sketch of the third holder for measurements in UHV. On the left the various parts of the holder are shown before being mounted. A couple of clips establish contact with the front of the device. The device, marked in blue, lies on a copper plate for the connection to the backside. Another copper plate is used as anode and collector. Six conductive screws fix the all structure. The dark cylinder on the bottom represents the wall of the UHV chamber. On the right the entire holder after assembling.*

Bibliography

[1] S.A. Buntin, L. J. Richter, R. R. Cavanagh, and D. S. King, **Optically driven surface reaction: Evidence for the role of hot electrons**, *Physical Review Letters*, Vol.61 (11), P. 1321-1324, 1988.

[2] J.W. Gadzuk and C. W. Clark, **Resonance enhanced electron stimulated desorption**, *Journal of Chemical Physics*, 91(5):3174-3181, 1989.

[3] J.W. Gadzuk, **Role of secondary electrons in hot-electron femtochemistry at surfaces using tunnel junctions**, *Journal of Vacuum Science & Technology A: Vacuum, Surfaces, and Films* , vol. 15, pages 1520-1525. AVS, 1997.

[4] D.J. DiMaria, M. V. Fischetti, J. Batey, L. Dori, E. Tierney, and J. Stasiak, **Direct observation of ballistic electrons in silicon dioxide**, *Physical Review Letters*, 57(25), p. 3213-3217, 1986.

[5] J. Cohen, **Tunnel emission into vacuum**, *Journal of Applied Physics*, 33(6), p. 1999-2000, 1962.

[6] H. Mimura, Y. Neo, H. Shimawaki, T. Matsumoto, and K. Yokoo, **Emission characteristics and application of semiconductor field emitters**, *Applied Surface Science*, 144:498-503, 2005.

[7] C.A. Mead, **Operation of tunnel-emitter devices**, *Journal of Applied Physics*, 32(4):646-652, 1961.

[8] D. Diesing, A.W. Hassel, M.M. Lohrengel, **Aluminium oxide tunnel junctions: influence of preparation technique, sample geometry and oxide thickness**, *Thin Solid Films* 342 (1999), p. 282-290, 1998.

[9] W.B. Nottingham, **Thermionic emission from tungsten and thoriated tungsten filaments**, *Physical Review*, 49, p. 78-97, 1936.

[10] R.N. Peacock, **Comparison of hot cathode and cold cathode ionization gauges**, *Journal of Vacuum Science & Technology A* , 9 (3) , p. 1977-1985,1991.

[11] M. Cahay, **Field emission properties of metallic nanostructures self assembled on nanoporous alumina and silicon templates**, *Journal of Vacuum Science & Technology B*, 26 (2), p. 885-890, 2008.

[12] S. Choker, *Field emission properties of carbon nanostructures, A review, International Workshop on Physics of Semiconductor Devices*, p. 820-826, 2007.

[13] N.S. Xu, S.E. Huq, **Novel cold cathode materials and applications**, *Materials Science and Engineering*, 48, p. 47-189, 2005.

[14] L. B. Thomsen, G. Nielsen, S. B. Vendelbo, M. Johansson, O. Hansen, and I. Chorkendorff, **Electron emission from ultra-large area mos electron emitters**, *Journal of Vacuum Science and Technology B*, 2009.

[15] M. Poppeller, E. Cartier, R. M. Tromp, *Microelectronic Engineering*, 46:183-186, 1999.

[16] H. Hopster, **Spin dependent mean-free path of low-energy electrons in ferromagnetic materials**, *Journal of Electron Spectroscopy and Related Phenomena*, 98-99 , p. 17-23, 1999.

[17] J. Bansmann, **Spin-polarization effects for electrons passing through thin iron and cobalt films**, *Solid State Communications*, 87 (5) , p. 467-469 ,1993.

[18] *Handbook of Chemistry and Physics*, 12-114, 2008.

[19] R. H. Fowler, L. W. Nordheim, **Electron emission in intense electric fields**, *Proceedings of the Royal Society of London A*, 119:173-181, 1928.

[20] J. P. Shiely, **Simulation of Tunneling in MOS Devices**, *Dissertation, Duke University* , 1999.

[21] C. B. Duke, **Tunneling in Solids**, *Academic Press* 1969.

[22] R. Tsu, L. Esaki, **Tunneling in a Finite Superlattice**, *Applied Physics Letters* vol. 22, no. 11, pp. 562-564, 1973.

[23] K. L. Jensen, **General formulation of thermal, field, and photoinduced electron emission**, *Journal of Applied Physics*, 102(024911), 2007.

[24] E. Schroedinger, **The current situation in quantum mechanics**, *Naturwissenschaften*, 23:844-849, 1935.

[25] L. Brillouin, **The ondulatory mechanics of Schrodinger; a general method of resolution by successive approximations**, *Comtes Rendus Hebdomadaires des Seances De L'Academie des Sciences*, 183:24-27, 1926.

[26] J. J. Quinn, **The range of hot electrons and holes in metals**, *Applied Physics Letters*, 2(9): 167169, 1963.

[27] W. F. Krolikowski, W. E. Spicer, **Photoemission studies of the noble metals**, *Physical Review B*, 1(2) 478-487, 1970.

[28] H. Kanter, **Slow-electron mean free paths in aluminum, silver, and gold**, *Physical Review B*, 1(2):522-536, 1970.

[29] M. Lenzlinger, E. H. Snow, **Fowler-Nordheim tunneling into thermally grown SiO2**, *Journal of Applied Physics*, 40:278-283, 1969.

[30] T. K. S. Wong, S. G. Ingram **Observational of Fowler-Nordheim tunnelling at atmospheric pressure using Au/Ti lateral tunnel diodes**, *Journal of Physics D.* , 26 (1993) 979-985., 1992.

[31] J.C. Rivière, **The work function of gold**, *Applied Physics Letters*, 8 (7) , p. 172, 1966.

[32] A. Alessandrini, **Work function dependence on the thickness and substrate of carbon contamination layers by Kelvin probe force microscopy**, *Philosophical Magazine Letters*, 83 (7) , p. 441-451. 2003.

[33] U. Yusupaliev, **Stoletov Constant and Effective Ionization Potential of a Diatomic Gas Molecule**, *Bulletin of the Lebedev Physics Institute*, Vol. 34(11), p. 334-339, 2007.

[34] L.Z. Fridlyand, **A theoretical determination of the Stoletov constant for a mixture of gases**, *Litovskii Fizicheskii Sbornik*, p. 543-552. ,1970.

[35] L.B. Loeb, **Fundamental Processes of Electrical Discharges in Gases**, *Gostekhizdat*, Moscow, 1950.

[36] D. Mathur, C . Badrinathan, **Experimental studies of metastable and dissociative states of doubly-charged molecular ions**, *Journal de Physique*, C1(50), 1989.

[37] A.A.G. Driskill-Smith, D.G. Hasko, H. Ahmed , **Fabrication and behavior of nanoscale field emission structures**, *Journal of Vacuum Science & Technology B*, Driskill-Smith, vol. 15 (6) , p. 2773-2776. ,1997.

[38] O.J. Orient, **Determination of the mean free path of slow electrons by the measurement of back-diffusion in helium and argon** , *Canadian Journal of Physics*, Vol. 43(3), p. 422-431, 1965.

[39] R.W. Crompton, D.J. Sutton, **Experimental Studies of the Motions of Slow Electrons in Air with Application to the Ionosphere**, *Proceedings of the Royal Society of London*, 218 (1135) , p. 507-519, 1953.

[40] J.S. Townsend, **Motion of Electrons in Gases**, *Proceedings of the Royal Society of London.*, Vol. 120, No. 786, 1928.

[41] L.H.G. Huxley , A. A. Zaazou, **Experimental and Theoretical Studies of the Behaviour of Slow Electrons in Air**, *Proceedings of the Royal Society of London*, Vol. 196, No. 1046 , pp. 402-426, 1949.

[42] R.A. Nielsen, **Electron and negative ion mobilities in oxygen, air, nitrous oxide and ammonia**, *Physical Review*, 51 , p. 69-75, 1937.

[43] L.W. Cochran, **Diffusion of slow electrons in gases**, *Physical Review*, 126 (5) , p. 1785-1788, 1962.

[44] Sang-Hun Seo, **Evolution of the electron energy distribution function in a planar inductive argon**, *Applied Physics Letters*, 76 (2) , p. 149-151 , 2000.

[45] T.Matsoukas, **Particle charging in low-pressure plasmas**, *Journal of Applied Physics*,7 (9) , p. 4285-4292, 1995.

[46] W.J. Graham, **Calculated values of the parameters of noble gas discharges**, *Physical Review*, 94 , p. 25-29, 1954.

[47] R.W. Crompton, D.J. Sutton, **Experimental Investigation of the Diffusion of Slow Electrons in Nitrogen and Hydrogen**, *Proceedings of the Royal Society of London*, 215 (1123), p.467-480; 1952.

[48] J.D. Cobine, E.C. Easton, **Timer for spark breakdown studies**, *Review of Scientific Instruments*, Vol.12, p. 301-305, 1941.

[49] C.J. Powell , **Energy and material dependence of the inelastic mean free path of low-energy electrons in solids**, *Journal of Vacuum Science & Technology A*,3 (3) , p. 1338-1342, 1985.

[50] B. Ziaja, R. A. London, J. Hajdu, **Ionization by impact electrons in solids, electron mean free path ftted over a wide energy range**, *Journal of Applied Physics* ,vol 99, 2006.

[51] J.V. Barth, **Adsorption, surface restructuring and alloy formation in the Na/Au(111) system**, *Surface Science*, 341 (1-2) , p. 62-91. , 1995.

[52] J.L. Larue, **The work function of submonolayer cesium-covered gold: A photoelectron spectroscopy study**, *Journal of Chemical Physics*, Issue Vol.129 Issue.2 , 129 (2) In: , 2008.

[53] G. Nielsen, **Electron emission from MOS electron emitters with clean and cesium covered gold surface**, *Applied Surface Science* , 255 (17) , p. 7657-7662 , 2009.

[54] W.E. Spicer, **Studies of the semiconducting properties of the compound CsAu**, *Physical review*, 115 (1) , p. 57-62, 1959.

[55] D.J. DiMaria, E. Cat-tier, and D. Arnolda, **Impact ionization, trap creation, degradation, and breakdown in silicon dioxide films on silicon**, *IBM Thomas J. Watson Research Center*, P.O. Box 218 ,1992.)

[56] D.J. DiMaria, **Defect generation under substrate-hot-electron injection into ultrathin silicon dioxide layers**, *Journal of applied physics*, vol 86(4), 1999.

[57] M. Born and R. Oppenheimer. **Quantum theory of the molecules**, *Annuals of Physics*, 84:457-84, 1927.

[58] A.L. Linsebigler, G. Lu, and J. T. Yates Jr. **Photocatalysis on tio2 surfaces: Principles, mechanisms, and selected results**, *Chemical Reviews* , 95:735-756, 1995.

[59] R.D. Ramsier and J. T. Yates. **Electron-stimulated desorption: Principles and applications**, *Surface Science Reports* , 12(6-8):246 - 378, 1991.

[60] F.J. Kao, D. G. Busch, D. Cohen, D. Gomes da Costa, and W. Ho. **Femtosecond laser desorption of molecularly adsorbed oxygen from pt(111)**, *Physical Review Letters* , 71(13):2094-2097, Sep 1993.

[61] S. Alavi and T. Seideman. **Reaction induced by a scanning tunneling microscope: Theory and application**, *The Journal of Chemical Physics*, 115(4):1882-1890, 2001.

[62] T.E. Madey. **History of desorption induced by electronic transitions**, *Surface Science*, 299-300:824 836, 1994.

[63] J.A. Misewich, T. F. Heinz, and D. M. Newns. **Desorption induced by multiple electronic transitions**, *Physical Review Letters*, 68(25):3737-3740, Jun 1992.

[64] P. Hohenberg and W. Kohn. **Inhomogeneous electron gas**, *Physical Review*, 136(3B):B864-B871, Nov 1964.

[65] J. Gavnholt, T. Olsen, M. Engelund, and J. Schiotz **Delta self-consistent field method to obtain potential energy surfaces of excited molecules on surfaces**, *Physical Review B*, 78(7):075441, 2008.

[66] T. Olsen, J. Gavnholt, and J. Schiotz. **Hot-electron-mediated desorption rates calculated from excited-state potential energy surfaces**, *Physical Review B*, 79(3):035403, 2009.